Supplementary Material

Changes in extreme temperatures of the Earth's desert regions over the next 100 years

Callum Leach, Kevin Ewans, Philip Jonathan

Overview

This supplementary material provides supporting information for the article referenced above.

Section SM1 provides further discussion of the literature on information criteria (such as AIC, BIC, DIC and WAIC), and non-stationary parametric GEV regression, to complement Section 1.

Section SM2 provides illustrations of regional annual minima time series for comparison with Figure 3.

Section SM3 provides a brief outline of the MCMC scheme for model parameter estimation, discussed in Section 3.2.

Section SM4 provides visual summaries of model fits for regional annual maxima (to be compared with Figure 6), and box-whisker plots of differences in return values ΔQ (to be compared with Figures 7-8).

Section SM5 provides visual summaries of model fits for regional annual minima (to be compared with corresponding figures for regional annual maxima in Figure 6 and Section SM4), and box-whisker plots of differences in return values for regional annual minima (to be compared with Figures 7-8).

Section SM6 gives box-whisker plots of $\Delta Q(\text{for maxima}) - \Delta Q(\text{for minima})$, comparing ΔQ for regional annual maxima and minima.

Section SM7 investigates the spatial distribution of regional annual maxima and minima (to be compared with Figure 12)

Section SM8 illustrates the distribution of complexity of fitted models (to be compared with Figure 13)

Section SM9 provides some background to the Bayesian model averaging performed in Section 6.3.

SM1 Literature review

This section should be read in conjunction with Section 1 of the main text.

SM1.1 Information criteria

Zhang et al. (2023) gives a more recent review of the use of information criteria for statistical model selection, focussing on the Akaike Information Criterion (AIC, Akaike 1974) and the so-called Bayesian Information Criterion (BIC, Schwarz 1978). The authors note that in application, adoption of different information criteria can result in the selection of different "optimal" models, yet it is generally unclear which criterion should be favoured. They further note that the choice of the most appropriate information criterion is problem-dependent, influenced by one or more of the underlying data-generating process, the nature of the postulated model forms, sample size and model performance criterion. For a Bayesian inference generating a sample from the joint posterior distribution of estimated model parameters, the Divergence Information Criterion (DIC, Spiegelhalter et al. 2002, Gelman et al. 2004) and the Widely Applicable Information Criterion (WAIC, Watanabe 2013,Vehtari et al. 2017) are often used. In comparing AIC and BIC, Zhang et al. (2023) notes that AIC tends to select more complex models, but that it is not generally possible to foresee which of AIC or BIC would yield models with best out-of-sample predictive performance for a particular model selection problem. Indeed, the authors recommend performing a study involving direct quantification of out-of-sample predictive performance using cross-validation, to quantify the relative performance of different information criteria on problems of the relevant type, as a rational basis for selecting the most appropriate criterion for that problem type. This suggestion was adopted by us in the current work to assess which of a range of criteria based on AIC, BIC, DIC and WAIC yields best performance in a specific extreme value prediction problem involving relatively small samples of CMIP6 climate model output for `tas`, below. The earlier article of Gelman et al. (2014) arrives at a similar conclusion regarding predictive information criteria for Bayesian models, including AIC, BIC, DIC and WAIC. The authors state that none of AIC, BIC, DIC and WAIC performs well universally: that AIC is poor in settings with prior information, that DIC is poor when the posterior distribution is not well summarised by its mean, and that WAIC relies on data partition and cross-validation, themselves problematic procedures in the presence of dependence. The authors lean towards cross-validation as their favoured approach. Kim et al. (2017) describes a simulation study to assess the relative performance of AIC, the corrected AIC (Hurvich and Tsai 1989), BIC and the likelihood ratio test (LRT) in identifying underlying stationary and non-stationary models with differing characteristics, from samples of varying sizes. The authors note that AIC tends to perform better for small samples (sample size ¡40), whereas BIC and LRT performance is better for larger samples. The driver of this difference in performance is that AIC tends to select more complex models than BIC and LRT.

We note that many other information criteria for model selection have been proposed and are used, including minimum description length (MDL, Rissanen 1978; related to BIC), the risk inflation criterion (RIC, Foster and George 1994; with an even stronger model complexity penalty than BIC, used in high-dimensional settings), and the Hannan–Quinn Information Criterion (HQIC, Hannan and Quinn 1979; used in time series modelling).

SM1.2 GEV regression for extreme temperatures

In a non-stationary extreme value setting, generalised extreme value (GEV) regression is often used to relate variation of block maxima of some environmental variable with respect to covariates. In the current work, we apply parametric GEV regression to understand temporal changes in the distribution of annual maxima of `tas`. In related work, Kharin and Zwiers (2005) uses parametric GEV regression, with linear variation of all GEV parameters in time, to quantify non-stationarity of annual maxima of various temperature indices. The regression is estimated using L-moments and maximum likelihood, and bootstrapping employed to provide a quantification of uncertainty. The authors show that spatially-averaged parameter estimates for GEV shape and scale show little change in time, whereas increases in temperature extremes can be predominantly explained by increases in the GEV location parameter: that is, global changes in temperature extremes tend to be associated primarily with the overall shift of distribution of annual extremes towards a warmer mean climate, and with only relatively small changes in the actual shape of the extreme temperature distribution. Changes in the distribution of extreme precipitation are more intricate. Zwiers et al. (2011) also uses GEV regression, now with non-stationary GEV location only, to quantify the influence on long return period daily temperature extremes at regional scales. Kharin et al. (2013) again uses GEV regression to update the analysis of Kharin and Zwiers (2005) for CMIP5 model outputs, estimated using both L-moments and maximum likelihood. Now, GEV location and scale are assumed to vary linearly in time, but GEV shape assumed time-invariant. Kharin et al. (2018) is a further follow-up paper, comparing CMIP5 and CMIP6 return values. Li et al. (2021) examines annual extremes of daily temperature from CMIP6 models, by fitting stationary GEV

models independently to each interval of a partition of the time domain into consecutive blocks. This is done, since the authors claim that it is not possible to fit non-stationary GEV models reliably to time series of climate model output with short length; we hope that the current work demonstrates that this claim is generally not true. Abdelmoaty and Papalexiou (2023) use a mixture of model selection information criteria, including AIC, BIC and the Anderson-Darling statistic, to select models for extreme precipitation in CMIP6 projections. Models considered involve linear representations for GEV regression location and scale. No conclusions are made about the best choice of information criterion to use in their study; the output of all criteria are used for model selection, but details are not given.

SM1.3 Related literature

A number of software packages for R and other programming languages provide functionality for parametric and non-parametric GEV regression (see e.g. Belzile et al. 2023). Diop and Niang (2023) use a bootstrap procedure for variable selection in GEV regression. Phatak et al. (2010) adopt a variable selection approach first proposed by Kiiveri (2008), incorporating a prior specification favouring sparse covariate descriptions, to characterise the covariate dependence of the location parameter in a GEV regression. Faulkner et al. (2024) use BIC to select physical covariates in non-stationary extreme value models of flood frequency in England and Wales. They note however that AIC may be a useful information criterion when taking a "more nuanced view of model selection". The python software developed for the scenario-coupled parametric GEV regression analysis is available via GitHub (at Leach and Jonathan 2026).

In a semi-parametric GEV regression setting, Nasri et al. (2013) report a B-spline model for extreme U.S. rainfall. Gardini (2023) proposes the use of Bayesian P-splines to characterise the non-linear effects of covariates on GEV parameters for samples of annual maxima of river discharge. Choice of functional form for covariate dependence is achieved using a grouped horseshoe prior to encourage shrinkage of non-relevant covariates. Richards and Huser (2026) model spatio-temporal extremes of wildfires using neural networks. In the related field of non-stationary peaks over threshold modelling, there are numerous examples of non-stationary non-parametric generalised Pareto regression in the environmental and engineering literature (see e.g. Jones et al. 2016, Randell et al. 2016). More generally, Lee et al. (2015) propose the use of Bayesian measures of surprise to determine suitable thresholds for extreme value models. These quantify the level of support for the proposed extremal model and threshold, without the need to specify any model alternatives, and allow direct comparison of competing threshold candidates with different numbers of threshold exceedances. Matear and Reddy (2025) describes a tool for sample size determination in stationary GEV fitting for climate applications, to ensure that estimates of extreme quantiles are obtained with the required precision.

A number of authors have explored different aspects of Bayesian inference in a parametric GEV regression setting. For example, Friederichs and Thorarinsdottir (2012) use the method of Hoff (2009) for Bayesian covariate selection in GEV regression. Castillo-Mateo et al. (2023) note that covariate selection in GEV regression is generally challenging, and use stochastic search variable selection for the selection of atmospheric covariates in modelling annual maximum temperature series for locations in Spain using GEV regression. Auld et al. (2023) examine whether the concentration of atmospheric carbon dioxide explains variation in the distribution of annual maximum daily maximum temperature in Europe. Model selection is performed using a hold-out sample with respect to various scoring rules for probabilistic forecasts, and AIC. The authors find good agreement in optimal model choice (from five candidates, with different combinations of no trends or of linear trends in GEV location and scale) across the scoring rules and AIC. Piironen and Vehtari (2017) provides a comparison of Bayesian predictive methods for model selection.

SM2 Illustrations of regional annual maxima and minima time series

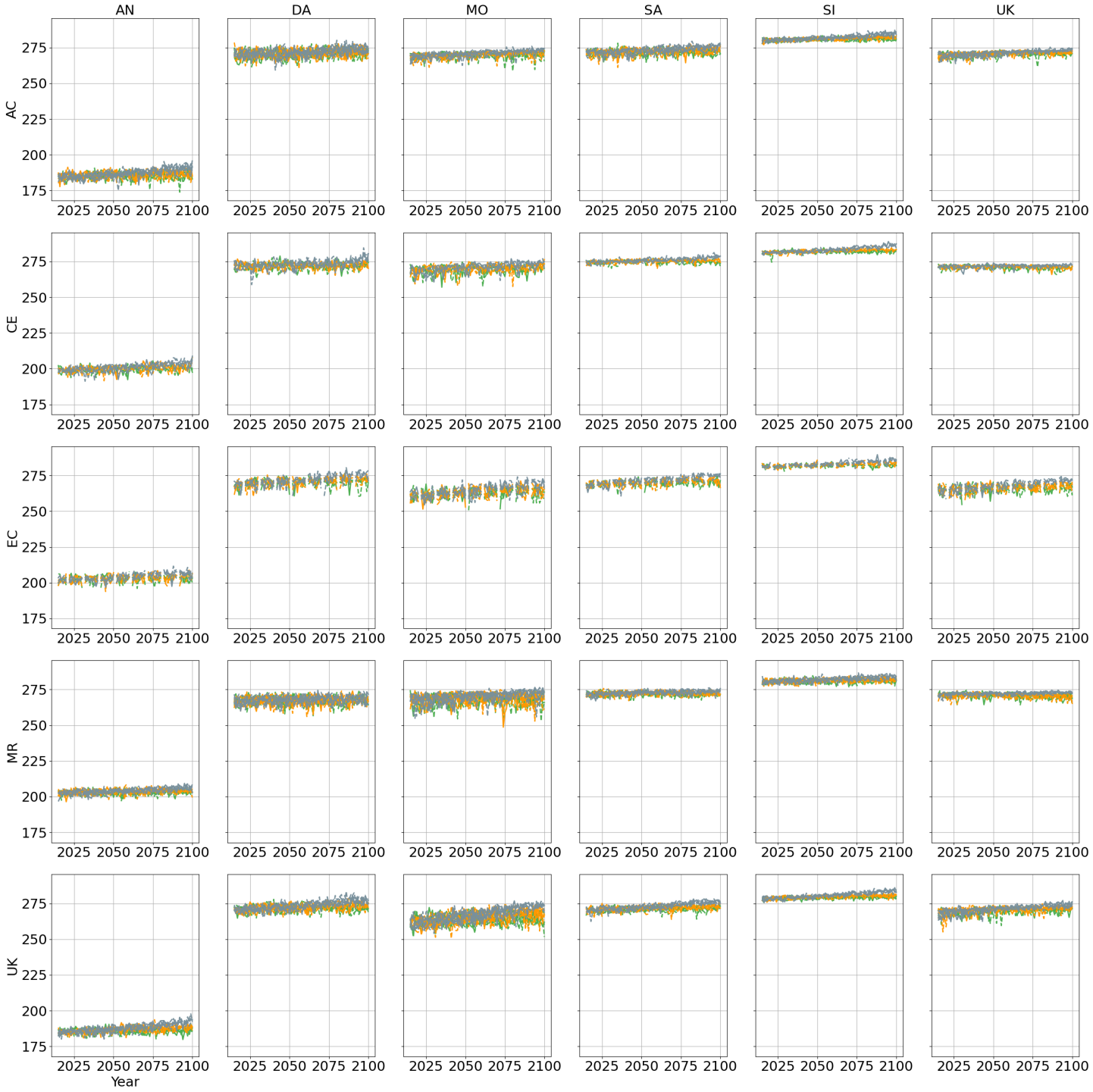

Figure SM1: Time series of regional annual minima of `tas` (K) by GCM (rows: `ACCESS-CM2`, `CESM2`, `EC-Earth3`, `MRI-ESM2-0` and `UKESM1-0-LL`) and region (column: : Antarctic, Dasht-e Lut, Mojave, Sahara, Simpson and UK). In each panel, climate scenarios are distinguished by colour: `SSP126` (green), `SSP245` (orange), `SSP245` (grey). Climate ensemble runs for each scenario are distinguished by line style. Corresponding spatial annual maxima time series are given in Figure 3 of the main text.

SM3 Bayesian inference

Inference for the GEV regression models described in Section 3.2 is performed using Markov chain Monte Carlo (MCMC, see e.g. Gamerman and Lopes 2006) following the method of Roberts and Rosenthal (2009). This procedure was reported previously in Ewans and Jonathan (2023), but is summarised here for completeness and ease of reference. All the parameters $\boldsymbol{\theta}$ of the model are jointly updated for a sequence of $n_B + n_S$ MCMC iterations. At each iteration, a new set of parameter values is proposed, and accepted according to the Metropolis-Hastings acceptance criterion based on (a) the sample likelihood evaluated at the current and candidate states, and (b) the values of the prior densities for parameters at the current and candidate states. Following n_B burn-in iterations, the Markov chain is judged to have converged, so that the subsequent n_S iterations provide a valid sample from the joint posterior distribution of parameters. Prior distributions were specified as follows: $\xi \sim U(-1, 0.2)$; $\sigma \sim U(0, \infty)$; $\mu \sim U(-\infty, \infty)$. Likelihoods for the models are available from the distributions given in the main text. An appropriate starting solution $\boldsymbol{\theta}_1$ for the MCMC inference was obtained by random sampling from the prior distributions of parameters, ensuring a valid likelihood.

For the first $n_S < n_B$ iterations, candidate parameter values $\boldsymbol{\theta}_k^c$ are proposed (independently) from $\boldsymbol{\theta}_k^c \sim N(\mathbf{0}, 0.1^2\boldsymbol{I})$ following Roberts and Rosenthal (2009). Thereafter $\boldsymbol{\theta}_k^c \sim (1-\beta)N\left(\boldsymbol{\theta}_{k-1}, 2.38^2\Sigma_k\right) + \beta N\left(\boldsymbol{\theta}_{k-1}, 0.1^2/4\right)$, where $\beta = 0.05$, Σ_k is the empirical variance-covariance matrix of parameters from the past k iterations, and $\boldsymbol{\theta}_{k-1}$ is the current value of parameters. Throughout, a candidate state is accepted using the standard Metropolis-Hastings acceptance criterion. Since prior distributions for parameters are uniform, and proposals symmetric, this criterion is effectively just a likelihood ratio. That is, we accept the candidate state with probability $\min(1, L(\boldsymbol{\theta}^c)/L(\boldsymbol{\theta}))$, where $L(\boldsymbol{\theta})$ and $L(\boldsymbol{\theta}^c)$ are the likelihoods evaluated at the current and candidate states respectively, with candidates lying outside their prior domains rejected.

SM4 Results for regional annual maxima

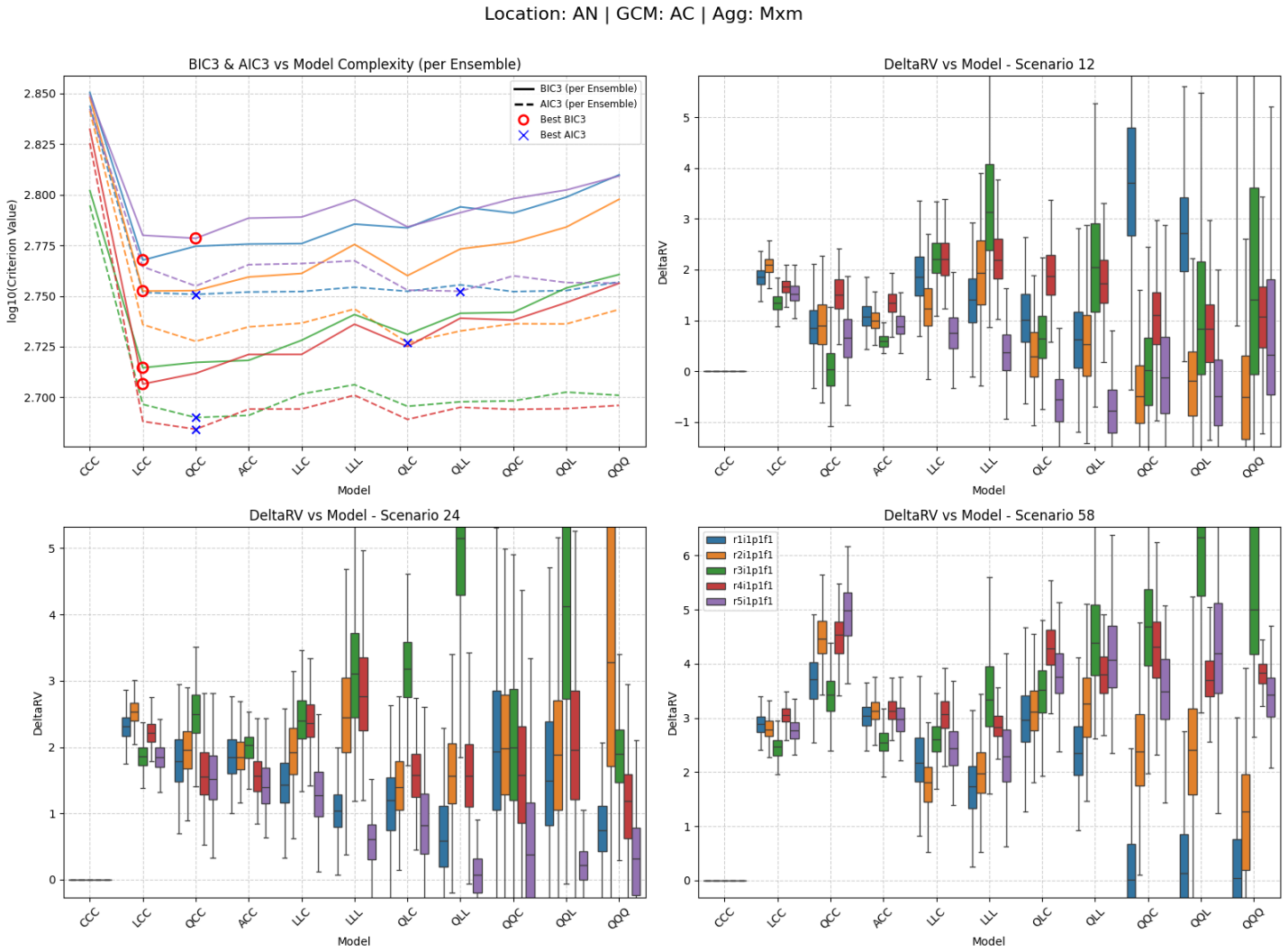

Figure SM2: Summary of scenario-coupled GEV regression for regional annual maxima of the Antarctic region using `ACCESS-CM2` GCM data. Top left: plots of BIC3 (solid line) and AIC3 (dashed line) for each available ensemble (distinguished by colour, see Table 2 of the main text and legend in bottom-right panel); optimal model choice using BIC3 (AIC3) indicated using red disc (blue cross). Top right: box-whisker plots summarising the distribution of the difference in the 100-year return value between 2025 and 2125 (ΔQ_1; see Equation 7) for climate scenario `SSP126` as a function of fitted model complexity (x-axis) and ensemble (distinguished by colour, with consistent ensemble colouring across panels); location of horizontal centre line of each box indicates posterior median of ΔQ_1; location of top (bottom) side of each box indicates 75%ile (25%ile) point, and top (bottom) of whiskers the 97.5%ile (2.5%ile) point of the posterior distribution. Bottom left and right: analogues of top right for scenarios `SSP245` (ΔQ_2) and `SSP585` (ΔQ_3). Value of ΔQ_j, $j = 1, 2, 3$ under model CCC is identically zero, and is omitted from bottom panels when convenient to provide better illustration of the variation in estimates under more complex models. For comparison with Figure 6 of the main text.

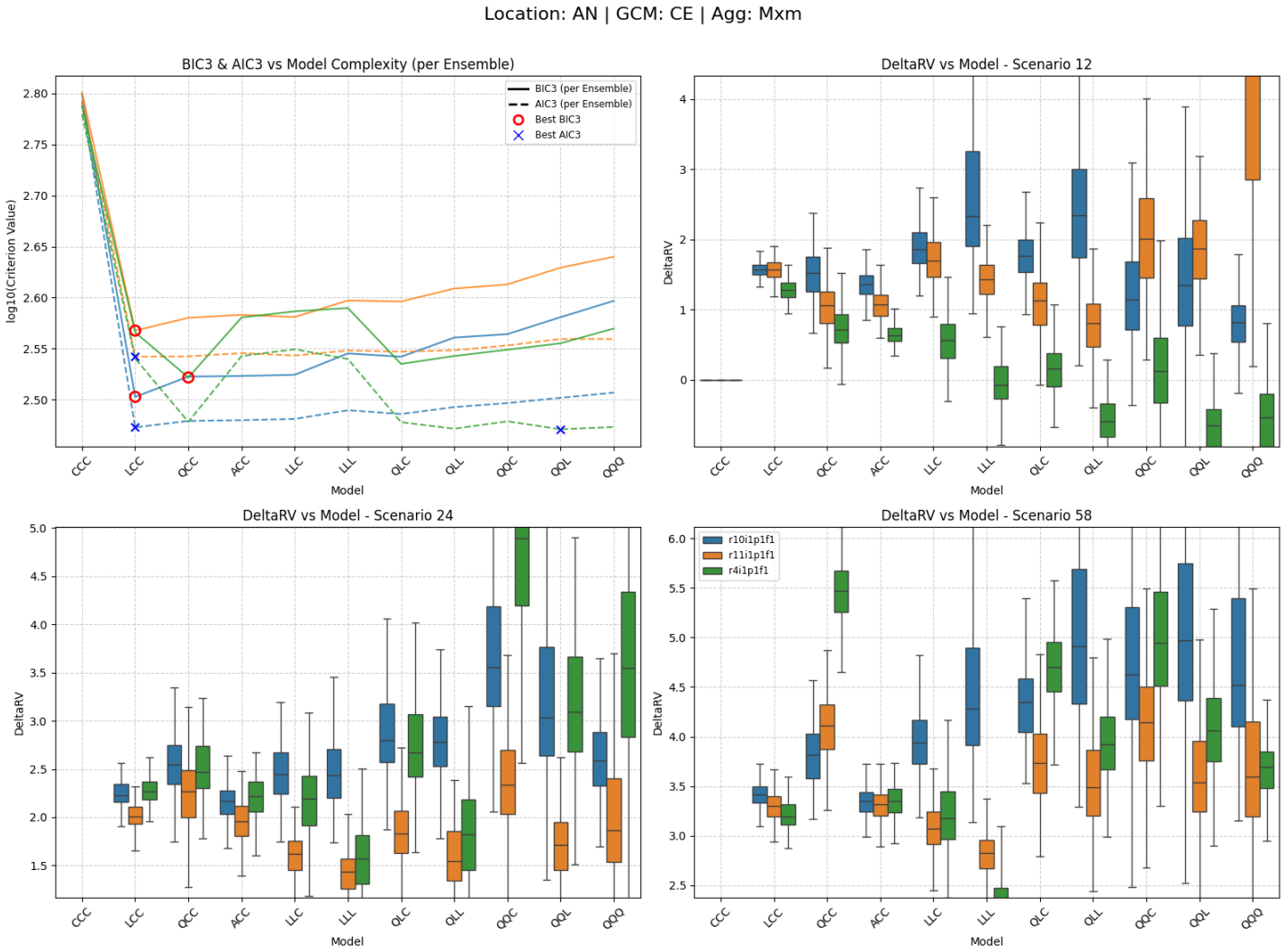

Figure SM3: Summary of scenario-coupled GEV regression for regional annual maxima of the Antarctic region using `CESM2` GCM data. Top left: plots of BIC3 (solid line) and AIC3 (dashed line) for each available ensemble (distinguished by colour, see Table 2 of the main text and legend in bottom-right panel); optimal model choice using BIC3 (AIC3) indicated using red disc (blue cross). Top right: box-whisker plots summarising the distribution of the difference in the 100-year return value between 2025 and 2125 (ΔQ_1; see Equation 7) for climate scenario `SSP126` as a function of fitted model complexity (x-axis) and ensemble (distinguished by colour, with consistent ensemble colouring across panels); location of horizontal centre line of each box indicates posterior median of ΔQ_1; location of top (bottom) side of each box indicates 75%ile (25%ile) point, and top (bottom) of whiskers the 97.5%ile (2.5%ile) point of the posterior distribution. Bottom left and right: analogues of top right for scenarios `SSP245` (ΔQ_2) and `SSP585` (ΔQ_3). Value of ΔQ_j, $j = 1, 2, 3$ under model CCC is identically zero, and is omitted from bottom panels when convenient to provide better illustration of the variation in estimates under more complex models. For comparison with Figure 6 of the main text.

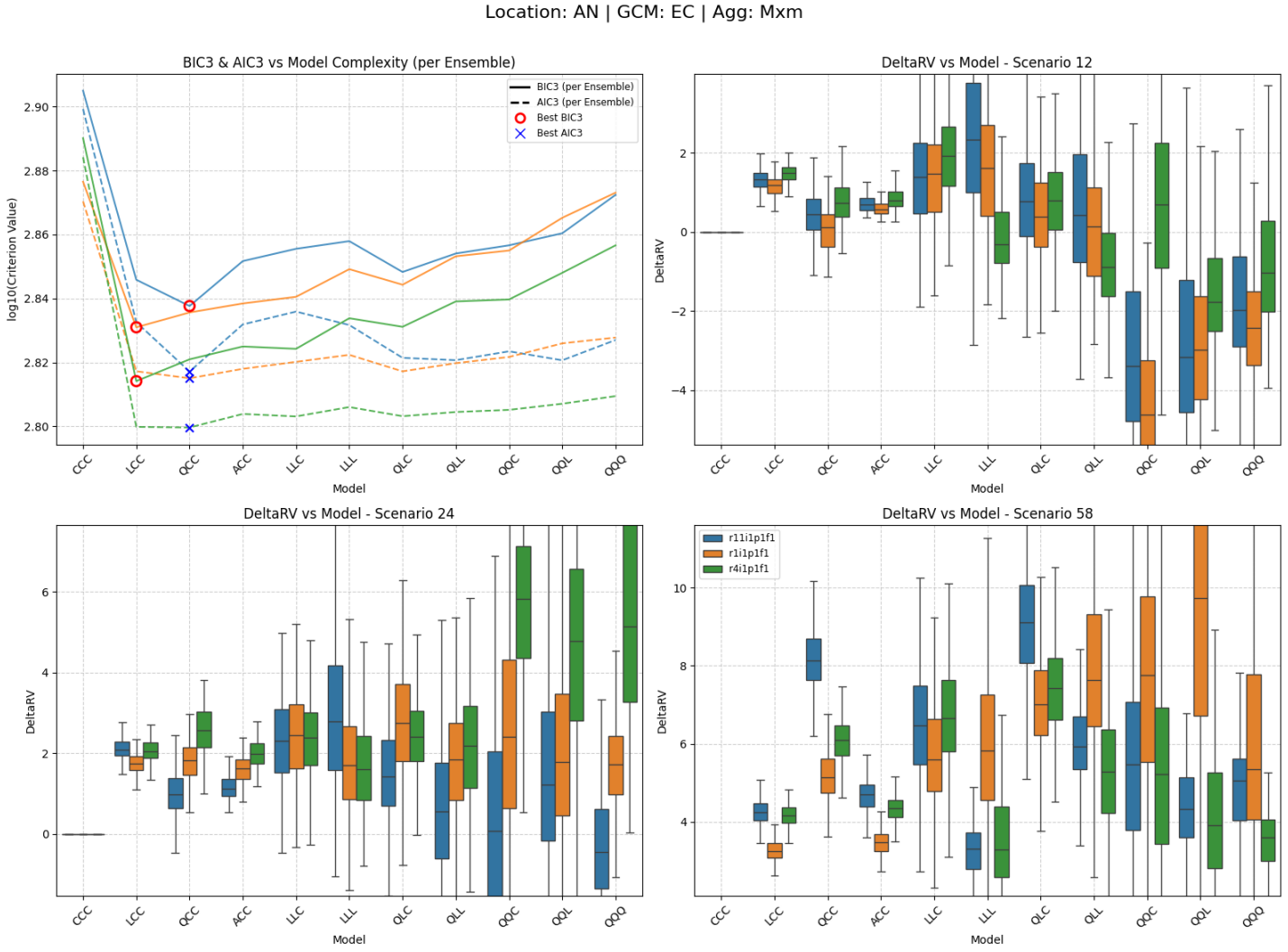

Figure SM4: Summary of scenario-coupled GEV regression for regional annual maxima of the Antarctic region using `EC-Earth3` GCM data. Top left: plots of BIC3 (solid line) and AIC3 (dashed line) for each available ensemble (distinguished by colour, see Table 2 of the main text and legend in bottom-right panel); optimal model choice using BIC3 (AIC3) indicated using red disc (blue cross). Top right: box-whisker plots summarising the distribution of the difference in the 100-year return value between 2025 and 2125 (ΔQ_1; see Equation 7) for climate scenario `SSP126` as a function of fitted model complexity (x-axis) and ensemble (distinguished by colour, with consistent ensemble colouring across panels); location of horizontal centre line of each box indicates posterior median of ΔQ_1; location of top (bottom) side of each box indicates 75%ile (25%ile) point, and top (bottom) of whiskers the 97.5%ile (2.5%ile) point of the posterior distribution. Bottom left and right: analogues of top right for scenarios `SSP245` (ΔQ_2) and `SSP585` (ΔQ_3). Value of ΔQ_j, $j = 1, 2, 3$ under model CCC is identically zero, and is omitted from bottom panels when convenient to provide better illustration of the variation in estimates under more complex models. For comparison with Figure 6 of the main text.

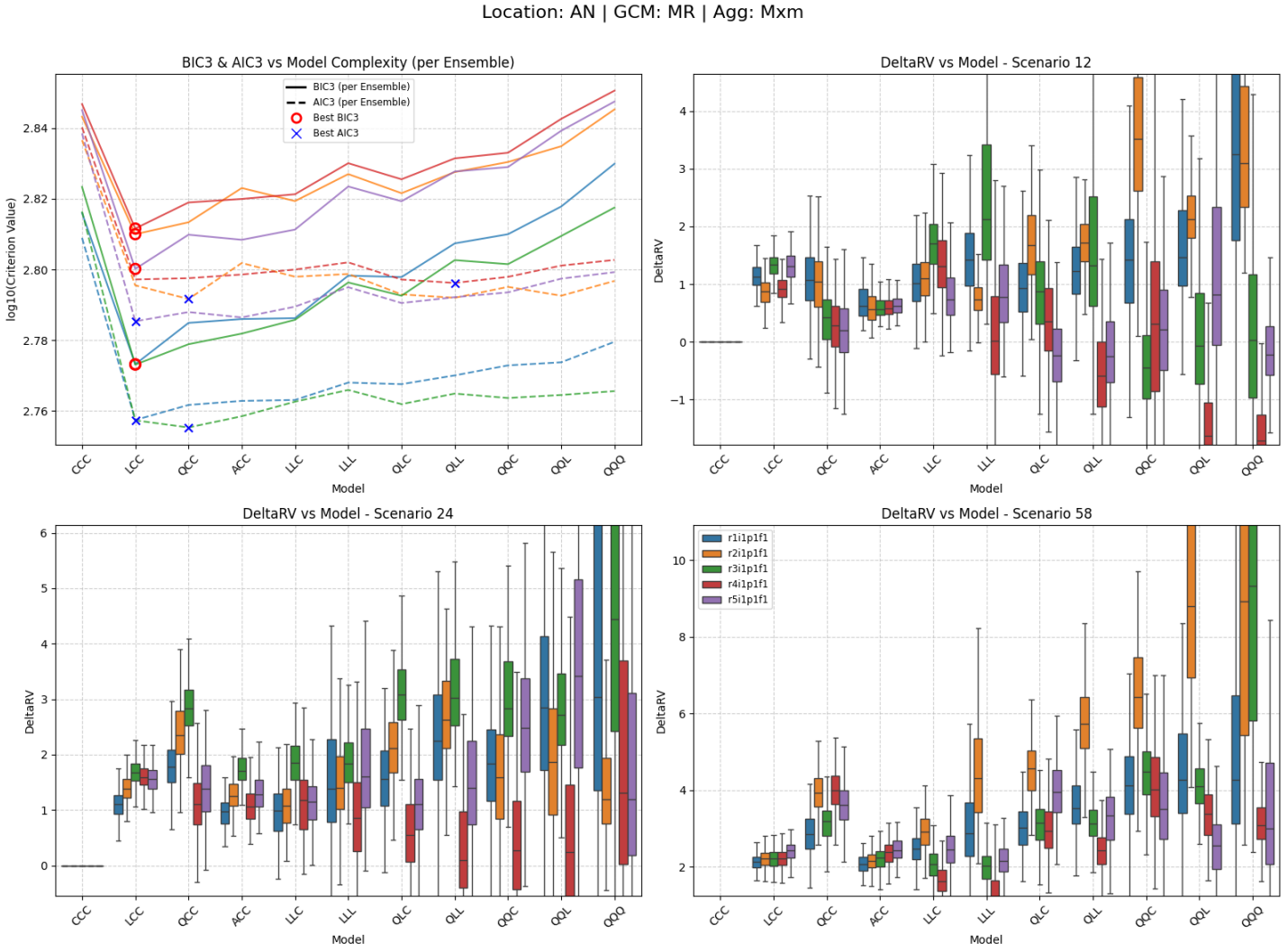

Figure SM5: Summary of scenario-coupled GEV regression for regional annual maxima of the Antarctic region using `MRI-ESM2-0` GCM data. Top left: plots of BIC3 (solid line) and AIC3 (dashed line) for each available ensemble (distinguished by colour, see Table 2 of the main text and legend in bottom-right panel); optimal model choice using BIC3 (AIC3) indicated using red disc (blue cross). Top right: box-whisker plots summarising the distribution of the difference in the 100-year return value between 2025 and 2125 (ΔQ_1; see Equation 7) for climate scenario `SSP126` as a function of fitted model complexity (x-axis) and ensemble (distinguished by colour, with consistent ensemble colouring across panels); location of horizontal centre line of each box indicates posterior median of ΔQ_1; location of top (bottom) side of each box indicates 75%ile (25%ile) point, and top (bottom) of whiskers the 97.5%ile (2.5%ile) point of the posterior distribution. Bottom left and right: analogues of top right for scenarios `SSP245` (ΔQ_2) and `SSP585` (ΔQ_3). Value of ΔQ_j, $j = 1, 2, 3$ under model CCC is identically zero, and is omitted from bottom panels when convenient to provide better illustration of the variation in estimates under more complex models. For comparison with Figure 6 of the main text.

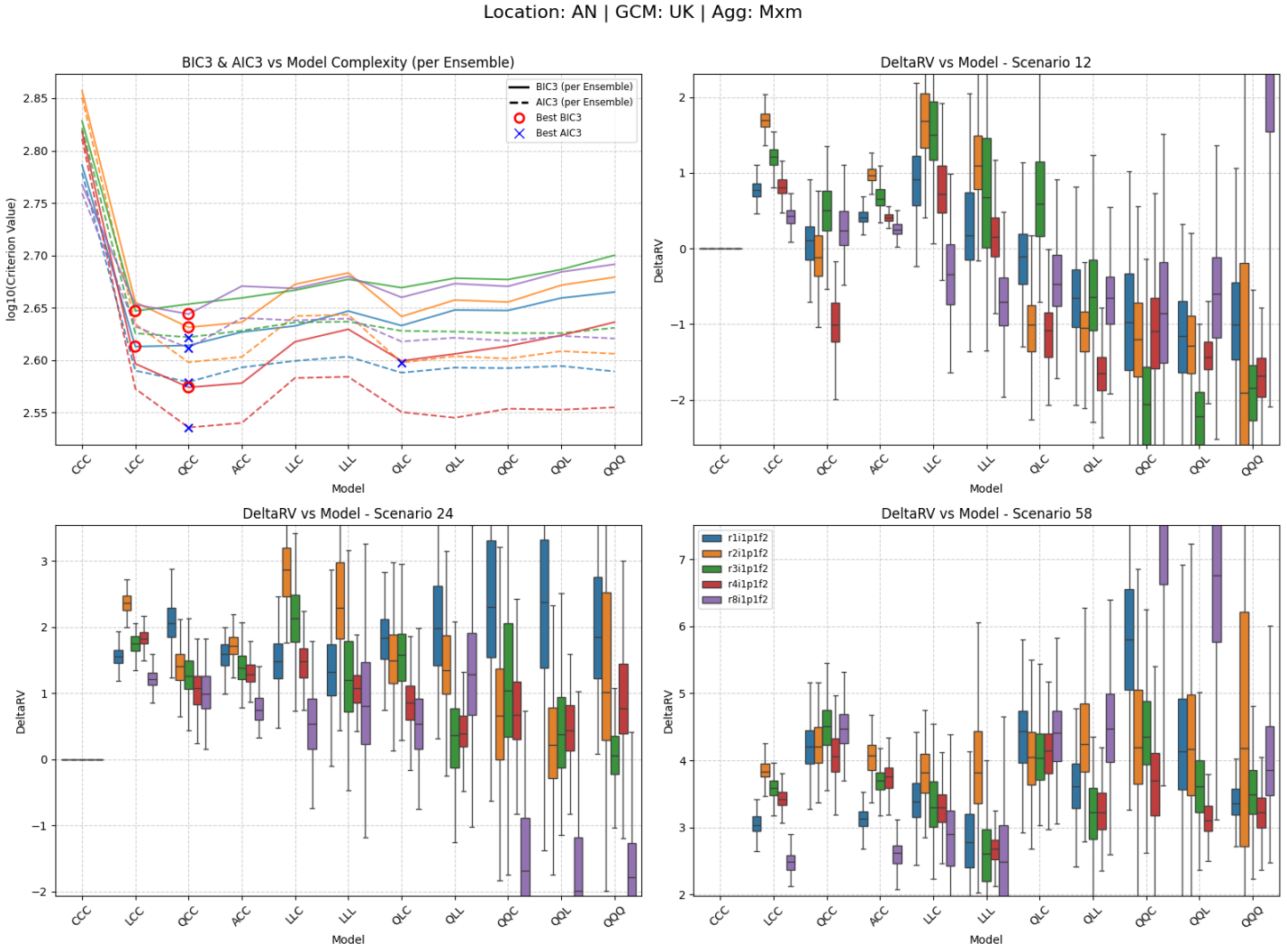

Figure SM6: Summary of scenario-coupled GEV regression for regional annual maxima of the Antarctic region using `UKESM1-0-LL` GCM data. Top left: plots of BIC3 (solid line) and AIC3 (dashed line) for each available ensemble (distinguished by colour, see Table 2 of the main text and legend in bottom-right panel); optimal model choice using BIC3 (AIC3) indicated using red disc (blue cross). Top right: box-whisker plots summarising the distribution of the difference in the 100-year return value between 2025 and 2125 (ΔQ_1; see Equation 7) for climate scenario `SSP126` as a function of fitted model complexity (x-axis) and ensemble (distinguished by colour, with consistent ensemble colouring across panels); location of horizontal centre line of each box indicates posterior median of ΔQ_1; location of top (bottom) side of each box indicates 75%ile (25%ile) point, and top (bottom) of whiskers the 97.5%ile (2.5%ile) point of the posterior distribution. Bottom left and right: analogues of top right for scenarios `SSP245` (ΔQ_2) and `SSP585` (ΔQ_3). Value of ΔQ_j, $j = 1, 2, 3$ under model CCC is identically zero, and is omitted from bottom panels when convenient to provide better illustration of the variation in estimates under more complex models. For comparison with Figure 6 of the main text.

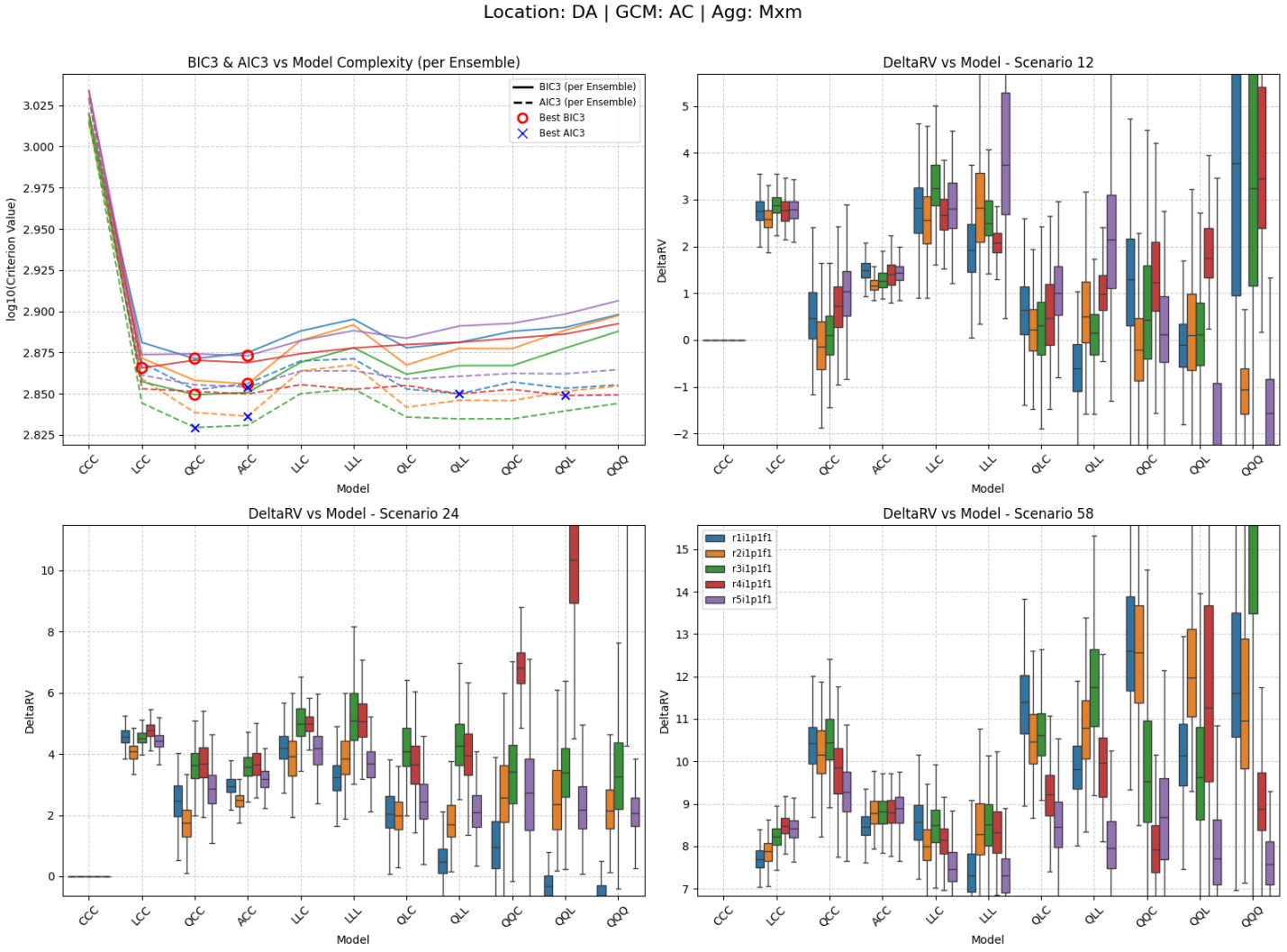

Figure SM7: Summary of scenario-coupled GEV regression for regional annual maxima of the Dasht-e Lut region using `ACCESS-CM2` GCM data. Top left: plots of BIC3 (solid line) and AIC3 (dashed line) for each available ensemble (distinguished by colour, see Table 2 of the main text and legend in bottom-right panel); optimal model choice using BIC3 (AIC3) indicated using red disc (blue cross). Top right: box-whisker plots summarising the distribution of the difference in the 100-year return value between 2025 and 2125 (ΔQ_1; see Equation 7) for climate scenario `SSP126` as a function of fitted model complexity (x-axis) and ensemble (distinguished by colour, with consistent ensemble colouring across panels); location of horizontal centre line of each box indicates posterior median of ΔQ_1; location of top (bottom) side of each box indicates 75%ile (25%ile) point, and top (bottom) of whiskers the 97.5%ile (2.5%ile) point of the posterior distribution. Bottom left and right: analogues of top right for scenarios `SSP245` (ΔQ_2) and `SSP585` (ΔQ_3). Value of ΔQ_j, $j = 1, 2, 3$ under model CCC is identically zero, and is omitted from bottom panels when convenient to provide better illustration of the variation in estimates under more complex models. For comparison with Figure 6 of the main text.

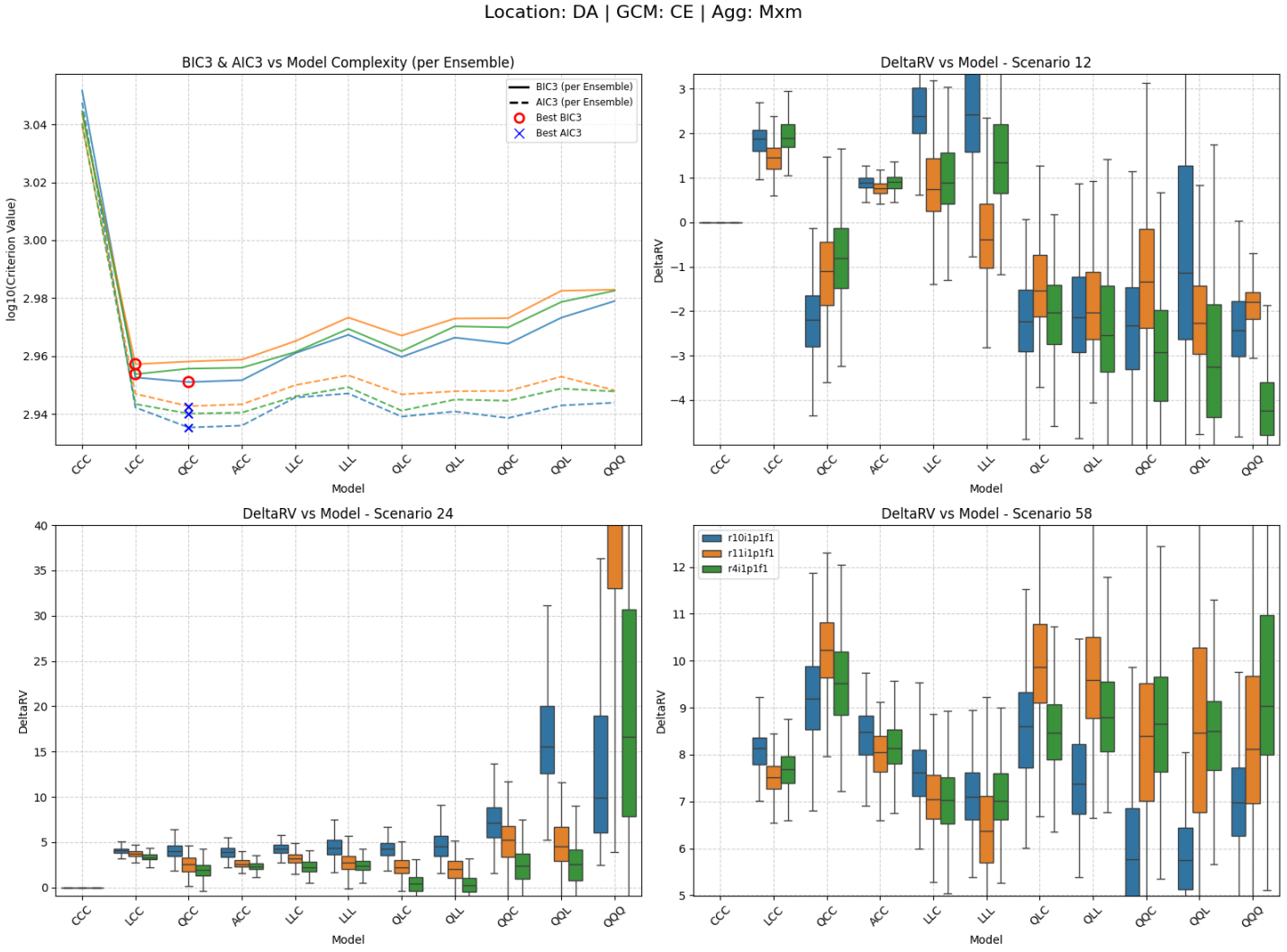

Figure SM8: Summary of scenario-coupled GEV regression for regional annual maxima of the Dasht-e Lut region using `CESM2` GCM data. Top left: plots of BIC3 (solid line) and AIC3 (dashed line) for each available ensemble (distinguished by colour, see Table 2 of the main text and legend in bottom-right panel); optimal model choice using BIC3 (AIC3) indicated using red disc (blue cross). Top right: box-whisker plots summarising the distribution of the difference in the 100-year return value between 2025 and 2125 (ΔQ_1; see Equation 7) for climate scenario `SSP126` as a function of fitted model complexity (x-axis) and ensemble (distinguished by colour, with consistent ensemble colouring across panels); location of horizontal centre line of each box indicates posterior median of ΔQ_1; location of top (bottom) side of each box indicates 75%ile (25%ile) point, and top (bottom) of whiskers the 97.5%ile (2.5%ile) point of the posterior distribution. Bottom left and right: analogues of top right for scenarios `SSP245` (ΔQ_2) and `SSP585` (ΔQ_3). Value of ΔQ_j, $j = 1, 2, 3$ under model CCC is identically zero, and is omitted from bottom panels when convenient to provide better illustration of the variation in estimates under more complex models. For comparison with Figure 6 of the main text.

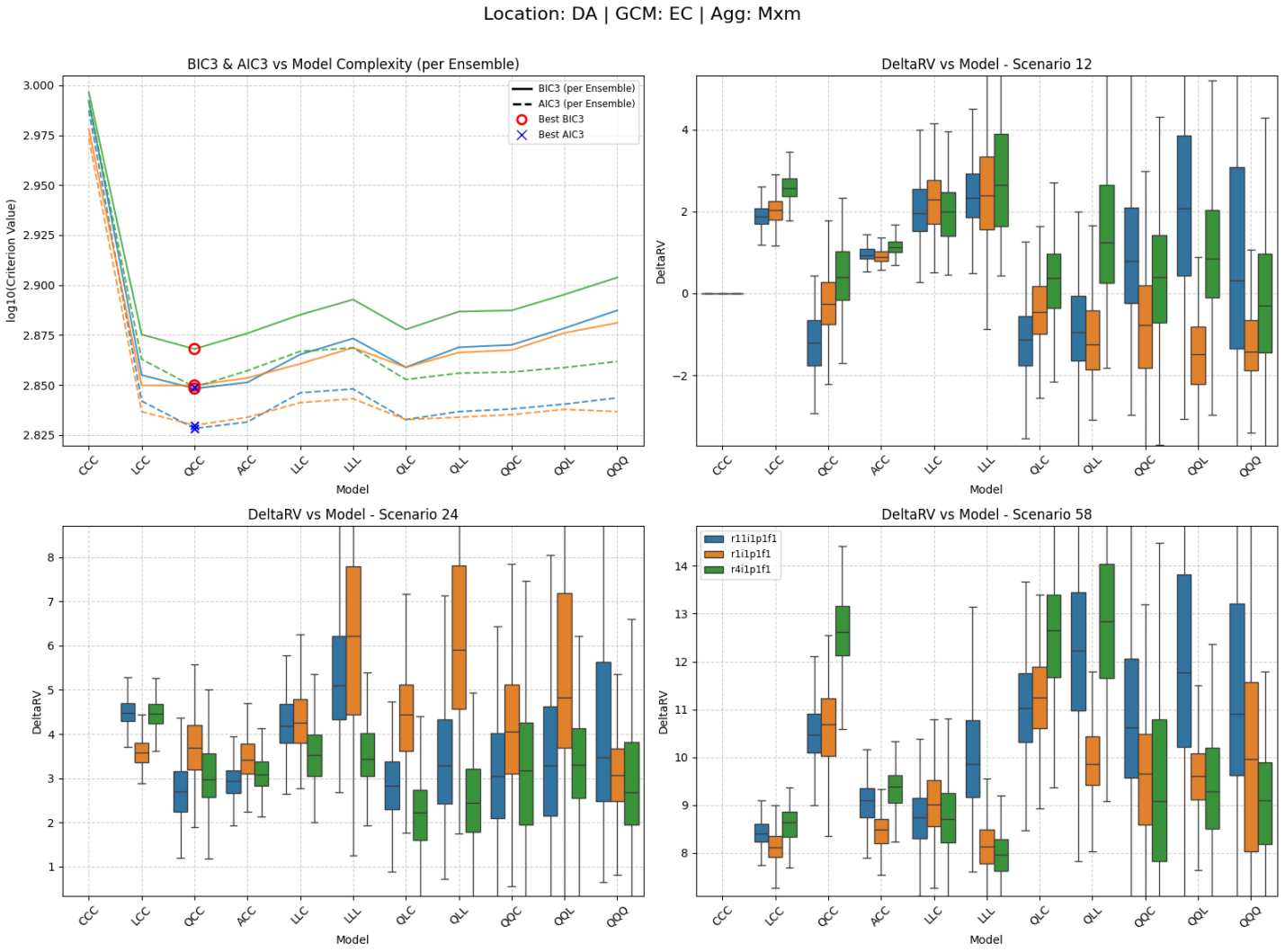

Figure SM9: Summary of scenario-coupled GEV regression for regional annual maxima of the Dasht-e Lut region using `EC-Earth3` GCM data. Top left: plots of BIC3 (solid line) and AIC3 (dashed line) for each available ensemble (distinguished by colour, see Table 2 of the main text and legend in bottom-right panel); optimal model choice using BIC3 (AIC3) indicated using red disc (blue cross). Top right: box-whisker plots summarising the distribution of the difference in the 100-year return value between 2025 and 2125 (ΔQ_1; see Equation 7) for climate scenario `SSP126` as a function of fitted model complexity (x-axis) and ensemble (distinguished by colour, with consistent ensemble colouring across panels); location of horizontal centre line of each box indicates posterior median of ΔQ_1; location of top (bottom) side of each box indicates 75%ile (25%ile) point, and top (bottom) of whiskers the 97.5%ile (2.5%ile) point of the posterior distribution. Bottom left and right: analogues of top right for scenarios `SSP245` (ΔQ_2) and `SSP585` (ΔQ_3). Value of ΔQ_j, $j = 1, 2, 3$ under model CCC is identically zero, and is omitted from bottom panels when convenient to provide better illustration of the variation in estimates under more complex models. For comparison with Figure 6 of the main text.

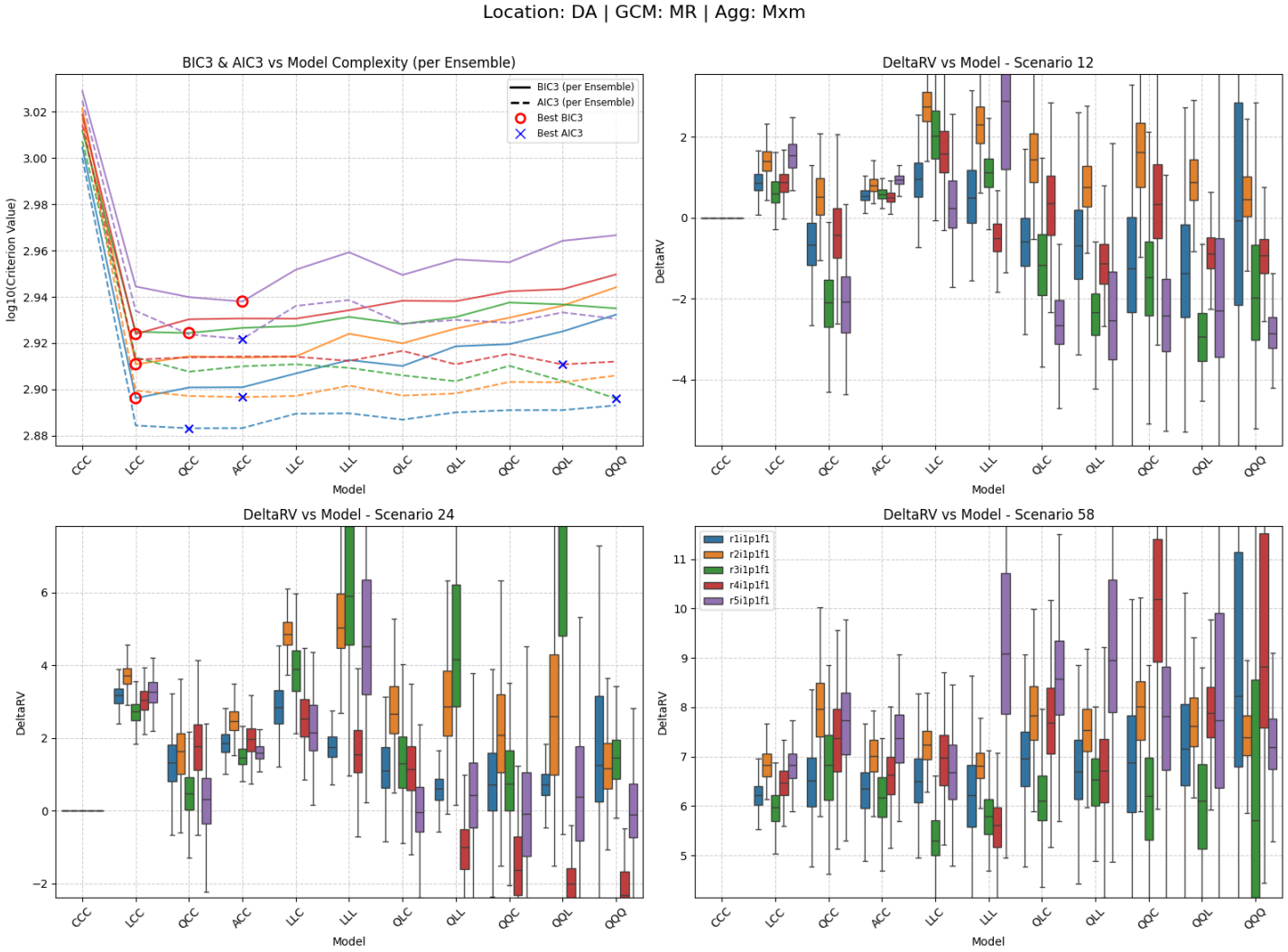

Figure SM10: Summary of scenario-coupled GEV regression for regional annual maxima of the Dasht-e Lut region using `MRI-ESM2-0` GCM data. Top left: plots of BIC3 (solid line) and AIC3 (dashed line) for each available ensemble (distinguished by colour, see Table 2 of the main text and legend in bottom-right panel); optimal model choice using BIC3 (AIC3) indicated using red disc (blue cross). Top right: box-whisker plots summarising the distribution of the difference in the 100-year return value between 2025 and 2125 (ΔQ_1; see Equation 7) for climate scenario `SSP126` as a function of fitted model complexity (x-axis) and ensemble (distinguished by colour, with consistent ensemble colouring across panels); location of horizontal centre line of each box indicates posterior median of ΔQ_1; location of top (bottom) side of each box indicates 75%ile (25%ile) point, and top (bottom) of whiskers the 97.5%ile (2.5%ile) point of the posterior distribution. Bottom left and right: analogues of top right for scenarios `SSP245` (ΔQ_2) and `SSP585` (ΔQ_3). Value of ΔQ_j, $j = 1, 2, 3$ under model CCC is identically zero, and is omitted from bottom panels when convenient to provide better illustration of the variation in estimates under more complex models. For comparison with Figure 6 of the main text.

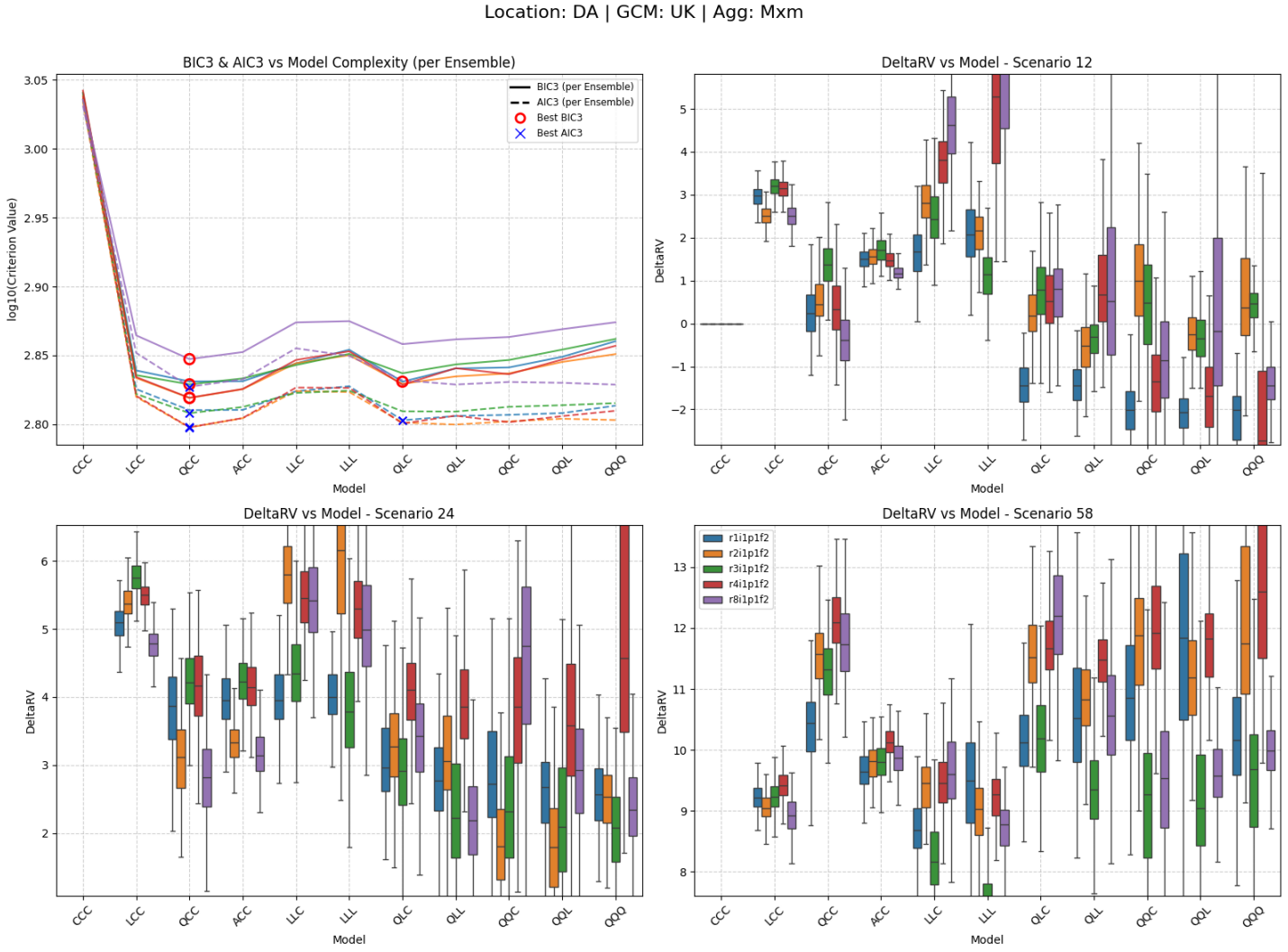

Figure SM11: Summary of scenario-coupled GEV regression for regional annual maxima of the Dasht-e Lut region using `UKESM1-0-LL` GCM data. Top left: plots of BIC3 (solid line) and AIC3 (dashed line) for each available ensemble (distinguished by colour, see Table 2 of the main text and legend in bottom-right panel); optimal model choice using BIC3 (AIC3) indicated using red disc (blue cross). Top right: box-whisker plots summarising the distribution of the difference in the 100-year return value between 2025 and 2125 (ΔQ_1; see Equation 7) for climate scenario `SSP126` as a function of fitted model complexity (x-axis) and ensemble (distinguished by colour, with consistent ensemble colouring across panels); location of horizontal centre line of each box indicates posterior median of ΔQ_1; location of top (bottom) side of each box indicates 75%ile (25%ile) point, and top (bottom) of whiskers the 97.5%ile (2.5%ile) point of the posterior distribution. Bottom left and right: analogues of top right for scenarios `SSP245` (ΔQ_2) and `SSP585` (ΔQ_3). Value of ΔQ_j, $j = 1, 2, 3$ under model CCC is identically zero, and is omitted from bottom panels when convenient to provide better illustration of the variation in estimates under more complex models. For comparison with Figure 6 of the main text.

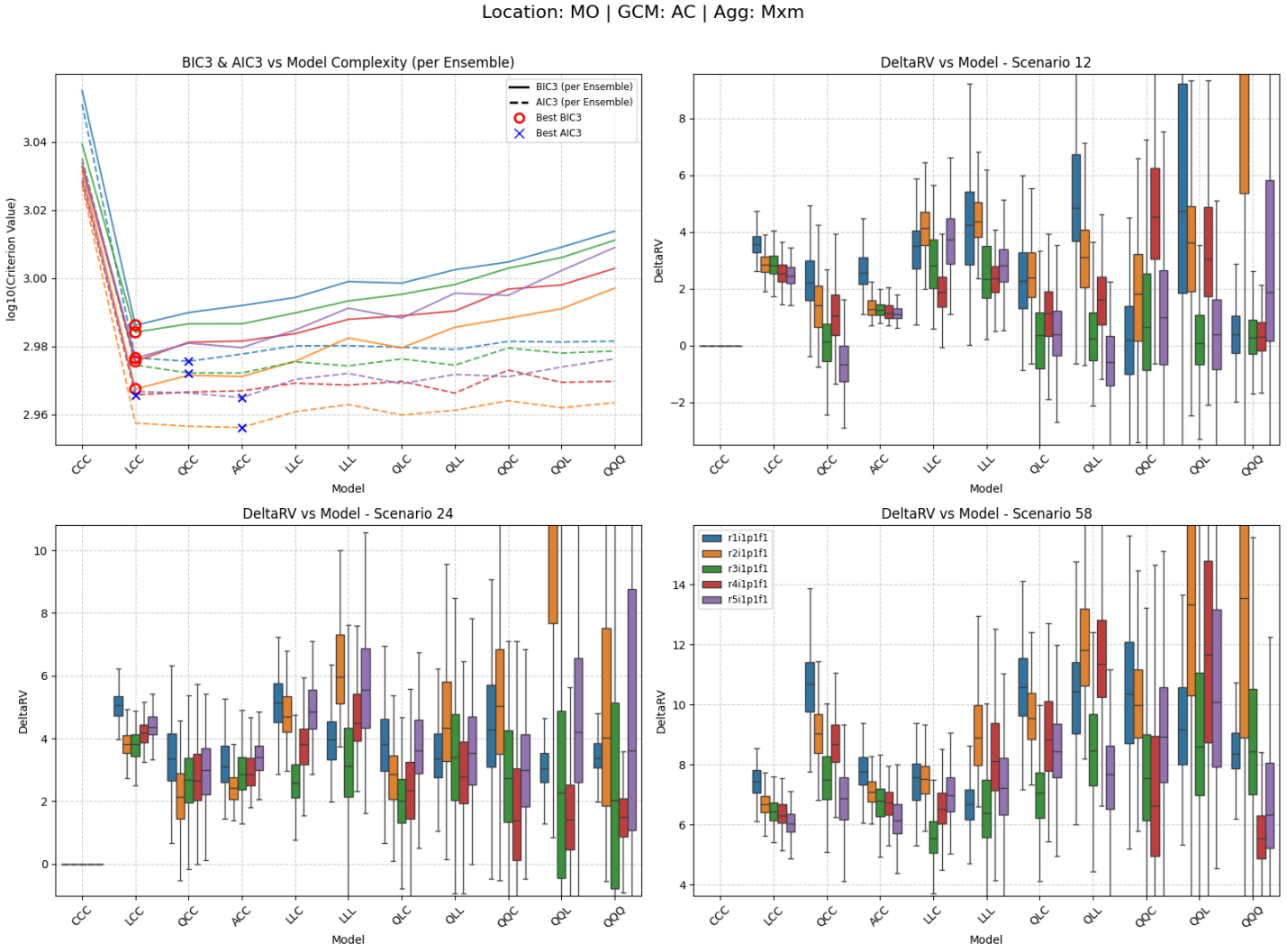

Figure SM12: Summary of scenario-coupled GEV regression for regional annual maxima of the Mojave region using `ACCESS-CM2` GCM data. Top left: plots of BIC3 (solid line) and AIC3 (dashed line) for each available ensemble (distinguished by colour, see Table 2 of the main text and legend in bottom-right panel); optimal model choice using BIC3 (AIC3) indicated using red disc (blue cross). Top right: box-whisker plots summarising the distribution of the difference in the 100-year return value between 2025 and 2125 (ΔQ_1; see Equation 7) for climate scenario `SSP126` as a function of fitted model complexity (x-axis) and ensemble (distinguished by colour, with consistent ensemble colouring across panels); location of horizontal centre line of each box indicates posterior median of ΔQ_1; location of top (bottom) side of each box indicates 75%ile (25%ile) point, and top (bottom) of whiskers the 97.5%ile (2.5%ile) point of the posterior distribution. Bottom left and right: analogues of top right for scenarios `SSP245` (ΔQ_2) and `SSP585` (ΔQ_3). Value of ΔQ_j, $j = 1, 2, 3$ under model CCC is identically zero, and is omitted from bottom panels when convenient to provide better illustration of the variation in estimates under more complex models. For comparison with Figure 6 of the main text.

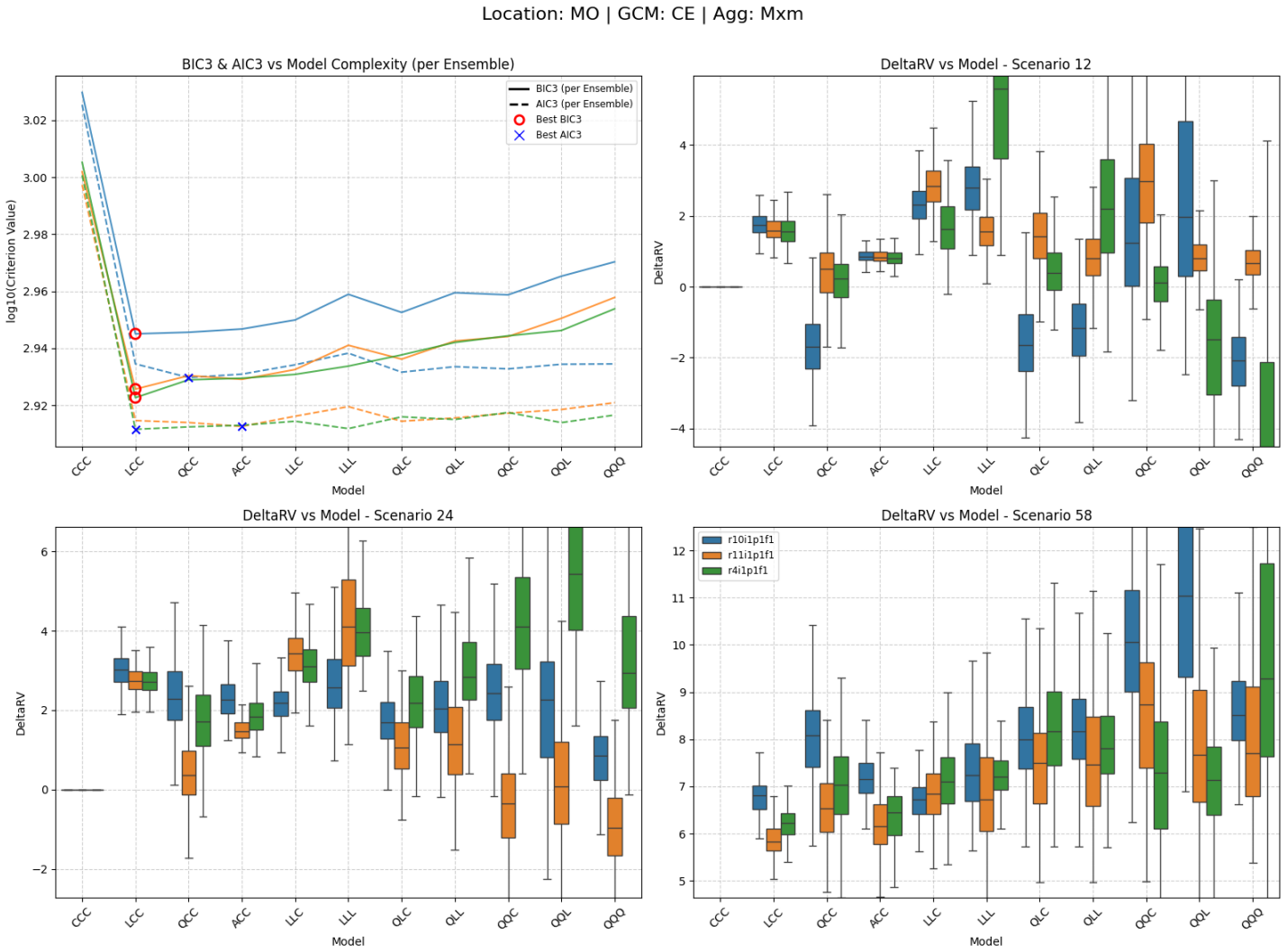

Figure SM13: Summary of scenario-coupled GEV regression for regional annual maxima of the Mojave region using `CESM2` GCM data. Top left: plots of BIC3 (solid line) and AIC3 (dashed line) for each available ensemble (distinguished by colour, see Table 2 of the main text and legend in bottom-right panel); optimal model choice using BIC3 (AIC3) indicated using red disc (blue cross). Top right: box-whisker plots summarising the distribution of the difference in the 100-year return value between 2025 and 2125 (ΔQ_1; see Equation 7) for climate scenario `SSP126` as a function of fitted model complexity (x-axis) and ensemble (distinguished by colour, with consistent ensemble colouring across panels); location of horizontal centre line of each box indicates posterior median of ΔQ_1; location of top (bottom) side of each box indicates 75%ile (25%ile) point, and top (bottom) of whiskers the 97.5%ile (2.5%ile) point of the posterior distribution. Bottom left and right: analogues of top right for scenarios `SSP245` (ΔQ_2) and `SSP585` (ΔQ_3). Value of ΔQ_j, $j = 1, 2, 3$ under model CCC is identically zero, and is omitted from bottom panels when convenient to provide better illustration of the variation in estimates under more complex models. For comparison with Figure 6 of the main text.

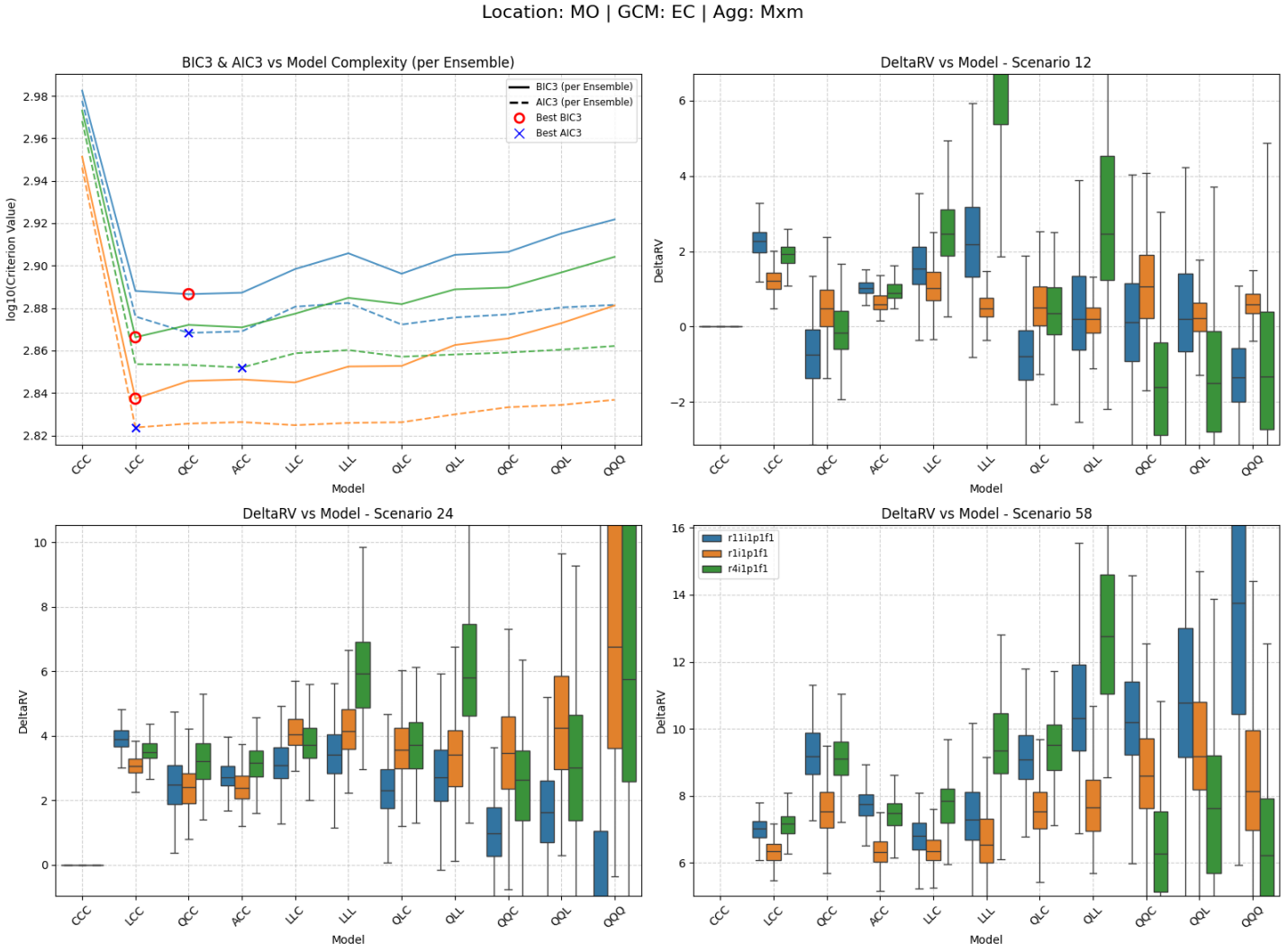

Figure SM14: Summary of scenario-coupled GEV regression for regional annual maxima of the Mojave region using `EC-Earth3` GCM data. Top left: plots of BIC3 (solid line) and AIC3 (dashed line) for each available ensemble (distinguished by colour, see Table 2 of the main text and legend in bottom-right panel); optimal model choice using BIC3 (AIC3) indicated using red disc (blue cross). Top right: box-whisker plots summarising the distribution of the difference in the 100-year return value between 2025 and 2125 (ΔQ_1; see Equation 7) for climate scenario `SSP126` as a function of fitted model complexity (x-axis) and ensemble (distinguished by colour, with consistent ensemble colouring across panels); location of horizontal centre line of each box indicates posterior median of ΔQ_1; location of top (bottom) side of each box indicates 75%ile (25%ile) point, and top (bottom) of whiskers the 97.5%ile (2.5%ile) point of the posterior distribution. Bottom left and right: analogues of top right for scenarios `SSP245` (ΔQ_2) and `SSP585` (ΔQ_3). Value of ΔQ_j, $j = 1, 2, 3$ under model CCC is identically zero, and is omitted from bottom panels when convenient to provide better illustration of the variation in estimates under more complex models. For comparison with Figure 6 of the main text.

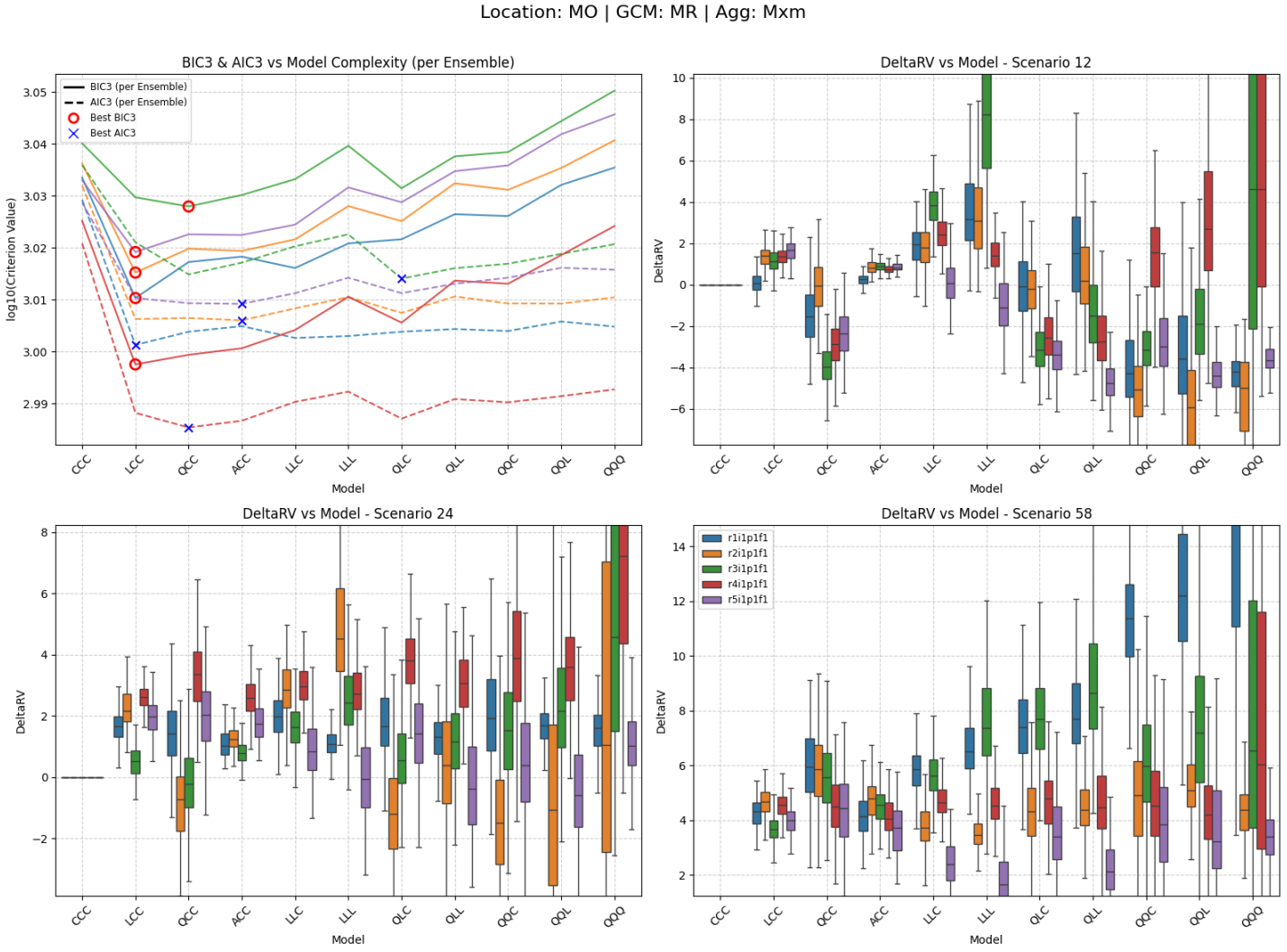

Figure SM15: Summary of scenario-coupled GEV regression for regional annual maxima of the Mojave region using `MRI-ESM2-0` GCM data. Top left: plots of BIC3 (solid line) and AIC3 (dashed line) for each available ensemble (distinguished by colour, see Table 2 of the main text and legend in bottom-right panel); optimal model choice using BIC3 (AIC3) indicated using red disc (blue cross). Top right: box-whisker plots summarising the distribution of the difference in the 100-year return value between 2025 and 2125 (ΔQ_1; see Equation 7) for climate scenario `SSP126` as a function of fitted model complexity (x-axis) and ensemble (distinguished by colour, with consistent ensemble colouring across panels); location of horizontal centre line of each box indicates posterior median of ΔQ_1; location of top (bottom) side of each box indicates 75%ile (25%ile) point, and top (bottom) of whiskers the 97.5%ile (2.5%ile) point of the posterior distribution. Bottom left and right: analogues of top right for scenarios `SSP245` (ΔQ_2) and `SSP585` (ΔQ_3). Value of ΔQ_j, $j = 1, 2, 3$ under model CCC is identically zero, and is omitted from bottom panels when convenient to provide better illustration of the variation in estimates under more complex models. For comparison with Figure 6 of the main text.

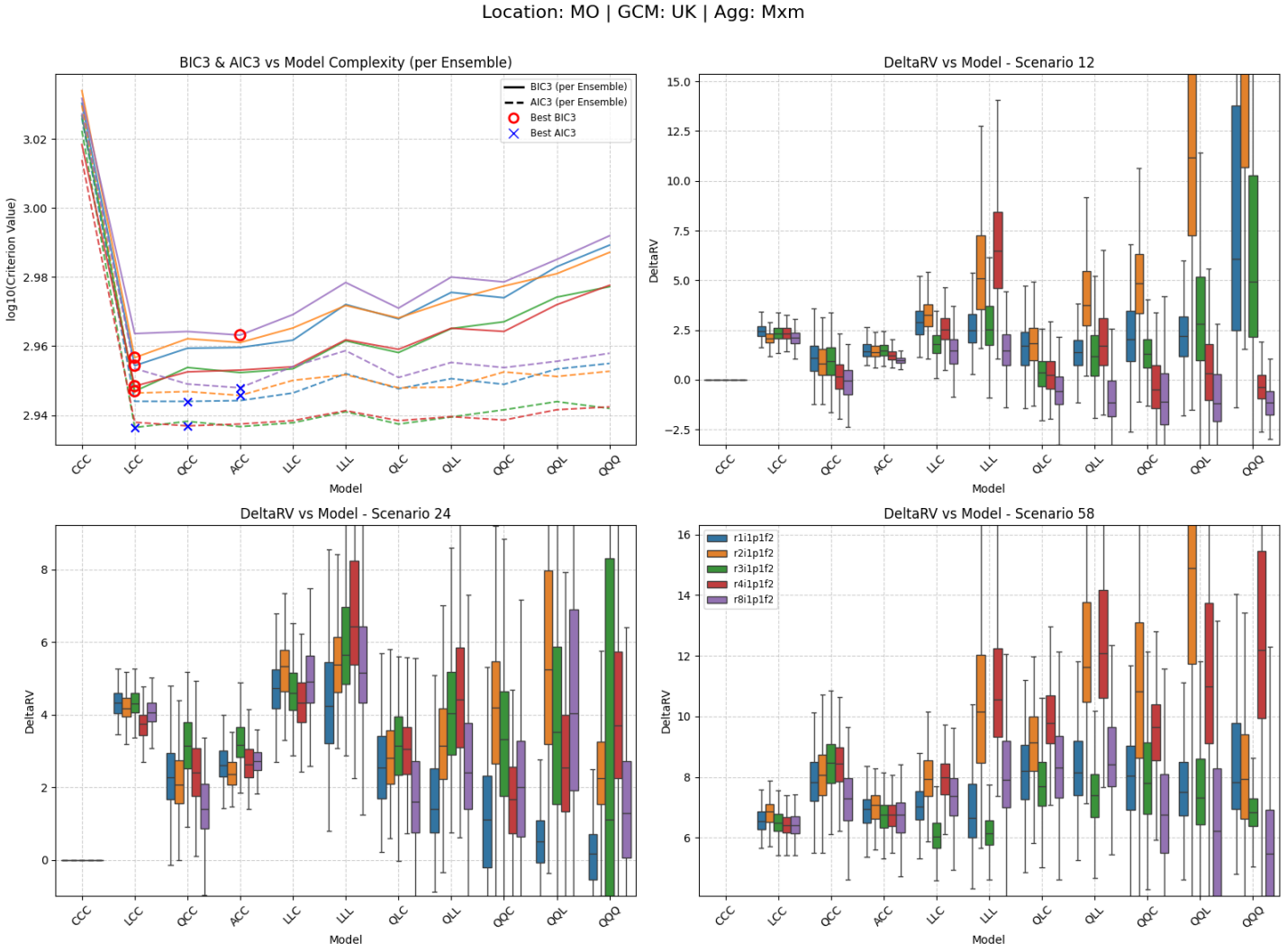

Figure SM16: Summary of scenario-coupled GEV regression for regional annual maxima of the Mojave region using `UKESM1-0-LL` GCM data. Top left: plots of BIC3 (solid line) and AIC3 (dashed line) for each available ensemble (distinguished by colour, see Table 2 of the main text and legend in bottom-right panel); optimal model choice using BIC3 (AIC3) indicated using red disc (blue cross). Top right: box-whisker plots summarising the distribution of the difference in the 100-year return value between 2025 and 2125 (ΔQ_1; see Equation 7) for climate scenario `SSP126` as a function of fitted model complexity (x-axis) and ensemble (distinguished by colour, with consistent ensemble colouring across panels); location of horizontal centre line of each box indicates posterior median of ΔQ_1; location of top (bottom) side of each box indicates 75%ile (25%ile) point, and top (bottom) of whiskers the 97.5%ile (2.5%ile) point of the posterior distribution. Bottom left and right: analogues of top right for scenarios `SSP245` (ΔQ_2) and `SSP585` (ΔQ_3). Value of ΔQ_j, $j = 1, 2, 3$ under model CCC is identically zero, and is omitted from bottom panels when convenient to provide better illustration of the variation in estimates under more complex models. For comparison with Figure 6 of the main text.

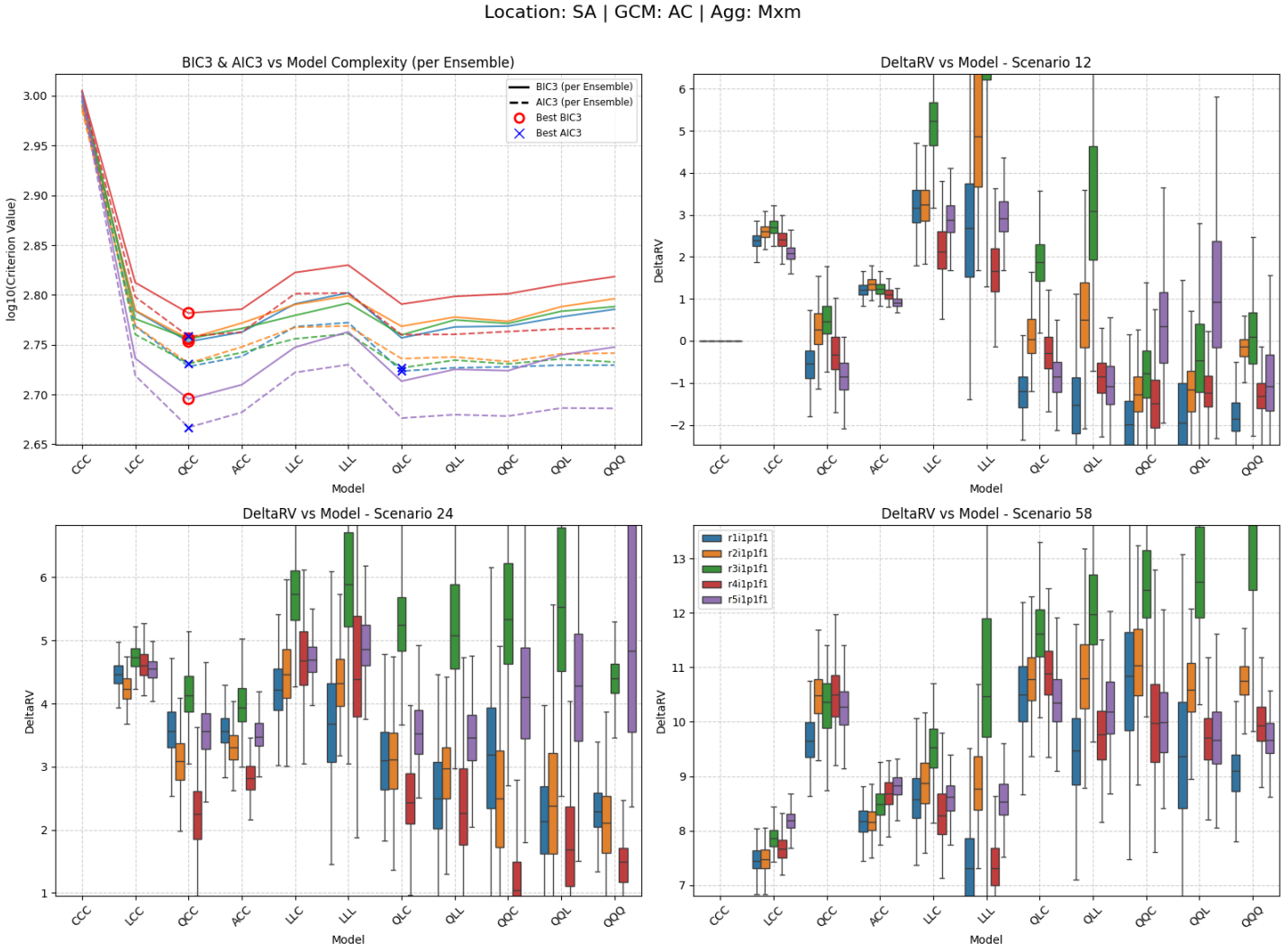

Figure SM17: Summary of scenario-coupled GEV regression for regional annual maxima of the Sahara region using `ACCESS-CM2` GCM data. Top left: plots of BIC3 (solid line) and AIC3 (dashed line) for each available ensemble (distinguished by colour, see Table 2 of the main text and legend in bottom-right panel); optimal model choice using BIC3 (AIC3) indicated using red disc (blue cross). Top right: box-whisker plots summarising the distribution of the difference in the 100-year return value between 2025 and 2125 (ΔQ_1; see Equation 7) for climate scenario `SSP126` as a function of fitted model complexity (x-axis) and ensemble (distinguished by colour, with consistent ensemble colouring across panels); location of horizontal centre line of each box indicates posterior median of ΔQ_1; location of top (bottom) side of each box indicates 75%ile (25%ile) point, and top (bottom) of whiskers the 97.5%ile (2.5%ile) point of the posterior distribution. Bottom left and right: analogues of top right for scenarios `SSP245` (ΔQ_2) and `SSP585` (ΔQ_3). Value of ΔQ_j, $j = 1, 2, 3$ under model CCC is identically zero, and is omitted from bottom panels when convenient to provide better illustration of the variation in estimates under more complex models. For comparison with Figure 6 of the main text.

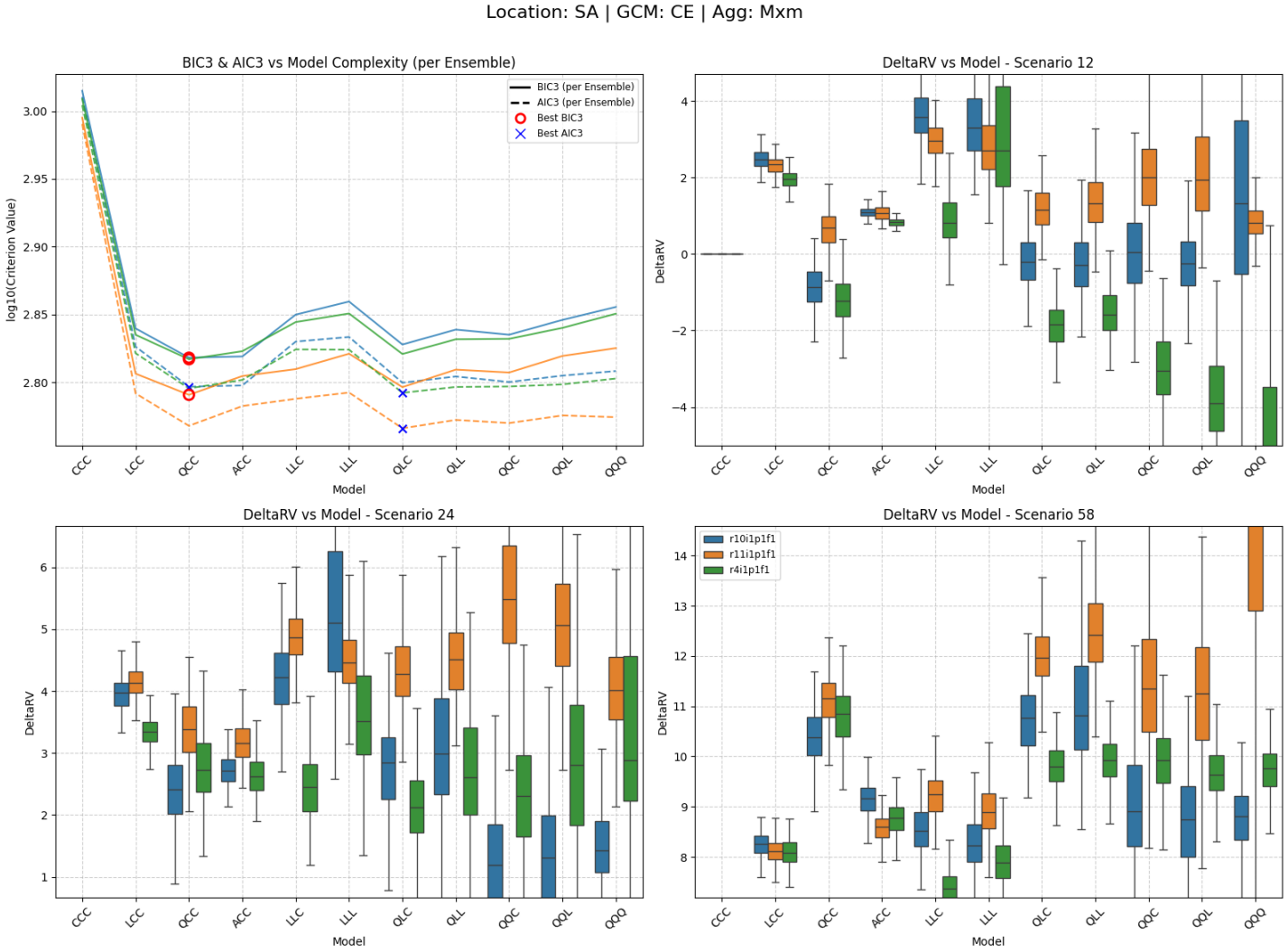

Figure SM18: Summary of scenario-coupled GEV regression for regional annual maxima of the Sahara region using `CESM2` GCM data. Top left: plots of BIC3 (solid line) and AIC3 (dashed line) for each available ensemble (distinguished by colour, see Table 2 of the main text and legend in bottom-right panel); optimal model choice using BIC3 (AIC3) indicated using red disc (blue cross). Top right: box-whisker plots summarising the distribution of the difference in the 100-year return value between 2025 and 2125 (ΔQ_1; see Equation 7) for climate scenario `SSP126` as a function of fitted model complexity (x-axis) and ensemble (distinguished by colour, with consistent ensemble colouring across panels); location of horizontal centre line of each box indicates posterior median of ΔQ_1; location of top (bottom) side of each box indicates 75%ile (25%ile) point, and top (bottom) of whiskers the 97.5%ile (2.5%ile) point of the posterior distribution. Bottom left and right: analogues of top right for scenarios `SSP245` (ΔQ_2) and `SSP585` (ΔQ_3). Value of ΔQ_j, $j = 1, 2, 3$ under model CCC is identically zero, and is omitted from bottom panels when convenient to provide better illustration of the variation in estimates under more complex models. For comparison with Figure 6 of the main text.

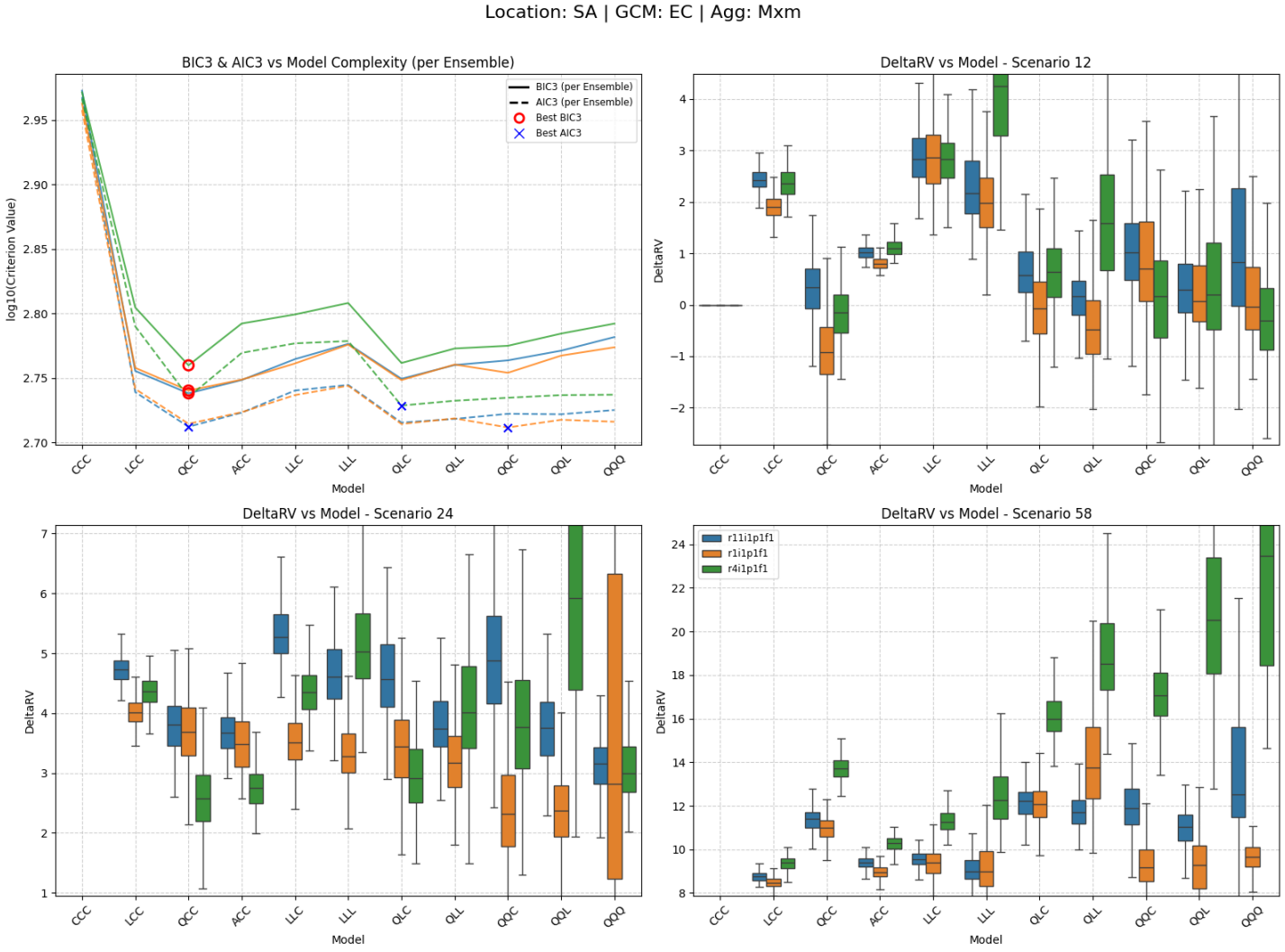

Figure SM19: Summary of scenario-coupled GEV regression for regional annual maxima of the Sahara region using `EC-Earth3` GCM data. Top left: plots of BIC3 (solid line) and AIC3 (dashed line) for each available ensemble (distinguished by colour, see Table 2 of the main text and legend in bottom-right panel); optimal model choice using BIC3 (AIC3) indicated using red disc (blue cross). Top right: box-whisker plots summarising the distribution of the difference in the 100-year return value between 2025 and 2125 (ΔQ_1; see Equation 7) for climate scenario `SSP126` as a function of fitted model complexity (x-axis) and ensemble (distinguished by colour, with consistent ensemble colouring across panels); location of horizontal centre line of each box indicates posterior median of ΔQ_1; location of top (bottom) side of each box indicates 75%ile (25%ile) point, and top (bottom) of whiskers the 97.5%ile (2.5%ile) point of the posterior distribution. Bottom left and right: analogues of top right for scenarios `SSP245` (ΔQ_2) and `SSP585` (ΔQ_3). Value of ΔQ_j, $j = 1, 2, 3$ under model CCC is identically zero, and is omitted from bottom panels when convenient to provide better illustration of the variation in estimates under more complex models. For comparison with Figure 6 of the main text.

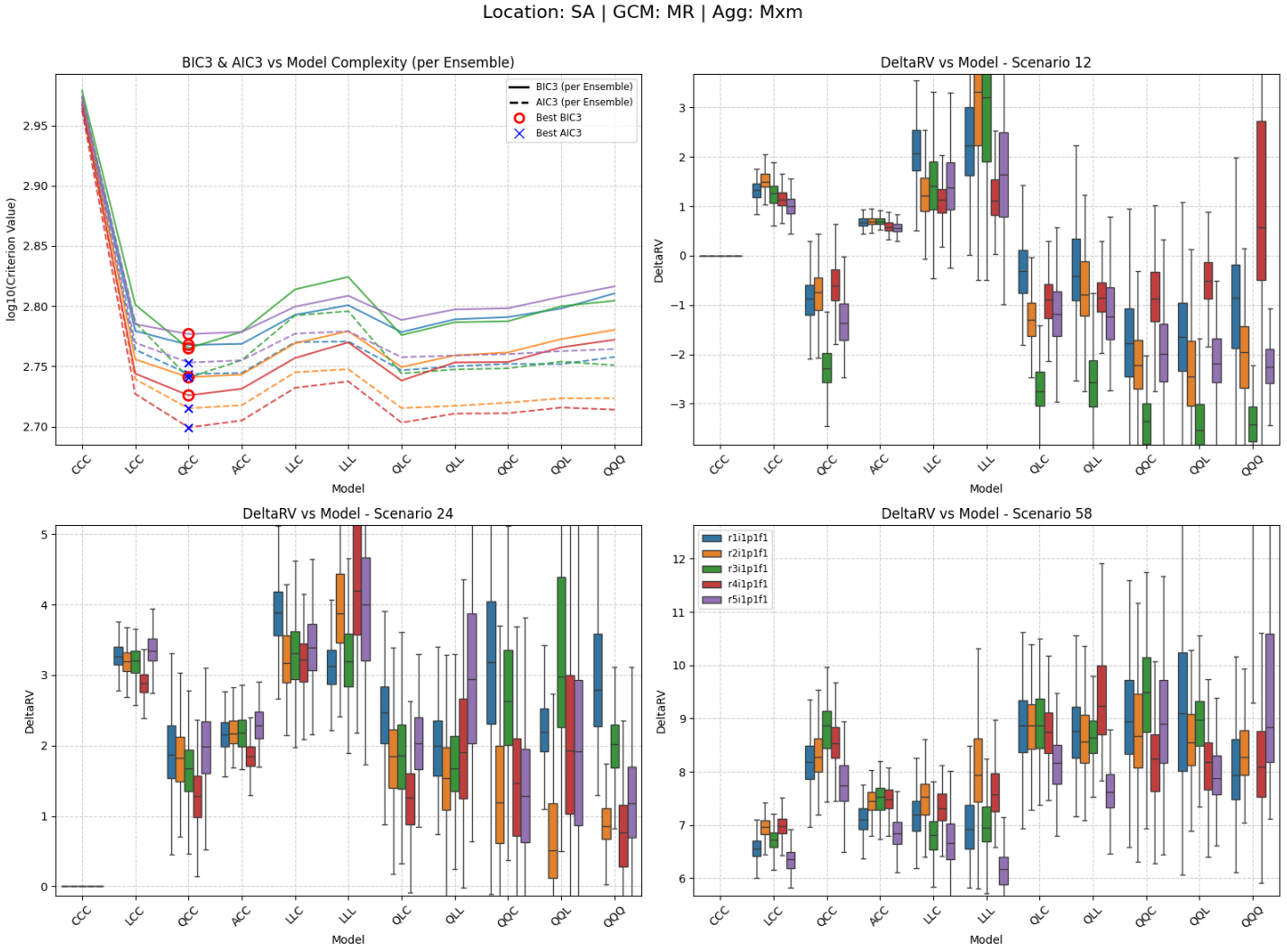

Figure SM20: Summary of scenario-coupled GEV regression for regional annual maxima of the Sahara region using `MRI-ESM2-0` GCM data. Top left: plots of BIC3 (solid line) and AIC3 (dashed line) for each available ensemble (distinguished by colour, see Table 2 of the main text and legend in bottom-right panel); optimal model choice using BIC3 (AIC3) indicated using red disc (blue cross). Top right: box-whisker plots summarising the distribution of the difference in the 100-year return value between 2025 and 2125 (ΔQ_1; see Equation 7) for climate scenario `SSP126` as a function of fitted model complexity (x-axis) and ensemble (distinguished by colour, with consistent ensemble colouring across panels); location of horizontal centre line of each box indicates posterior median of ΔQ_1; location of top (bottom) side of each box indicates 75%ile (25%ile) point, and top (bottom) of whiskers the 97.5%ile (2.5%ile) point of the posterior distribution. Bottom left and right: analogues of top right for scenarios `SSP245` (ΔQ_2) and `SSP585` (ΔQ_3). Value of ΔQ_j, $j = 1, 2, 3$ under model CCC is identically zero, and is omitted from bottom panels when convenient to provide better illustration of the variation in estimates under more complex models. For comparison with Figure 6 of the main text.

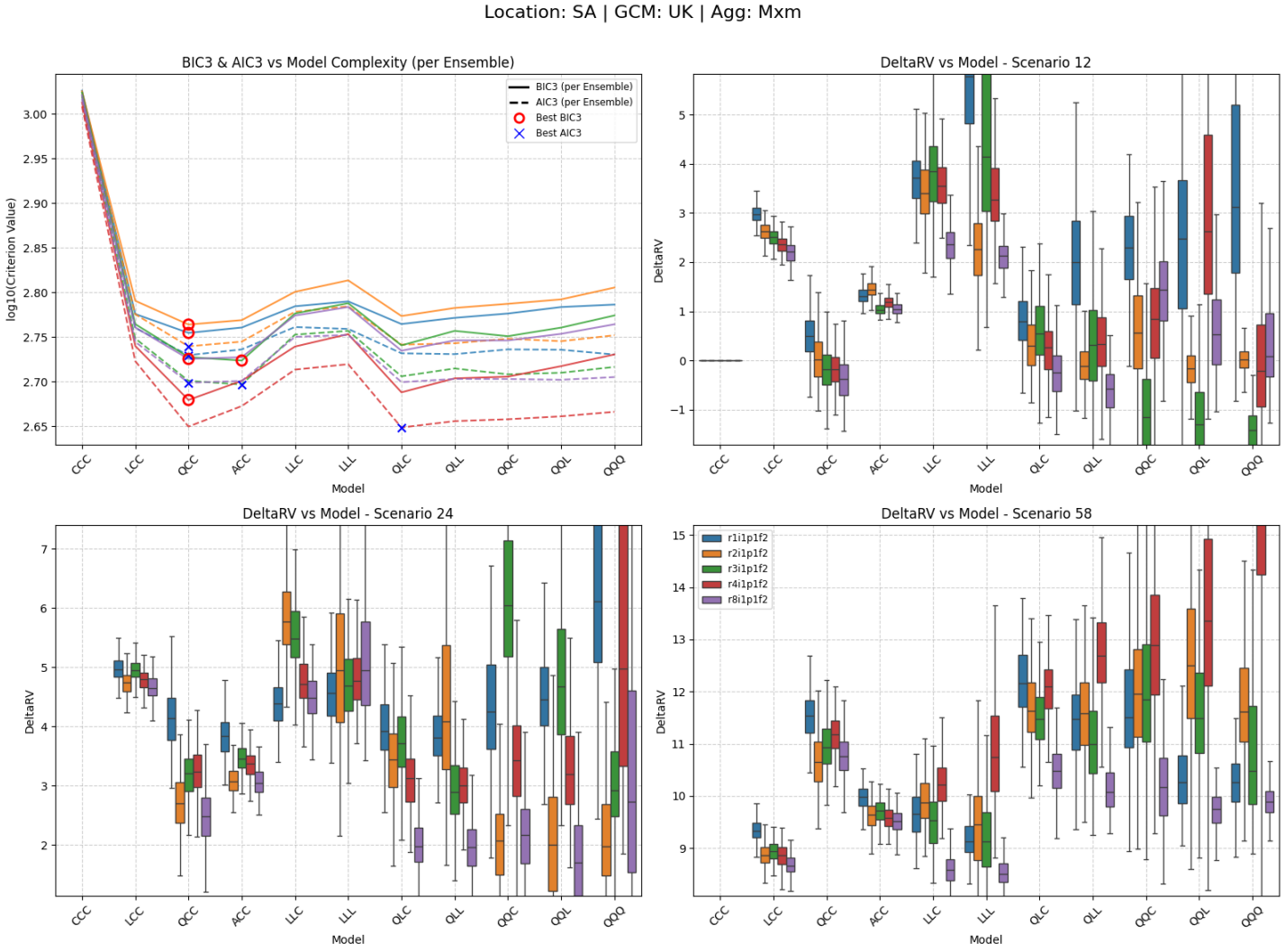

Figure SM21: Summary of scenario-coupled GEV regression for regional annual maxima of the Sahara region using `UKESM1-0-LL` GCM data. Top left: plots of BIC3 (solid line) and AIC3 (dashed line) for each available ensemble (distinguished by colour, see Table 2 of the main text and legend in bottom-right panel); optimal model choice using BIC3 (AIC3) indicated using red disc (blue cross). Top right: box-whisker plots summarising the distribution of the difference in the 100-year return value between 2025 and 2125 (ΔQ_1; see Equation 7) for climate scenario `SSP126` as a function of fitted model complexity (x-axis) and ensemble (distinguished by colour, with consistent ensemble colouring across panels); location of horizontal centre line of each box indicates posterior median of ΔQ_1; location of top (bottom) side of each box indicates 75%ile (25%ile) point, and top (bottom) of whiskers the 97.5%ile (2.5%ile) point of the posterior distribution. Bottom left and right: analogues of top right for scenarios `SSP245` (ΔQ_2) and `SSP585` (ΔQ_3). Value of ΔQ_j, $j = 1, 2, 3$ under model CCC is identically zero, and is omitted from bottom panels when convenient to provide better illustration of the variation in estimates under more complex models. For comparison with Figure 6 of the main text.

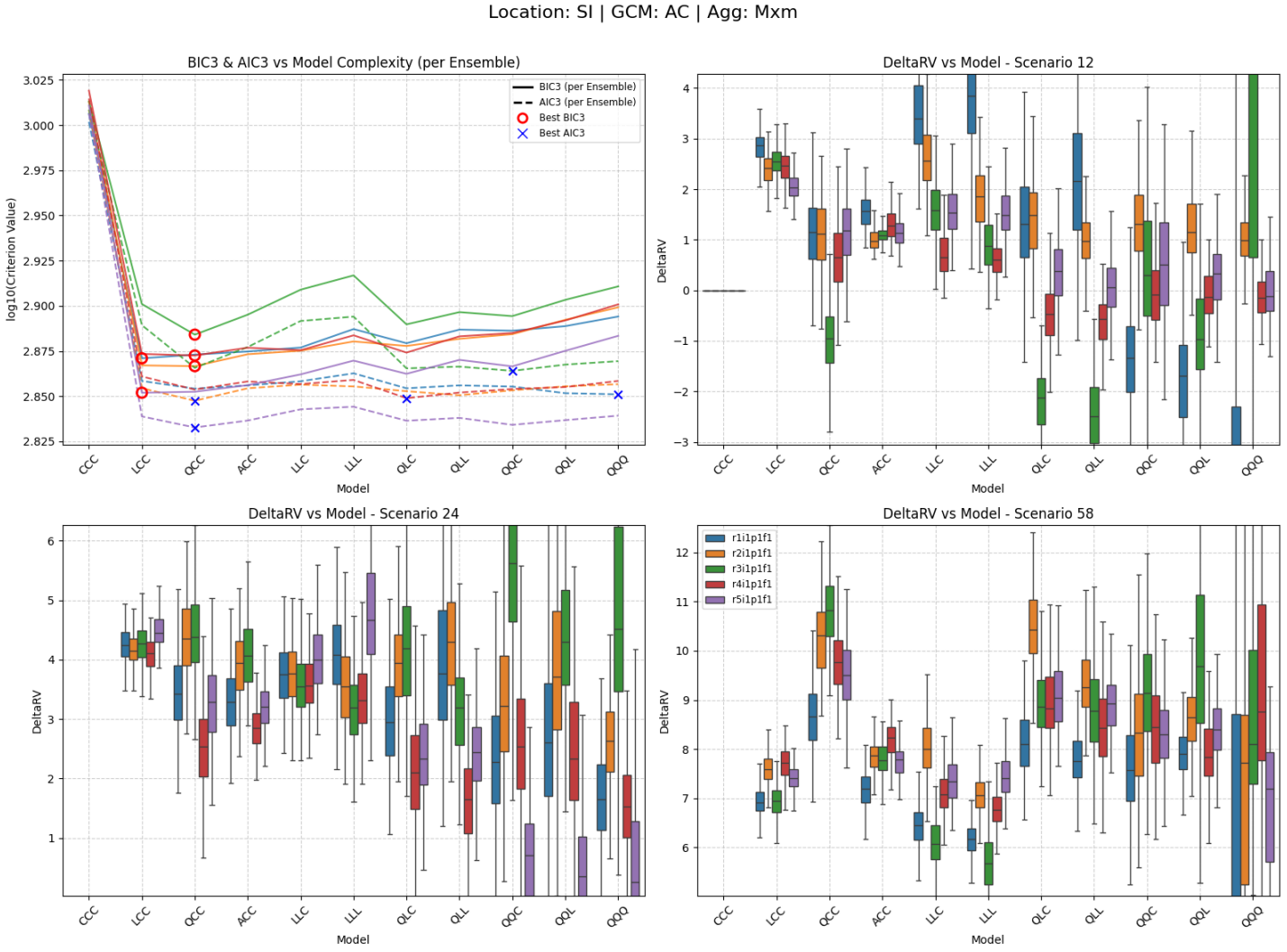

Figure SM22: Summary of scenario-coupled GEV regression for regional annual maxima of the Simpson region using `ACCESS-CM2` GCM data. Top left: plots of BIC3 (solid line) and AIC3 (dashed line) for each available ensemble (distinguished by colour, see Table 2 of the main text and legend in bottom-right panel); optimal model choice using BIC3 (AIC3) indicated using red disc (blue cross). Top right: box-whisker plots summarising the distribution of the difference in the 100-year return value between 2025 and 2125 (ΔQ_1; see Equation 7) for climate scenario `SSP126` as a function of fitted model complexity (x-axis) and ensemble (distinguished by colour, with consistent ensemble colouring across panels); location of horizontal centre line of each box indicates posterior median of ΔQ_1; location of top (bottom) side of each box indicates 75%ile (25%ile) point, and top (bottom) of whiskers the 97.5%ile (2.5%ile) point of the posterior distribution. Bottom left and right: analogues of top right for scenarios `SSP245` (ΔQ_2) and `SSP585` (ΔQ_3). Value of ΔQ_j, $j = 1, 2, 3$ under model CCC is identically zero, and is omitted from bottom panels when convenient to provide better illustration of the variation in estimates under more complex models. For comparison with Figure 6 of the main text.

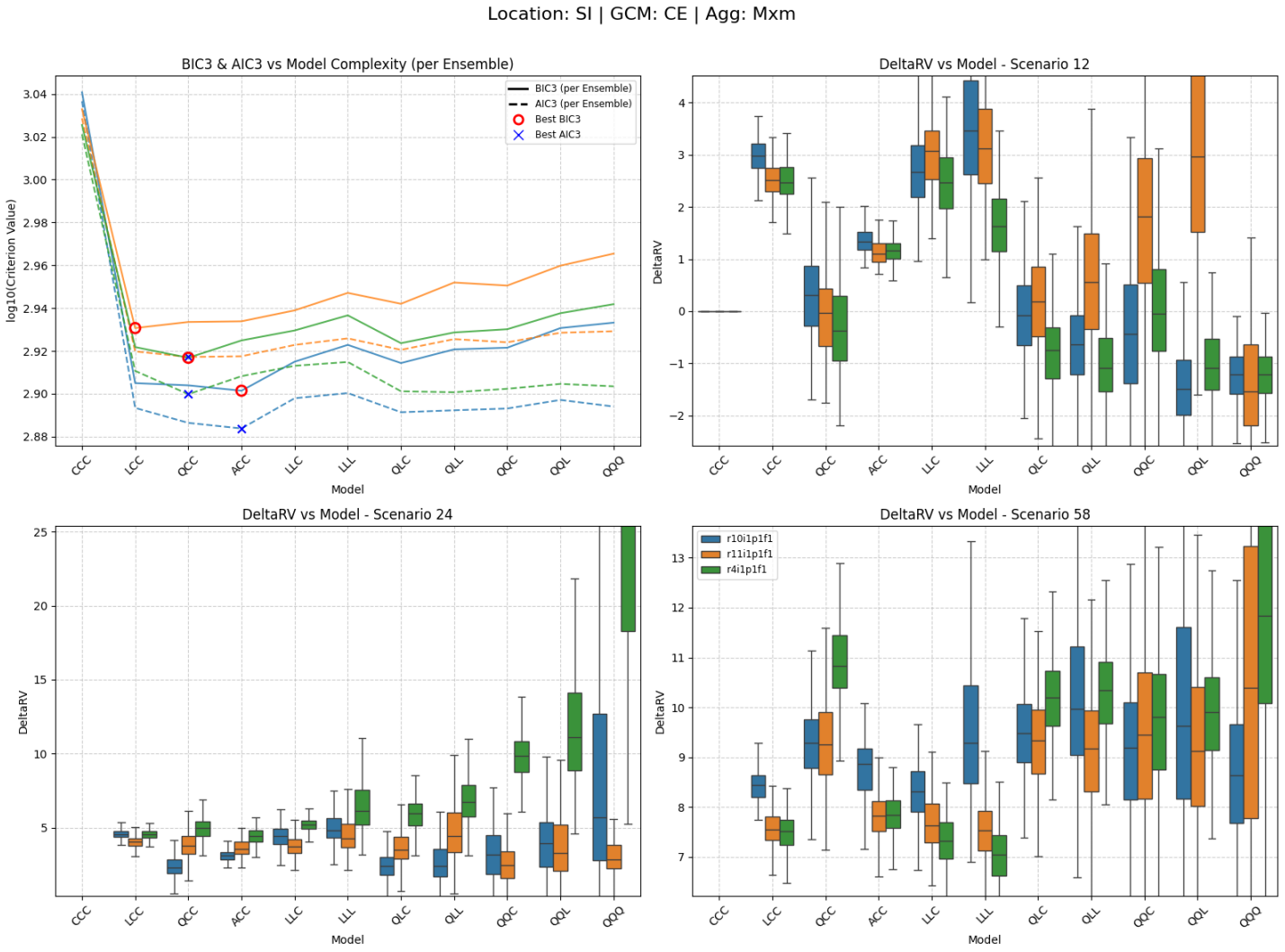

Figure SM23: Summary of scenario-coupled GEV regression for regional annual maxima of the Simpson region using `CESM2` GCM data. Top left: plots of BIC3 (solid line) and AIC3 (dashed line) for each available ensemble (distinguished by colour, see Table 2 of the main text and legend in bottom-right panel); optimal model choice using BIC3 (AIC3) indicated using red disc (blue cross). Top right: box-whisker plots summarising the distribution of the difference in the 100-year return value between 2025 and 2125 (ΔQ_1; see Equation 7) for climate scenario `SSP126` as a function of fitted model complexity (x-axis) and ensemble (distinguished by colour, with consistent ensemble colouring across panels); location of horizontal centre line of each box indicates posterior median of ΔQ_1; location of top (bottom) side of each box indicates 75%ile (25%ile) point, and top (bottom) of whiskers the 97.5%ile (2.5%ile) point of the posterior distribution. Bottom left and right: analogues of top right for scenarios `SSP245` (ΔQ_2) and `SSP585` (ΔQ_3). Value of ΔQ_j, $j = 1, 2, 3$ under model CCC is identically zero, and is omitted from bottom panels when convenient to provide better illustration of the variation in estimates under more complex models. For comparison with Figure 6 of the main text.

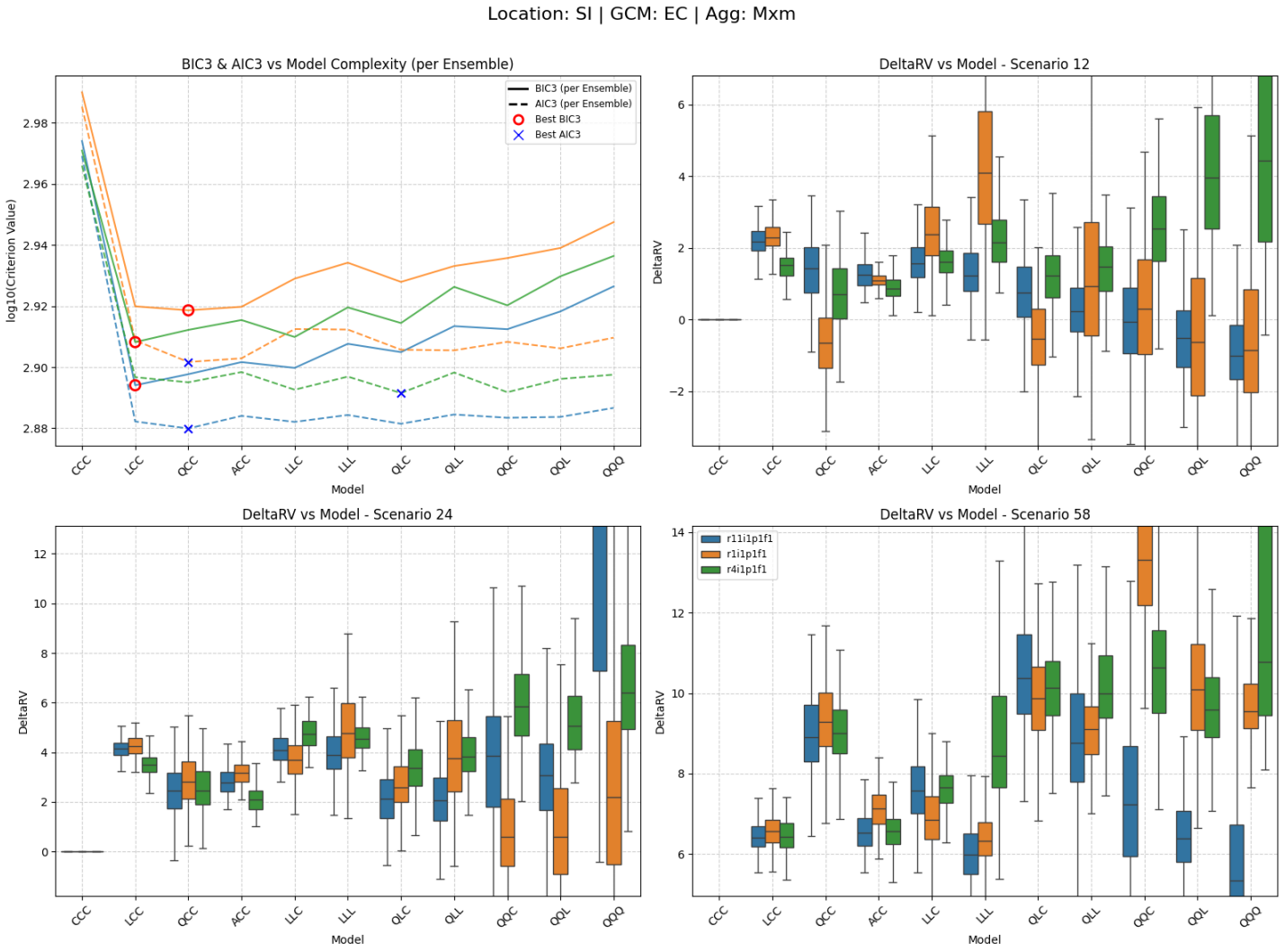

Figure SM24: Summary of scenario-coupled GEV regression for regional annual maxima of the Simpson region using `EC-Earth3` GCM data. Top left: plots of BIC3 (solid line) and AIC3 (dashed line) for each available ensemble (distinguished by colour, see Table 2 of the main text and legend in bottom-right panel); optimal model choice using BIC3 (AIC3) indicated using red disc (blue cross). Top right: box-whisker plots summarising the distribution of the difference in the 100-year return value between 2025 and 2125 (ΔQ_1; see Equation 7) for climate scenario `SSP126` as a function of fitted model complexity (x-axis) and ensemble (distinguished by colour, with consistent ensemble colouring across panels); location of horizontal centre line of each box indicates posterior median of ΔQ_1; location of top (bottom) side of each box indicates 75%ile (25%ile) point, and top (bottom) of whiskers the 97.5%ile (2.5%ile) point of the posterior distribution. Bottom left and right: analogues of top right for scenarios `SSP245` (ΔQ_2) and `SSP585` (ΔQ_3). Value of ΔQ_j, $j = 1, 2, 3$ under model CCC is identically zero, and is omitted from bottom panels when convenient to provide better illustration of the variation in estimates under more complex models. For comparison with Figure 6 of the main text.

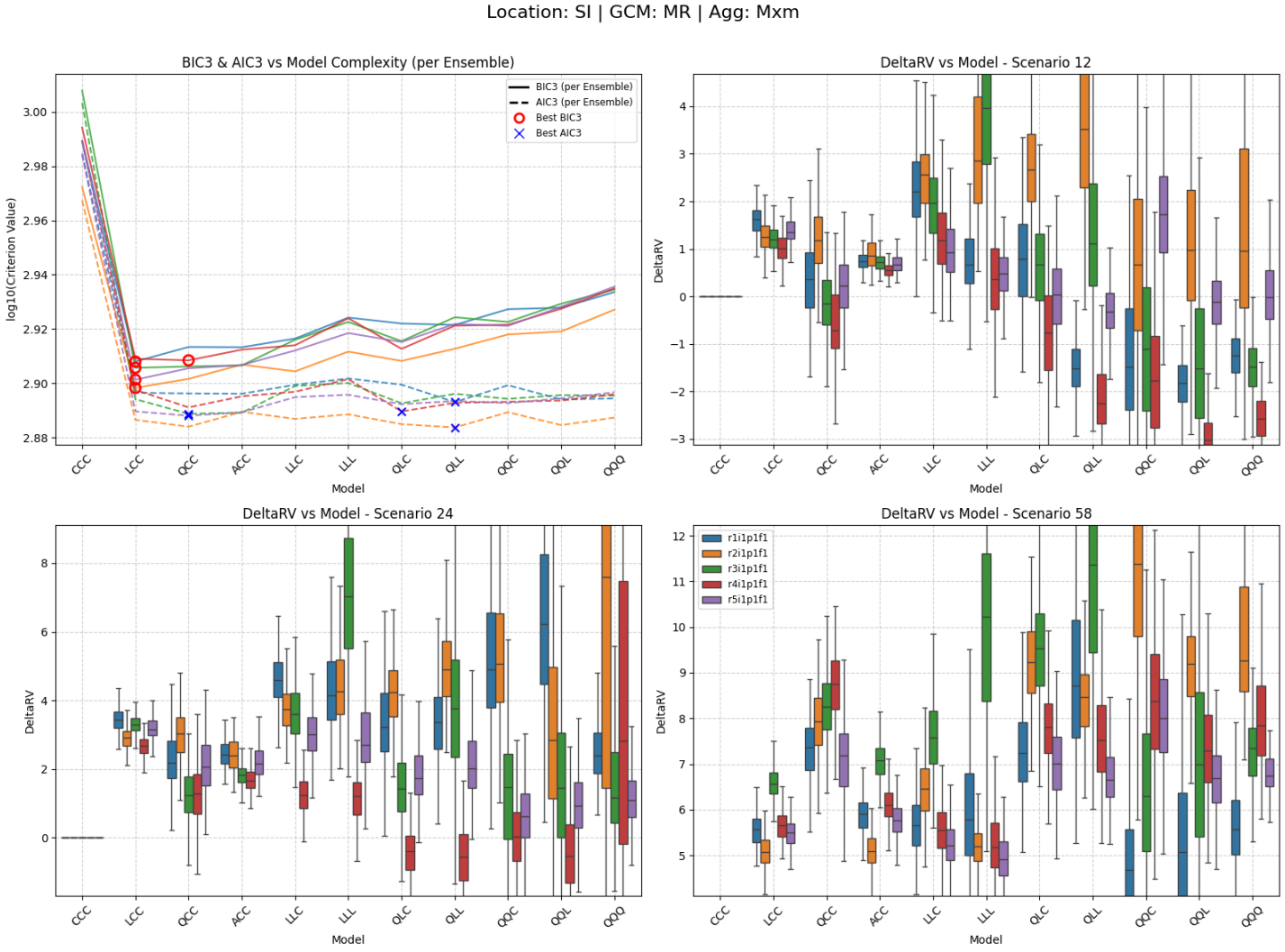

Figure SM25: Summary of scenario-coupled GEV regression for regional annual maxima of the Simpson region using `MRI-ESM2-0` GCM data. Top left: plots of BIC3 (solid line) and AIC3 (dashed line) for each available ensemble (distinguished by colour, see Table 2 of the main text and legend in bottom-right panel); optimal model choice using BIC3 (AIC3) indicated using red disc (blue cross). Top right: box-whisker plots summarising the distribution of the difference in the 100-year return value between 2025 and 2125 (ΔQ_1; see Equation 7) for climate scenario `SSP126` as a function of fitted model complexity (x-axis) and ensemble (distinguished by colour, with consistent ensemble colouring across panels); location of horizontal centre line of each box indicates posterior median of ΔQ_1; location of top (bottom) side of each box indicates 75%ile (25%ile) point, and top (bottom) of whiskers the 97.5%ile (2.5%ile) point of the posterior distribution. Bottom left and right: analogues of top right for scenarios `SSP245` (ΔQ_2) and `SSP585` (ΔQ_3). Value of ΔQ_j, $j = 1, 2, 3$ under model CCC is identically zero, and is omitted from bottom panels when convenient to provide better illustration of the variation in estimates under more complex models. For comparison with Figure 6 of the main text.

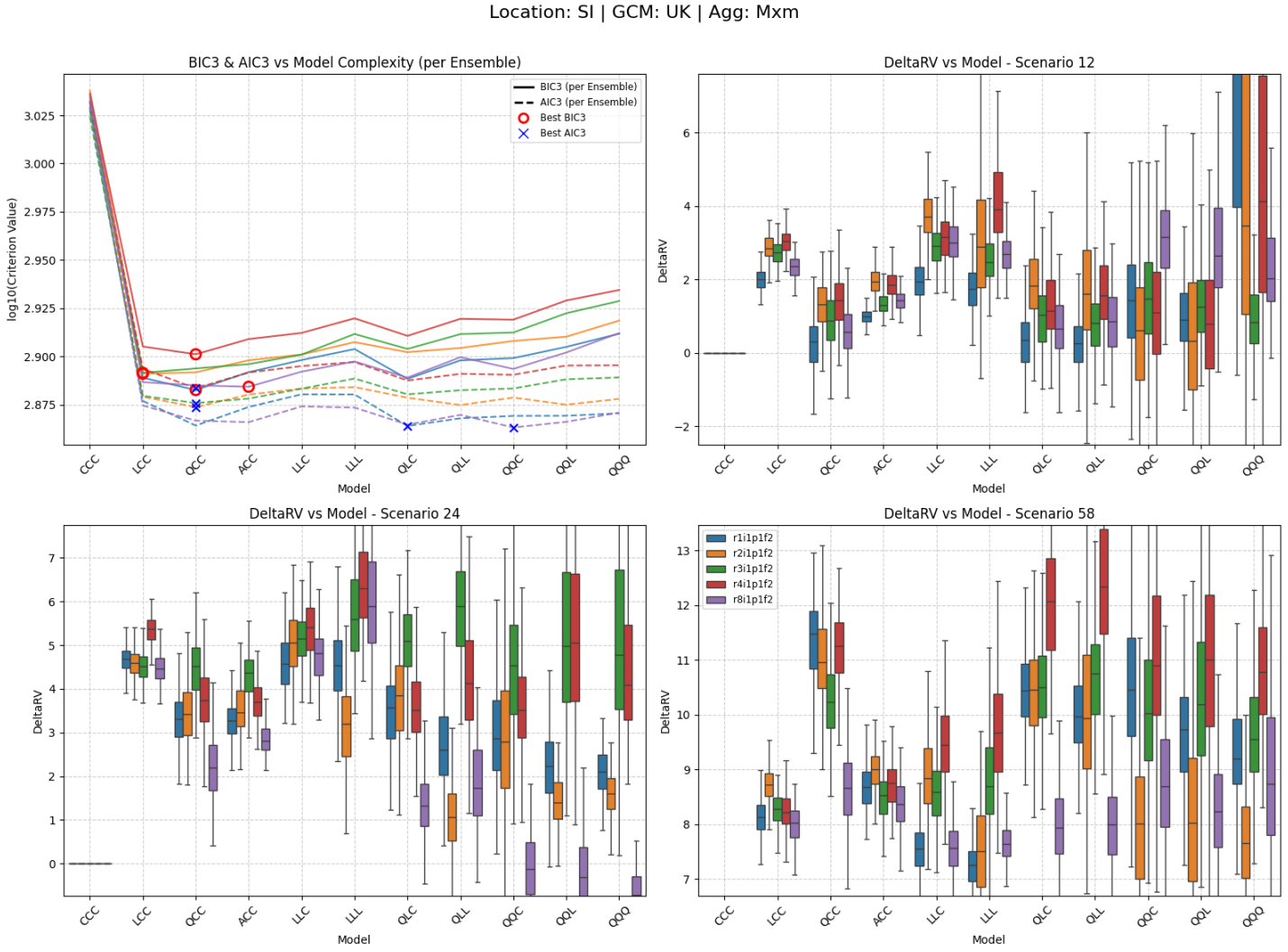

Figure SM26: Summary of scenario-coupled GEV regression for regional annual maxima of the Simpson region using `UKESM1-0-LL` GCM data. Top left: plots of BIC3 (solid line) and AIC3 (dashed line) for each available ensemble (distinguished by colour, see Table 2 of the main text and legend in bottom-right panel); optimal model choice using BIC3 (AIC3) indicated using red disc (blue cross). Top right: box-whisker plots summarising the distribution of the difference in the 100-year return value between 2025 and 2125 (ΔQ_1; see Equation 7) for climate scenario `SSP126` as a function of fitted model complexity (x-axis) and ensemble (distinguished by colour, with consistent ensemble colouring across panels); location of horizontal centre line of each box indicates posterior median of ΔQ_1; location of top (bottom) side of each box indicates 75%ile (25%ile) point, and top (bottom) of whiskers the 97.5%ile (2.5%ile) point of the posterior distribution. Bottom left and right: analogues of top right for scenarios `SSP245` (ΔQ_2) and `SSP585` (ΔQ_3). Value of ΔQ_j, $j = 1, 2, 3$ under model CCC is identically zero, and is omitted from bottom panels when convenient to provide better illustration of the variation in estimates under more complex models. For comparison with Figure 6 of the main text.

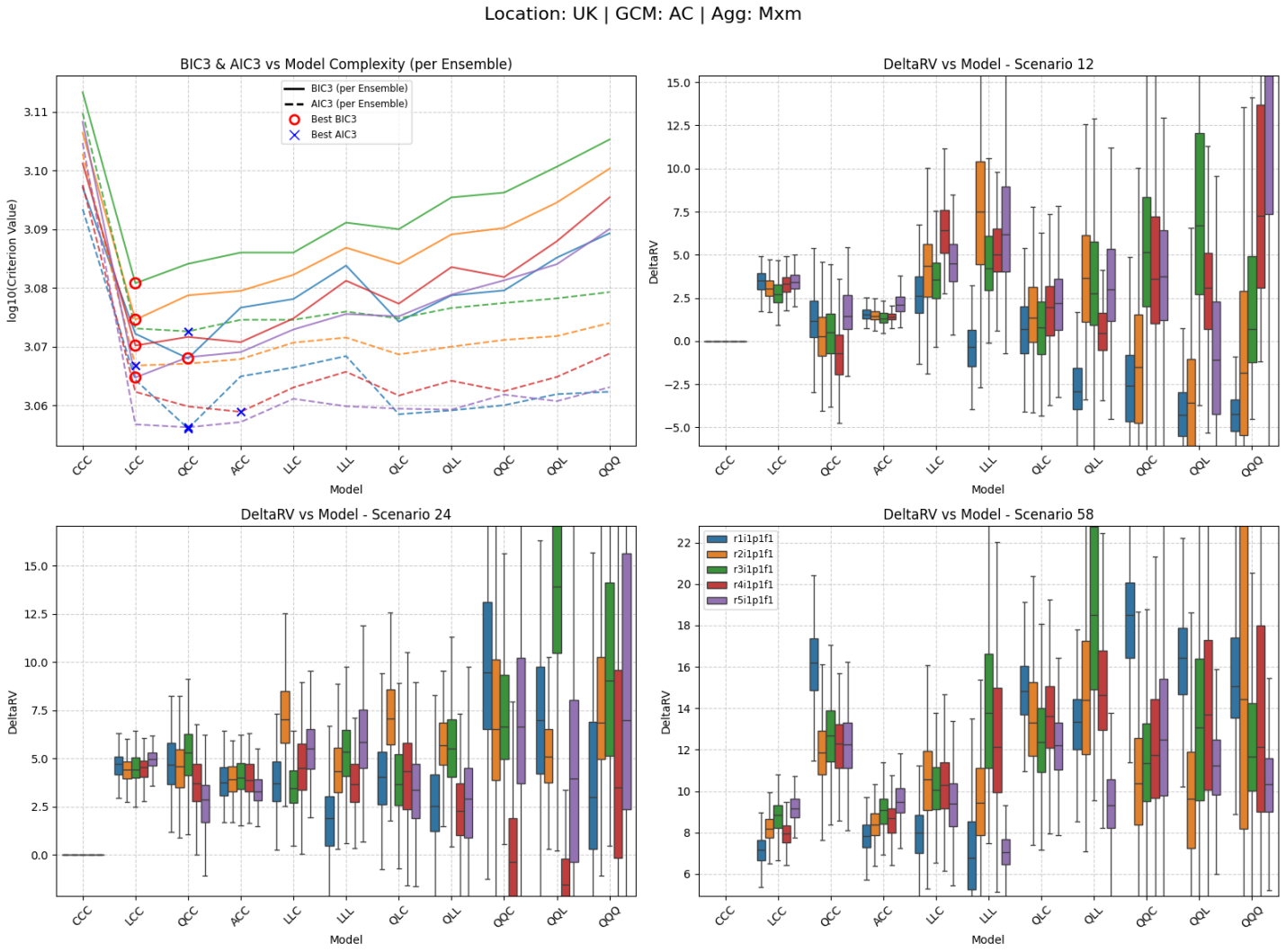

Figure SM27: Summary of scenario-coupled GEV regression for regional annual maxima of the UK region using `ACCESS-CM2` GCM data. Top left: plots of BIC3 (solid line) and AIC3 (dashed line) for each available ensemble (distinguished by colour, see Table 2 of the main text and legend in bottom-right panel); optimal model choice using BIC3 (AIC3) indicated using red disc (blue cross). Top right: box-whisker plots summarising the distribution of the difference in the 100-year return value between 2025 and 2125 (ΔQ_1; see Equation 7) for climate scenario `SSP126` as a function of fitted model complexity (x-axis) and ensemble (distinguished by colour, with consistent ensemble colouring across panels); location of horizontal centre line of each box indicates posterior median of ΔQ_1; location of top (bottom) side of each box indicates 75%ile (25%ile) point, and top (bottom) of whiskers the 97.5%ile (2.5%ile) point of the posterior distribution. Bottom left and right: analogues of top right for scenarios `SSP245` (ΔQ_2) and `SSP585` (ΔQ_3). Value of ΔQ_j, $j = 1, 2, 3$ under model CCC is identically zero, and is omitted from bottom panels when convenient to provide better illustration of the variation in estimates under more complex models. For comparison with Figure 6 of the main text.

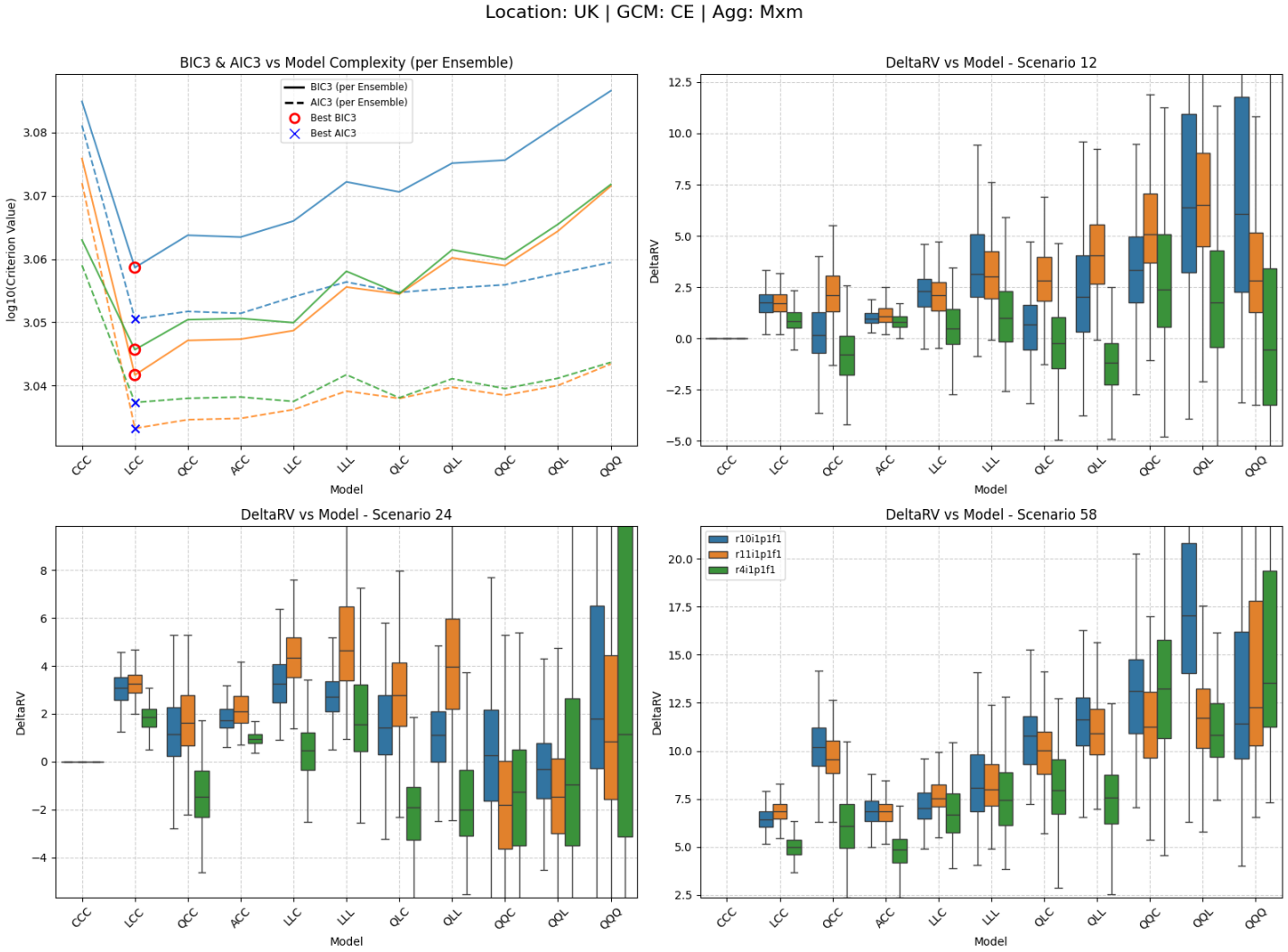

Figure SM28: Summary of scenario-coupled GEV regression for regional annual maxima of the UK region using `CESM2` GCM data. Top left: plots of BIC3 (solid line) and AIC3 (dashed line) for each available ensemble (distinguished by colour, see Table 2 of the main text and legend in bottom-right panel); optimal model choice using BIC3 (AIC3) indicated using red disc (blue cross). Top right: box-whisker plots summarising the distribution of the difference in the 100-year return value between 2025 and 2125 (ΔQ_1; see Equation 7) for climate scenario `SSP126` as a function of fitted model complexity (x-axis) and ensemble (distinguished by colour, with consistent ensemble colouring across panels); location of horizontal centre line of each box indicates posterior median of ΔQ_1; location of top (bottom) side of each box indicates 75%ile (25%ile) point, and top (bottom) of whiskers the 97.5%ile (2.5%ile) point of the posterior distribution. Bottom left and right: analogues of top right for scenarios `SSP245` (ΔQ_2) and `SSP585` (ΔQ_3). Value of ΔQ_j, $j = 1, 2, 3$ under model CCC is identically zero, and is omitted from bottom panels when convenient to provide better illustration of the variation in estimates under more complex models. For comparison with Figure 6 of the main text.

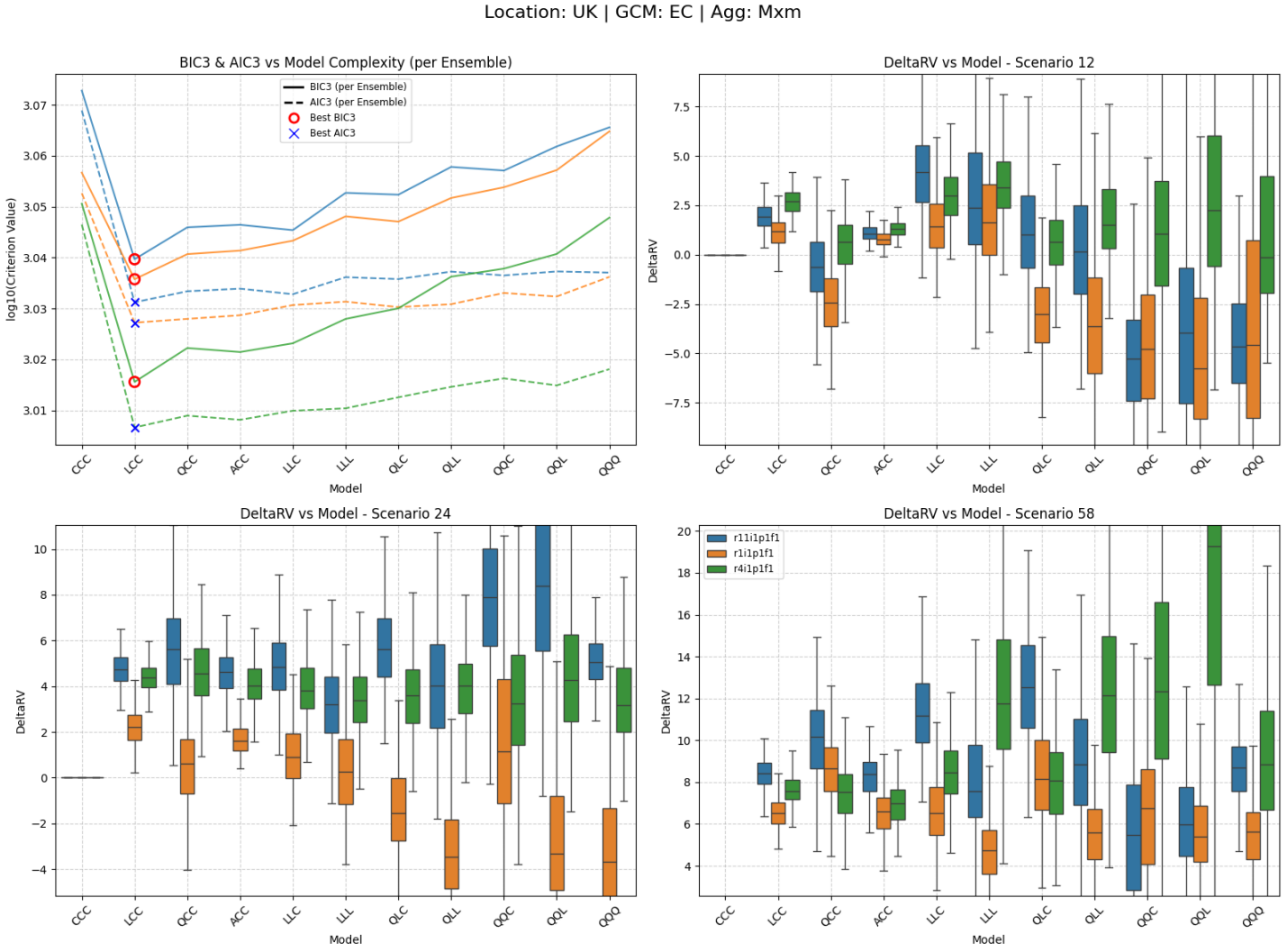

Figure SM29: Summary of scenario-coupled GEV regression for regional annual maxima of the UK region using `EC-Earth3` GCM data. Top left: plots of BIC3 (solid line) and AIC3 (dashed line) for each available ensemble (distinguished by colour, see Table 2 of the main text and legend in bottom-right panel); optimal model choice using BIC3 (AIC3) indicated using red disc (blue cross). Top right: box-whisker plots summarising the distribution of the difference in the 100-year return value between 2025 and 2125 (ΔQ_1; see Equation 7) for climate scenario `SSP126` as a function of fitted model complexity (x-axis) and ensemble (distinguished by colour, with consistent ensemble colouring across panels); location of horizontal centre line of each box indicates posterior median of ΔQ_1; location of top (bottom) side of each box indicates 75%ile (25%ile) point, and top (bottom) of whiskers the 97.5%ile (2.5%ile) point of the posterior distribution. Bottom left and right: analogues of top right for scenarios `SSP245` (ΔQ_2) and `SSP585` (ΔQ_3). Value of ΔQ_j, $j = 1, 2, 3$ under model CCC is identically zero, and is omitted from bottom panels when convenient to provide better illustration of the variation in estimates under more complex models. For comparison with Figure 6 of the main text.

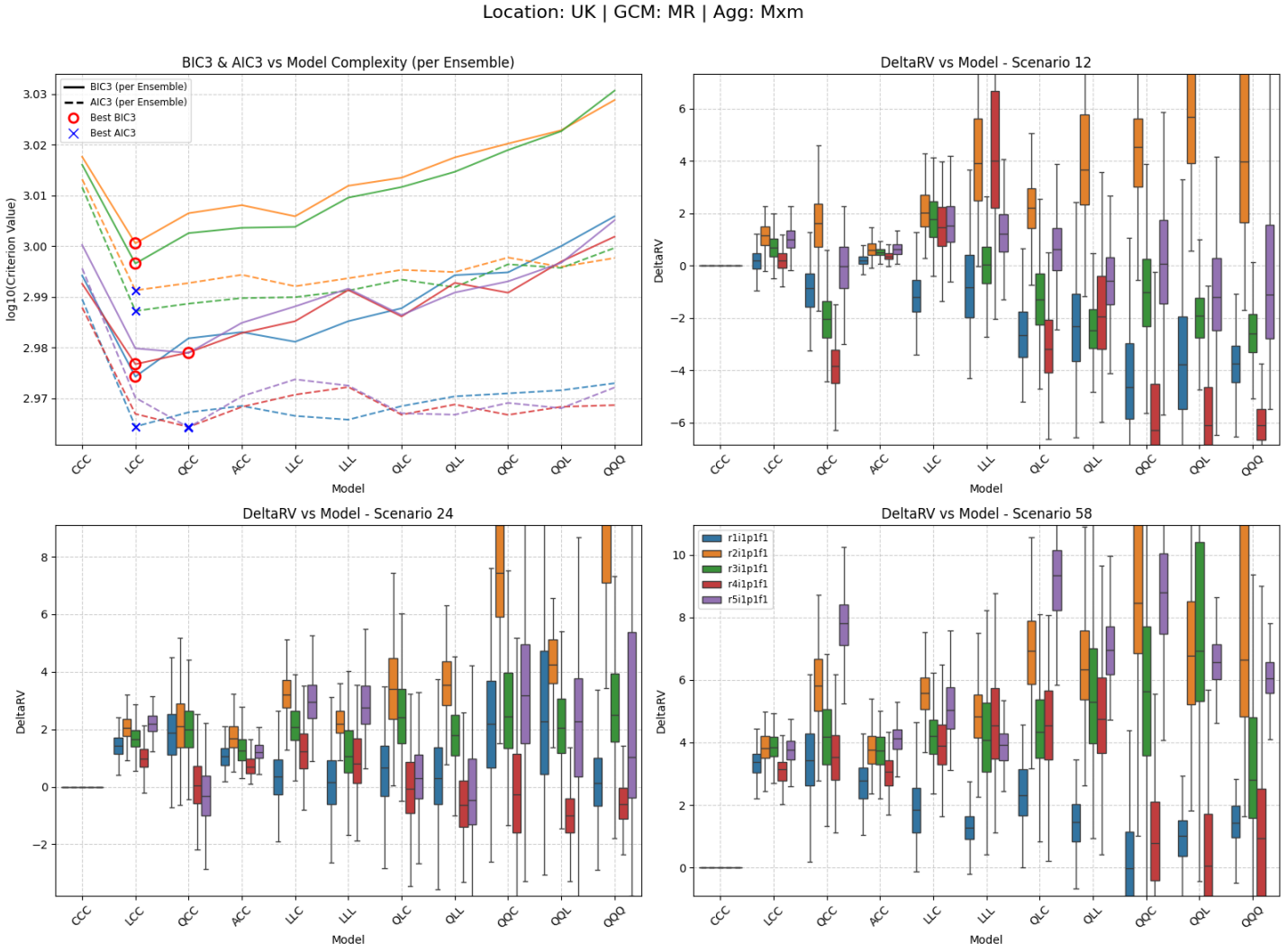

Figure SM30: Summary of scenario-coupled GEV regression for regional annual maxima of the UK region using `MRI-ESM2-0` GCM data. Top left: plots of BIC3 (solid line) and AIC3 (dashed line) for each available ensemble (distinguished by colour, see Table 2 of the main text and legend in bottom-right panel); optimal model choice using BIC3 (AIC3) indicated using red disc (blue cross). Top right: box-whisker plots summarising the distribution of the difference in the 100-year return value between 2025 and 2125 (ΔQ_1; see Equation 7) for climate scenario `SSP126` as a function of fitted model complexity (x-axis) and ensemble (distinguished by colour, with consistent ensemble colouring across panels); location of horizontal centre line of each box indicates posterior median of ΔQ_1; location of top (bottom) side of each box indicates 75%ile (25%ile) point, and top (bottom) of whiskers the 97.5%ile (2.5%ile) point of the posterior distribution. Bottom left and right: analogues of top right for scenarios `SSP245` (ΔQ_2) and `SSP585` (ΔQ_3). Value of ΔQ_j, $j = 1, 2, 3$ under model CCC is identically zero, and is omitted from bottom panels when convenient to provide better illustration of the variation in estimates under more complex models. For comparison with Figure 6 of the main text.

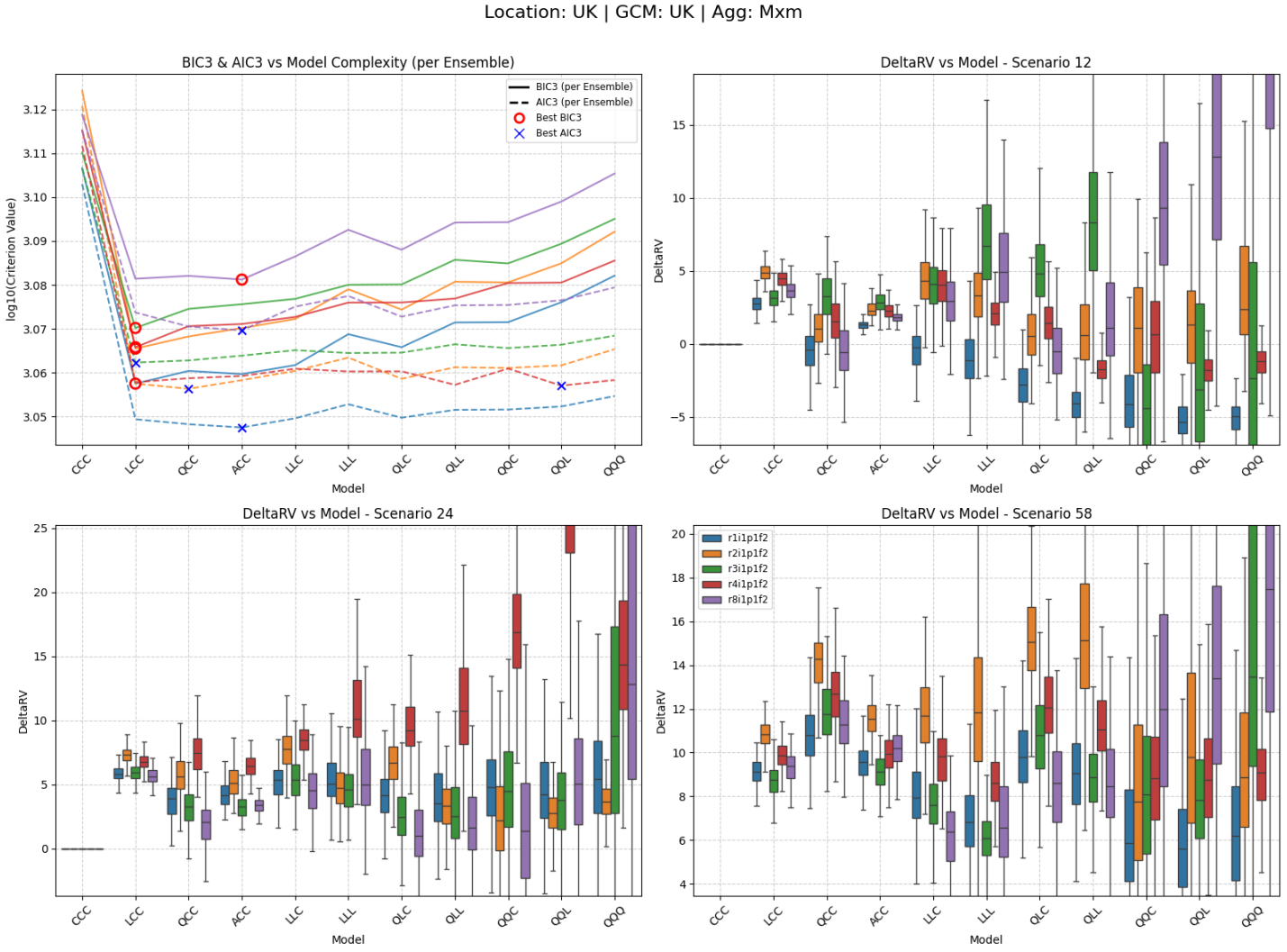

Figure SM31: Summary of scenario-coupled GEV regression for regional annual maxima of the UK region using `UKESM1-0-LL` GCM data. Top left: plots of BIC3 (solid line) and AIC3 (dashed line) for each available ensemble (distinguished by colour, see Table 2 of the main text and legend in bottom-right panel); optimal model choice using BIC3 (AIC3) indicated using red disc (blue cross). Top right: box-whisker plots summarising the distribution of the difference in the 100-year return value between 2025 and 2125 (ΔQ_1; see Equation 7) for climate scenario `SSP126` as a function of fitted model complexity (x-axis) and ensemble (distinguished by colour, with consistent ensemble colouring across panels); location of horizontal centre line of each box indicates posterior median of ΔQ_1; location of top (bottom) side of each box indicates 75%ile (25%ile) point, and top (bottom) of whiskers the 97.5%ile (2.5%ile) point of the posterior distribution. Bottom left and right: analogues of top right for scenarios `SSP245` (ΔQ_2) and `SSP585` (ΔQ_3). Value of ΔQ_j, $j = 1, 2, 3$ under model CCC is identically zero, and is omitted from bottom panels when convenient to provide better illustration of the variation in estimates under more complex models. For comparison with Figure 6 of the main text.

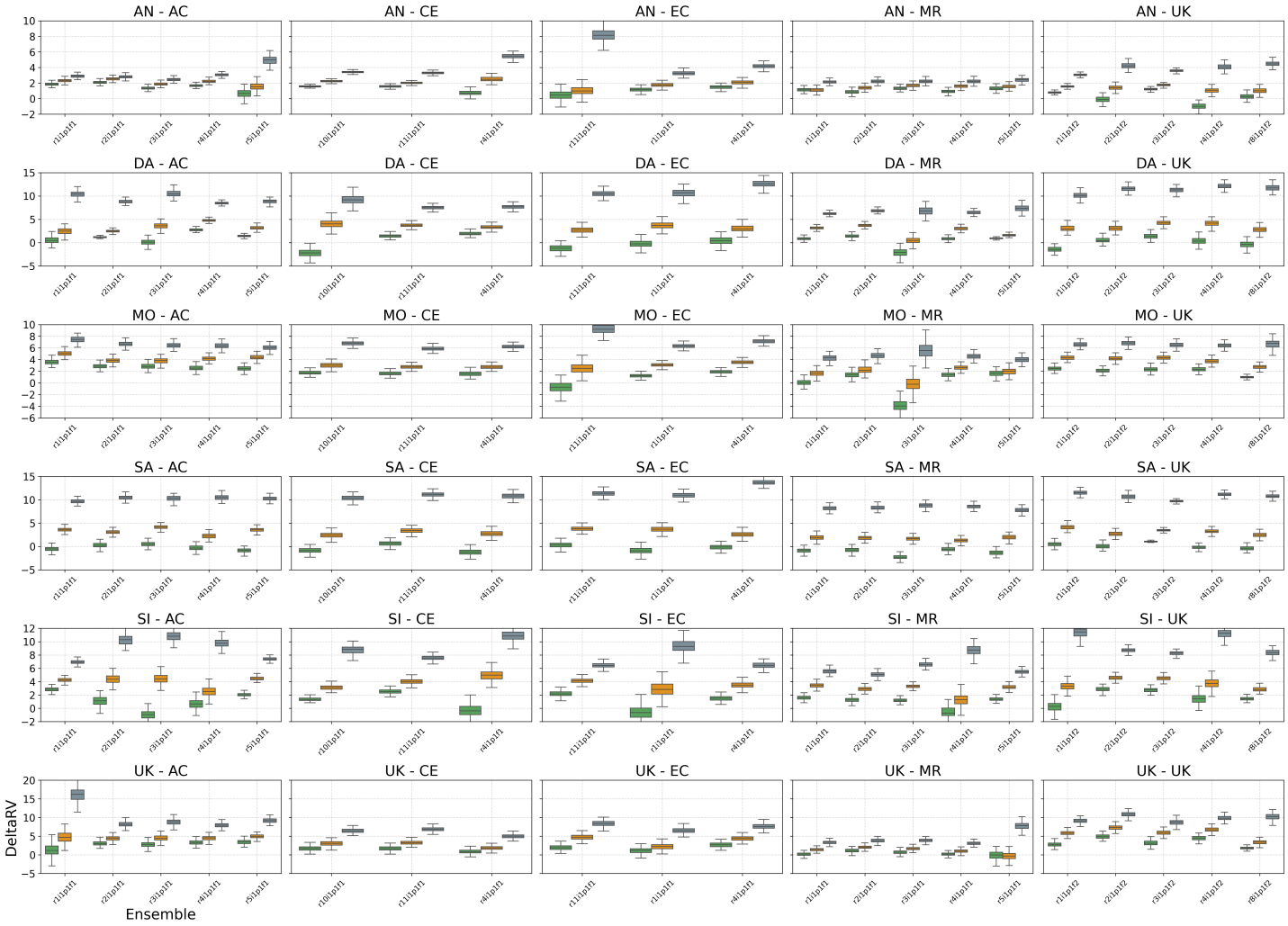

Figure SM32: Summary of inferences for return value differences ΔQ_j, $j = 1, 2, 3$ (see Equation 7) of regional annual maxima using BIC3 for model selection. Each panel shows box-whisker plots summarising the posterior distribution of ΔQ for climate scenarios `SSP126` ($j = 1$, green), `SSP245` ($j = 2$, orange) and `SSP585` ($j = 3$, grey) for each of up to five climate ensembles. Different panels show inferences for specific combinations of regions and locations; see Tables 1 and 2 for region and GCM acronyms.

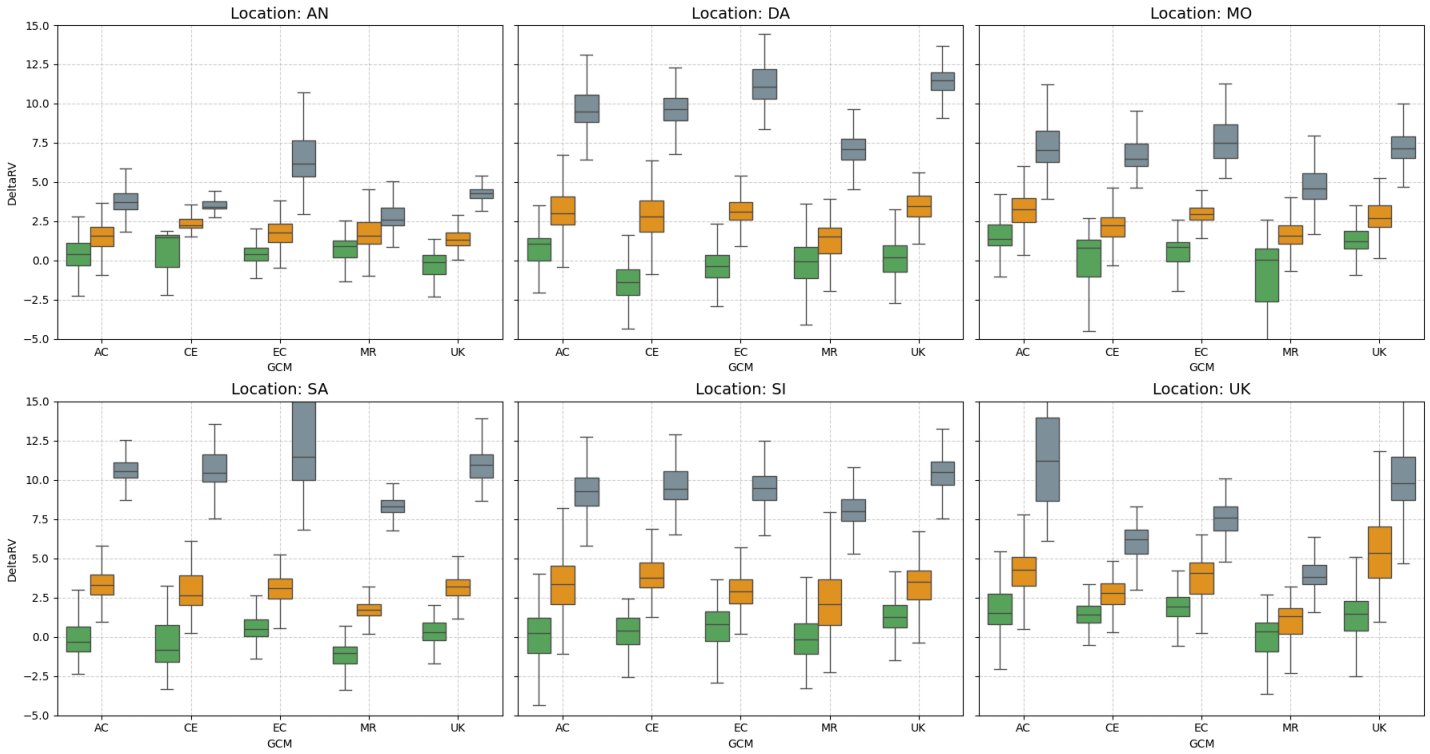

Figure SM33: Summary of inferences for return value differences ΔQ_j, $j = 1, 2, 3$ (see Equation 7) of regional annual maxima using AIC3 for model selection, aggregated over climate ensemble. Each panel shows box-whisker plots summarising the posterior distribution of ΔQ for climate scenarios `SSP126` ($j = 1$, green), `SSP245` ($j = 2$, orange) and `SSP585` ($j = 3$, grey) and each of five GCMs (`ACCESS-CM2`, `CESM2`, `EC-Earth3`, `MRI-ESM2-0`, `UKESM1-0-LL`). Left to right, top to bottom, panels show inferences for the Antarctic, Dasht-e Lut, Mojave, Sahara, Simpson and UK regions. For comparison with Figure 7.

Figure SM34: Summary of inferences for return value differences ΔQ_j, $j = 1, 2, 3$ (see Equation 7) of regional annual maxima using AIC3 for model selection. Each panel shows box-whisker plots summarising the posterior distribution of ΔQ for climate scenarios `SSP126` ($j = 1$, green), `SSP245` ($j = 2$, orange) and `SSP585` ($j = 3$, grey) for each of up to five climate ensembles. Different panels show inferences for specific combinations of regions and locations; see Tables 1 and 2 for region and GCM acronyms.

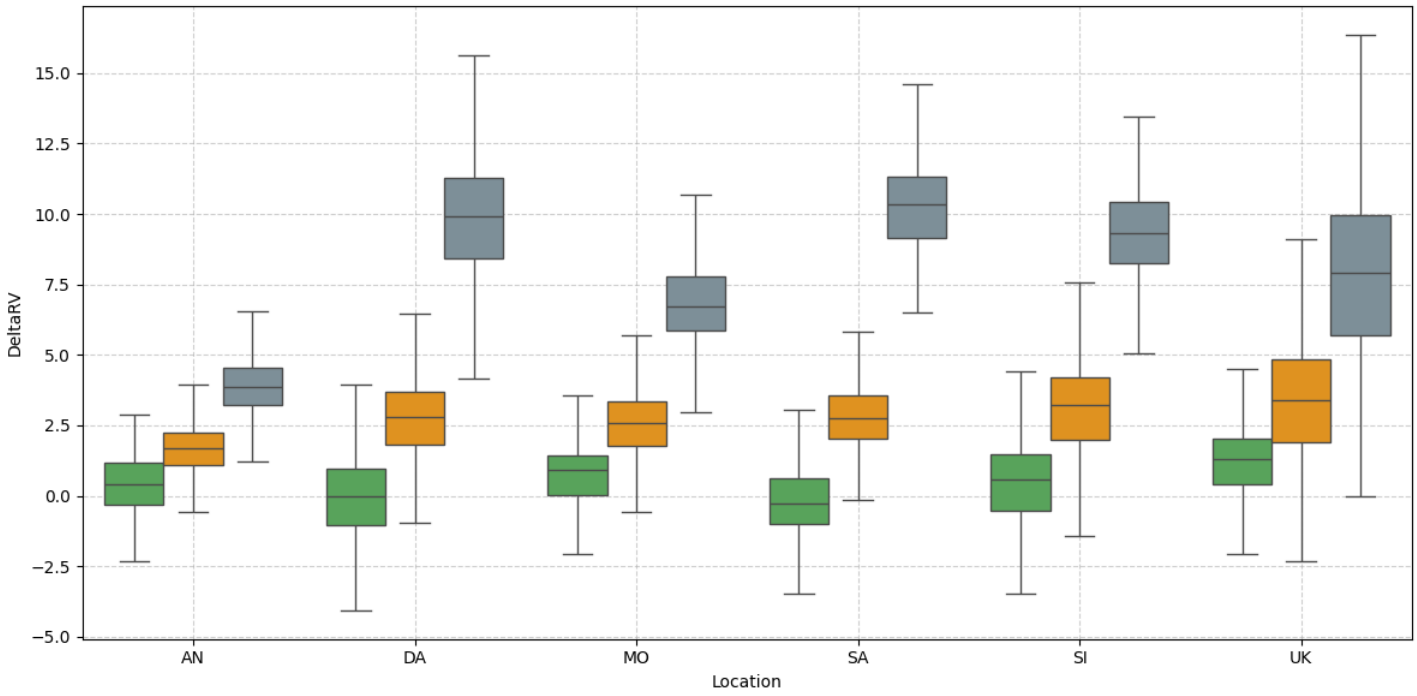

Figure SM35: Summary of inferences for return value differences ΔQ_j, $j = 1, 2, 3$ (see Equation 7) of regional annual maxima using AIC3 for model selection, aggregated over climate ensemble and GCM. Box-whisker plots summarise the posterior distribution of ΔQ for climate scenarios `SSP126` ($j = 1$, green), `SSP245` ($j = 2$, orange) and `SSP585` ($j = 3$, grey) for the Antarctic, Dasht-e Lut, Mojave, Sahara, Simpson and UK regions.

SM5 Results for regional annual minima

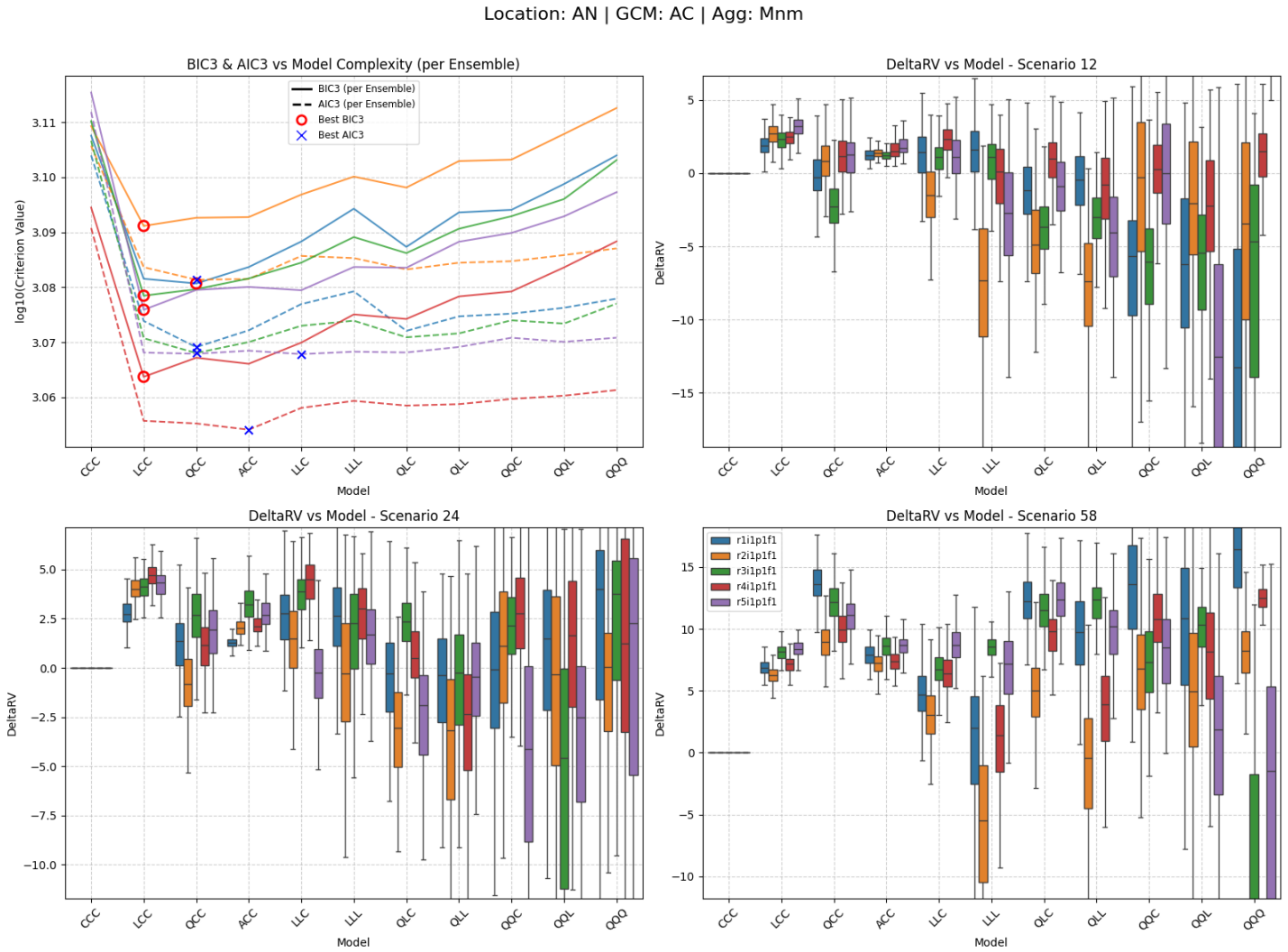

Figure SM36: Summary of scenario-coupled GEV regression for regional annual minima of the Antarctic region using `ACCESS-CM2` GCM data. Top left: plots of BIC3 (solid line) and AIC3 (dashed line) for each available ensemble (distinguished by colour, see Table 2 of the main text and legend in bottom-right panel); optimal model choice using BIC3 (AIC3) indicated using red disc (blue cross). Top right: box-whisker plots summarising the distribution of the difference in the 100-year return value between 2025 and 2125 (ΔQ_1; see Equation 7) for climate scenario `SSP126` as a function of fitted model complexity (x-axis) and ensemble (distinguished by colour, with consistent ensemble colouring across panels); location of horizontal centre line of each box indicates posterior median of ΔQ_1; location of top (bottom) side of each box indicates 75%ile (25%ile) point, and top (bottom) of whiskers the 97.5%ile (2.5%ile) point of the posterior distribution. Bottom left and right: analogues of top right for scenarios `SSP245` (ΔQ_2) and `SSP585` (ΔQ_3). Value of ΔQ_j, $j = 1, 2, 3$ under model CCC is identically zero, and is omitted from bottom panels when convenient to provide better illustration of the variation in estimates under more complex models. For comparison with Figure 6 of the main text.

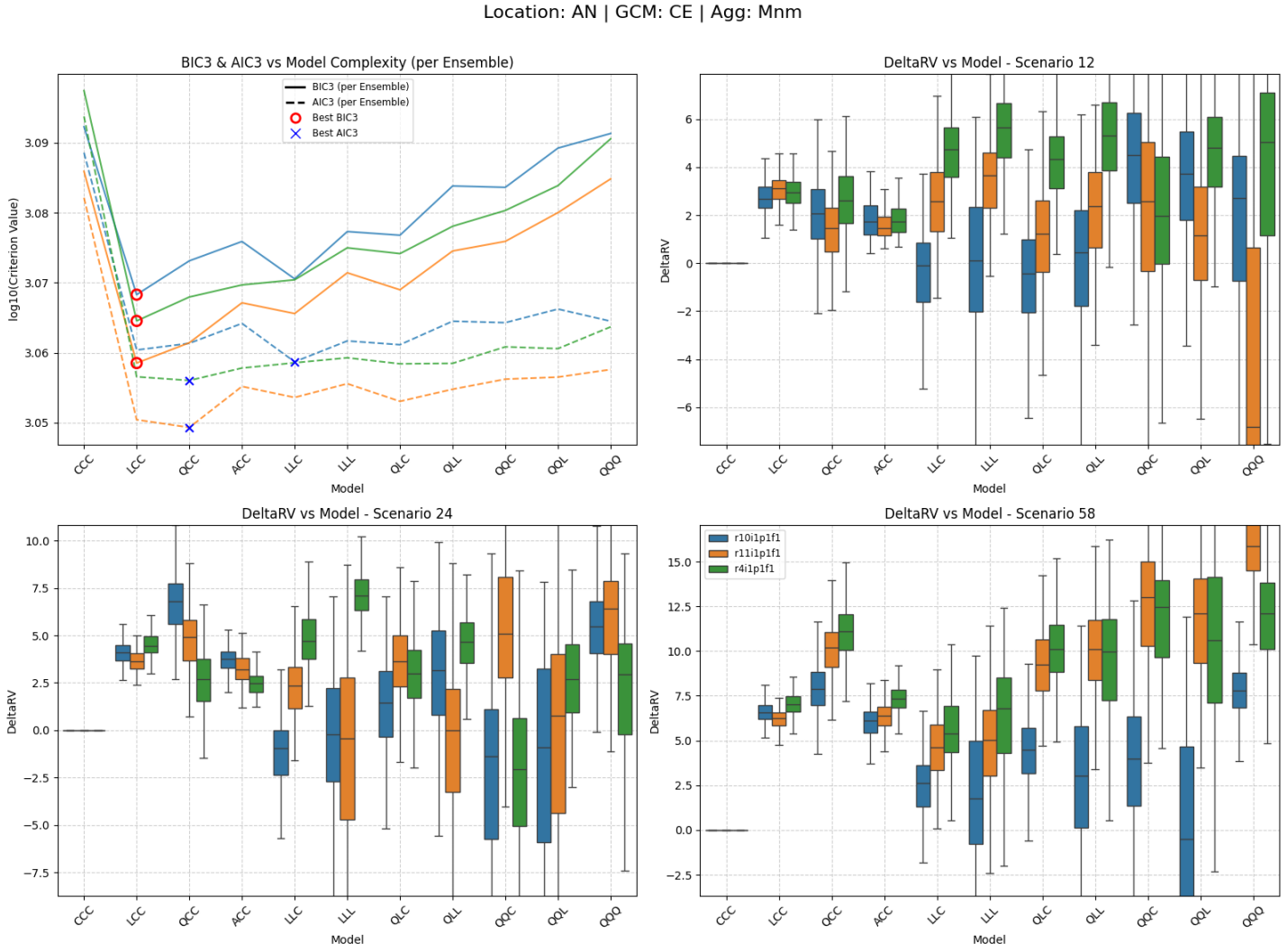

Figure SM37: Summary of scenario-coupled GEV regression for regional annual minima of the Antarctic region using `CESM2` GCM data. Top left: plots of BIC3 (solid line) and AIC3 (dashed line) for each available ensemble (distinguished by colour, see Table 2 of the main text and legend in bottom-right panel); optimal model choice using BIC3 (AIC3) indicated using red disc (blue cross). Top right: box-whisker plots summarising the distribution of the difference in the 100-year return value between 2025 and 2125 (ΔQ_1; see Equation 7) for climate scenario `SSP126` as a function of fitted model complexity (x-axis) and ensemble (distinguished by colour, with consistent ensemble colouring across panels); location of horizontal centre line of each box indicates posterior median of ΔQ_1; location of top (bottom) side of each box indicates 75%ile (25%ile) point, and top (bottom) of whiskers the 97.5%ile (2.5%ile) point of the posterior distribution. Bottom left and right: analogues of top right for scenarios `SSP245` (ΔQ_2) and `SSP585` (ΔQ_3). Value of ΔQ_j, $j = 1, 2, 3$ under model CCC is identically zero, and is omitted from bottom panels when convenient to provide better illustration of the variation in estimates under more complex models. For comparison with Figure 6 of the main text.

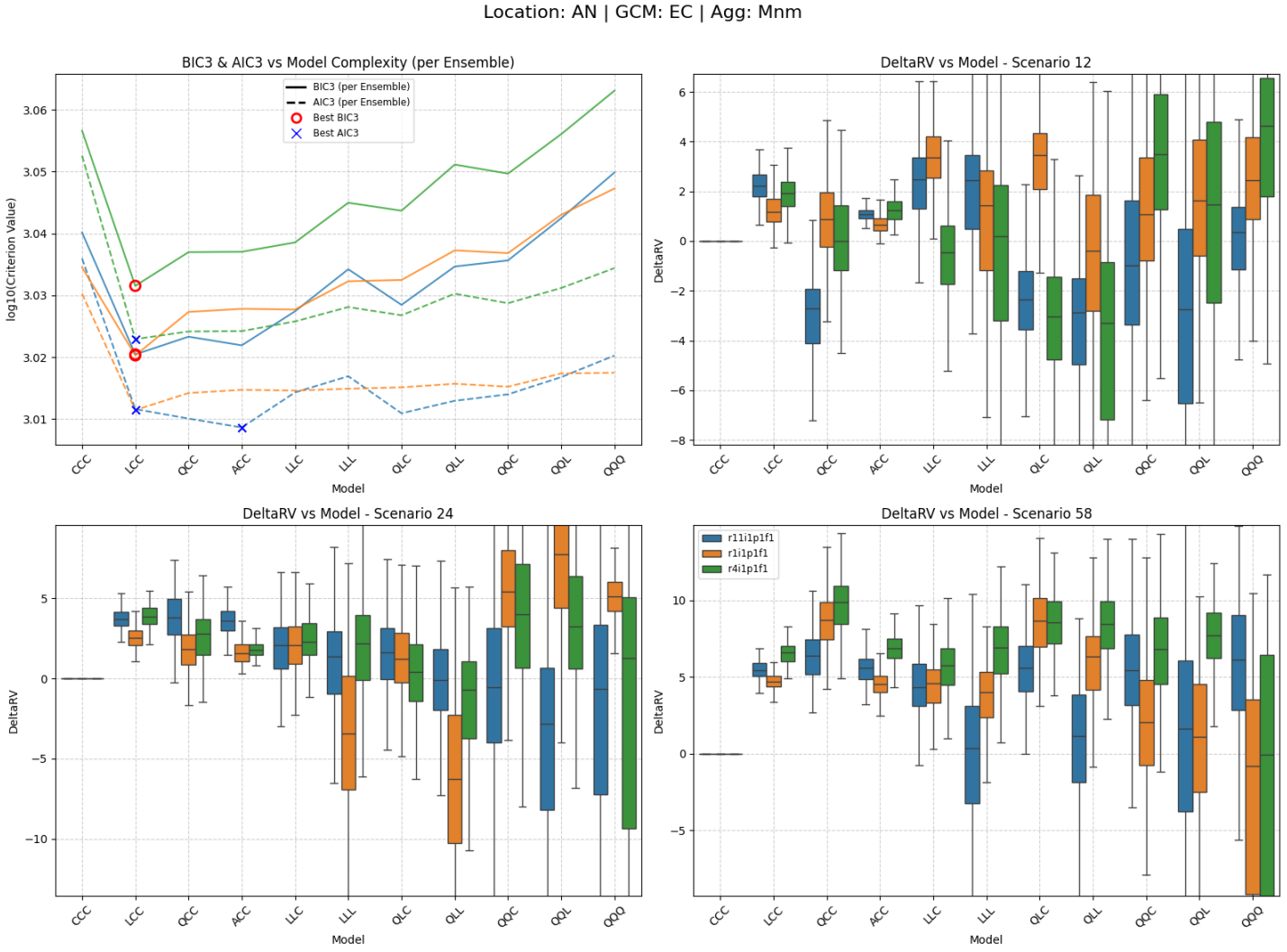

Figure SM38: Summary of scenario-coupled GEV regression for regional annual minima of the Antarctic region using `EC-Earth3` GCM data. Top left: plots of BIC3 (solid line) and AIC3 (dashed line) for each available ensemble (distinguished by colour, see Table 2 of the main text and legend in bottom-right panel); optimal model choice using BIC3 (AIC3) indicated using red disc (blue cross). Top right: box-whisker plots summarising the distribution of the difference in the 100-year return value between 2025 and 2125 (ΔQ_1; see Equation 7) for climate scenario `SSP126` as a function of fitted model complexity (x-axis) and ensemble (distinguished by colour, with consistent ensemble colouring across panels); location of horizontal centre line of each box indicates posterior median of ΔQ_1; location of top (bottom) side of each box indicates 75%ile (25%ile) point, and top (bottom) of whiskers the 97.5%ile (2.5%ile) point of the posterior distribution. Bottom left and right: analogues of top right for scenarios `SSP245` (ΔQ_2) and `SSP585` (ΔQ_3). Value of ΔQ_j, $j = 1, 2, 3$ under model CCC is identically zero, and is omitted from bottom panels when convenient to provide better illustration of the variation in estimates under more complex models. For comparison with Figure 6 of the main text.

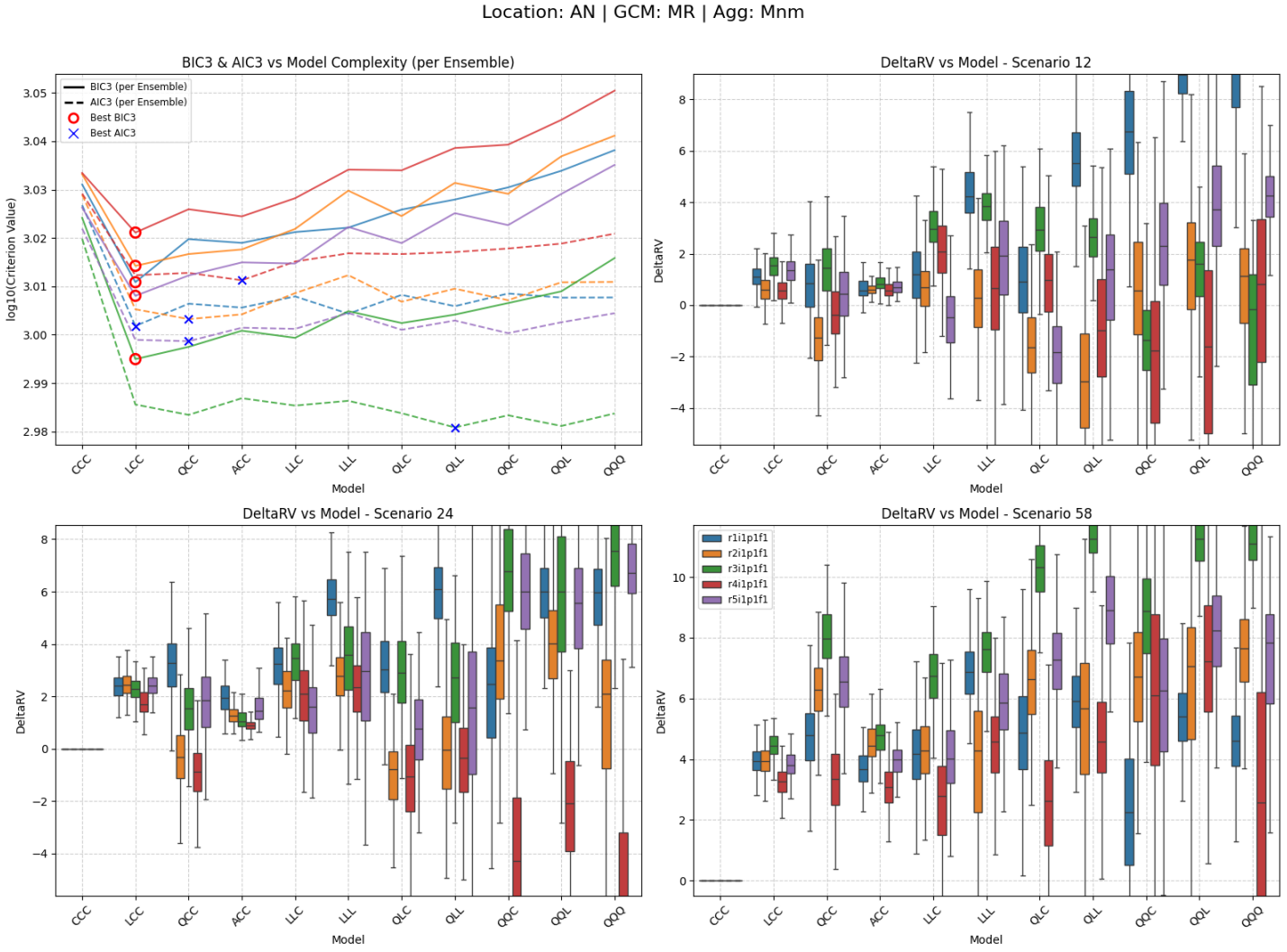

Figure SM39: Summary of scenario-coupled GEV regression for regional annual minima of the Antarctic region using `MRI-ESM2-0` GCM data. Top left: plots of BIC3 (solid line) and AIC3 (dashed line) for each available ensemble (distinguished by colour, see Table 2 of the main text and legend in bottom-right panel); optimal model choice using BIC3 (AIC3) indicated using red disc (blue cross). Top right: box-whisker plots summarising the distribution of the difference in the 100-year return value between 2025 and 2125 (ΔQ_1; see Equation 7) for climate scenario `SSP126` as a function of fitted model complexity (x-axis) and ensemble (distinguished by colour, with consistent ensemble colouring across panels); location of horizontal centre line of each box indicates posterior median of ΔQ_1; location of top (bottom) side of each box indicates 75%ile (25%ile) point, and top (bottom) of whiskers the 97.5%ile (2.5%ile) point of the posterior distribution. Bottom left and right: analogues of top right for scenarios `SSP245` (ΔQ_2) and `SSP585` (ΔQ_3). Value of ΔQ_j, $j = 1, 2, 3$ under model CCC is identically zero, and is omitted from bottom panels when convenient to provide better illustration of the variation in estimates under more complex models. For comparison with Figure 6 of the main text.

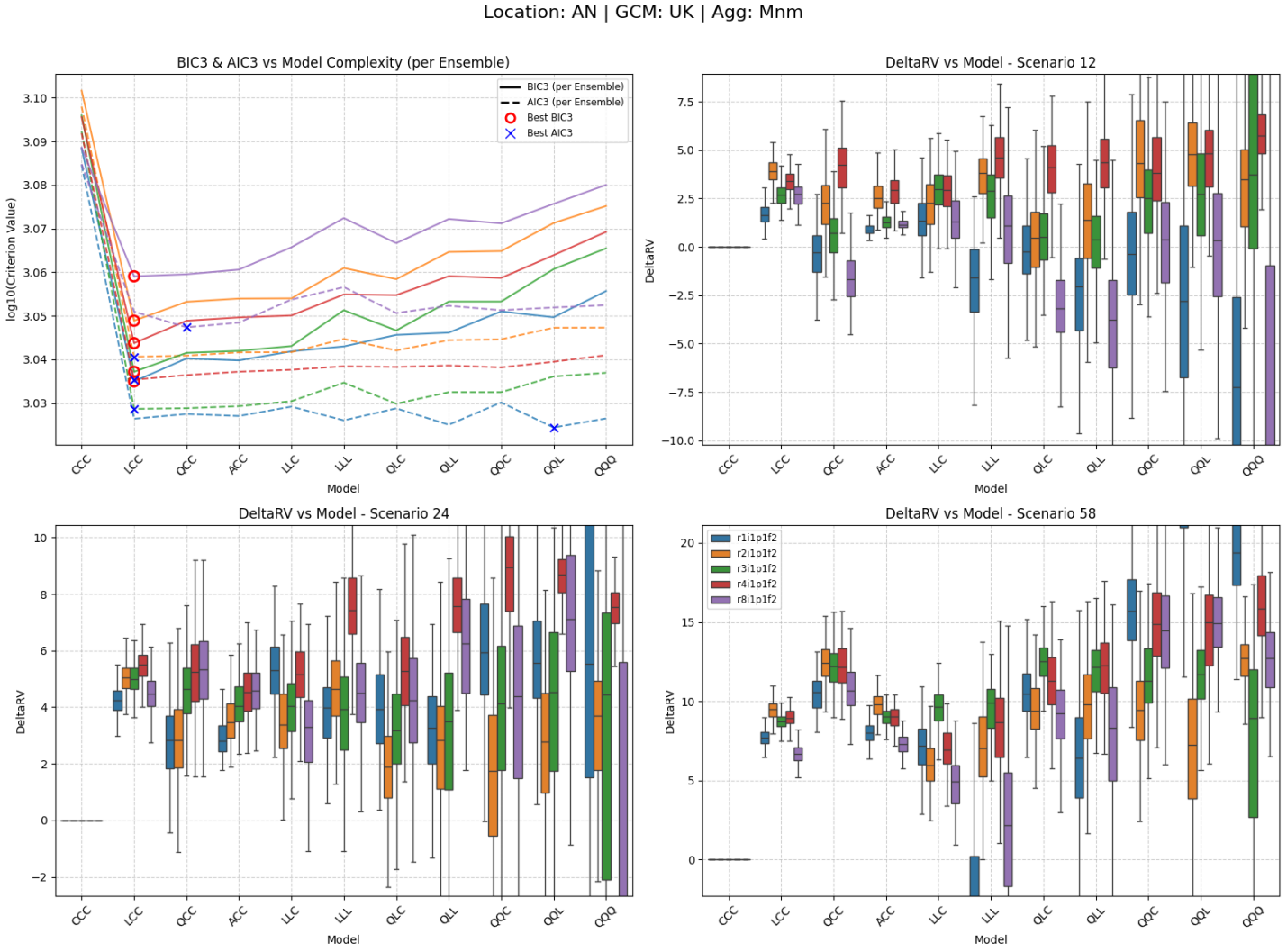

Figure SM40: Summary of scenario-coupled GEV regression for regional annual minima of the Antarctic region using `UKESM1-0-LL` GCM data. Top left: plots of BIC3 (solid line) and AIC3 (dashed line) for each available ensemble (distinguished by colour, see Table 2 of the main text and legend in bottom-right panel); optimal model choice using BIC3 (AIC3) indicated using red disc (blue cross). Top right: box-whisker plots summarising the distribution of the difference in the 100-year return value between 2025 and 2125 (ΔQ_1; see Equation 7) for climate scenario `SSP126` as a function of fitted model complexity (x-axis) and ensemble (distinguished by colour, with consistent ensemble colouring across panels); location of horizontal centre line of each box indicates posterior median of ΔQ_1; location of top (bottom) side of each box indicates 75%ile (25%ile) point, and top (bottom) of whiskers the 97.5%ile (2.5%ile) point of the posterior distribution. Bottom left and right: analogues of top right for scenarios `SSP245` (ΔQ_2) and `SSP585` (ΔQ_3). Value of ΔQ_j, $j = 1, 2, 3$ under model CCC is identically zero, and is omitted from bottom panels when convenient to provide better illustration of the variation in estimates under more complex models. For comparison with Figure 6 of the main text.

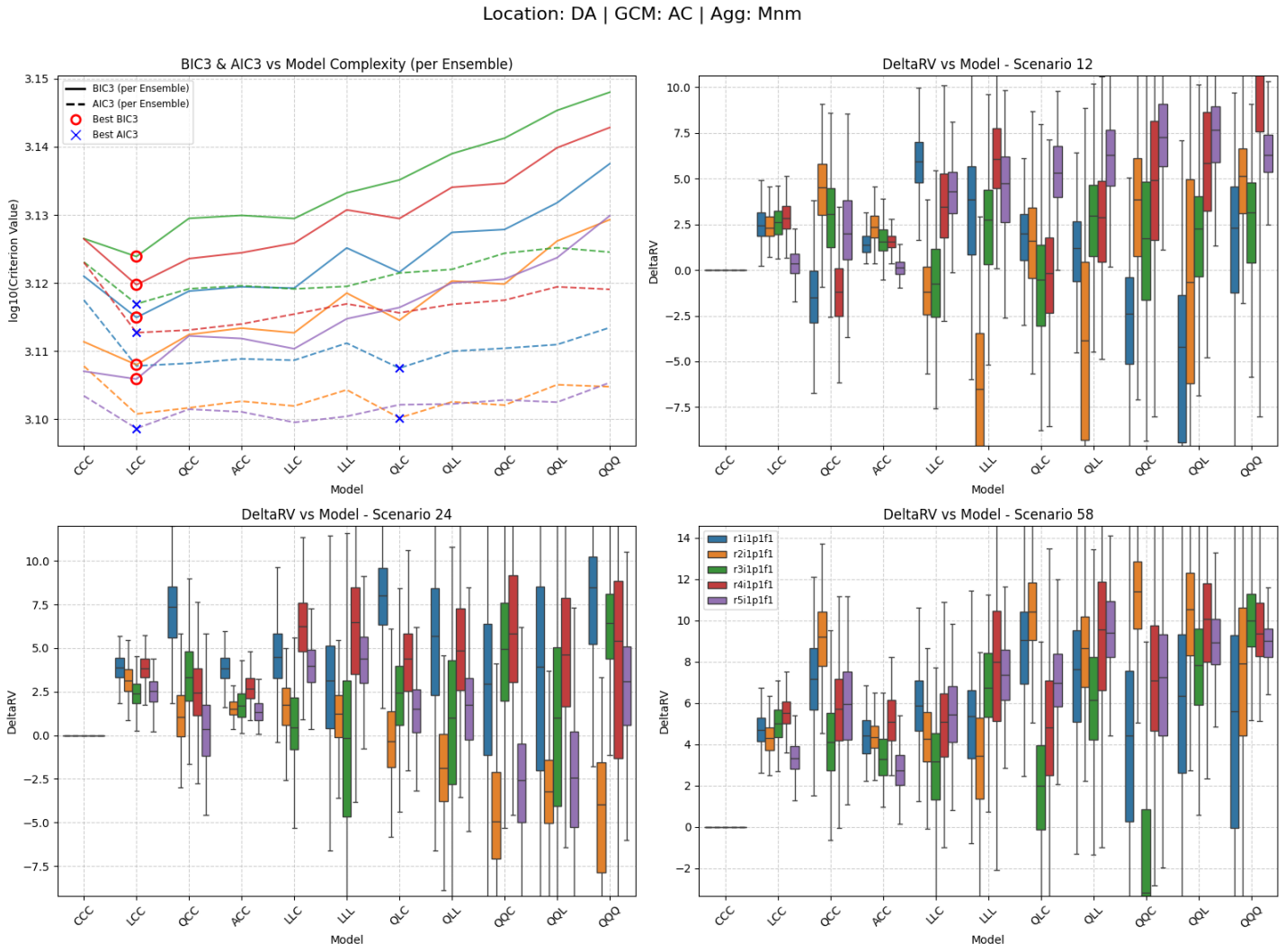

Figure SM41: Summary of scenario-coupled GEV regression for regional annual minima of the Dasht-e Lut region using `ACCESS-CM2` GCM data. Top left: plots of BIC3 (solid line) and AIC3 (dashed line) for each available ensemble (distinguished by colour, see Table 2 of the main text and legend in bottom-right panel); optimal model choice using BIC3 (AIC3) indicated using red disc (blue cross). Top right: box-whisker plots summarising the distribution of the difference in the 100-year return value between 2025 and 2125 (ΔQ_1; see Equation 7) for climate scenario `SSP126` as a function of fitted model complexity (x-axis) and ensemble (distinguished by colour, with consistent ensemble colouring across panels); location of horizontal centre line of each box indicates posterior median of ΔQ_1; location of top (bottom) side of each box indicates 75%ile (25%ile) point, and top (bottom) of whiskers the 97.5%ile (2.5%ile) point of the posterior distribution. Bottom left and right: analogues of top right for scenarios `SSP245` (ΔQ_2) and `SSP585` (ΔQ_3). Value of ΔQ_j, $j = 1, 2, 3$ under model CCC is identically zero, and is omitted from bottom panels when convenient to provide better illustration of the variation in estimates under more complex models. For comparison with Figure 6 of the main text.

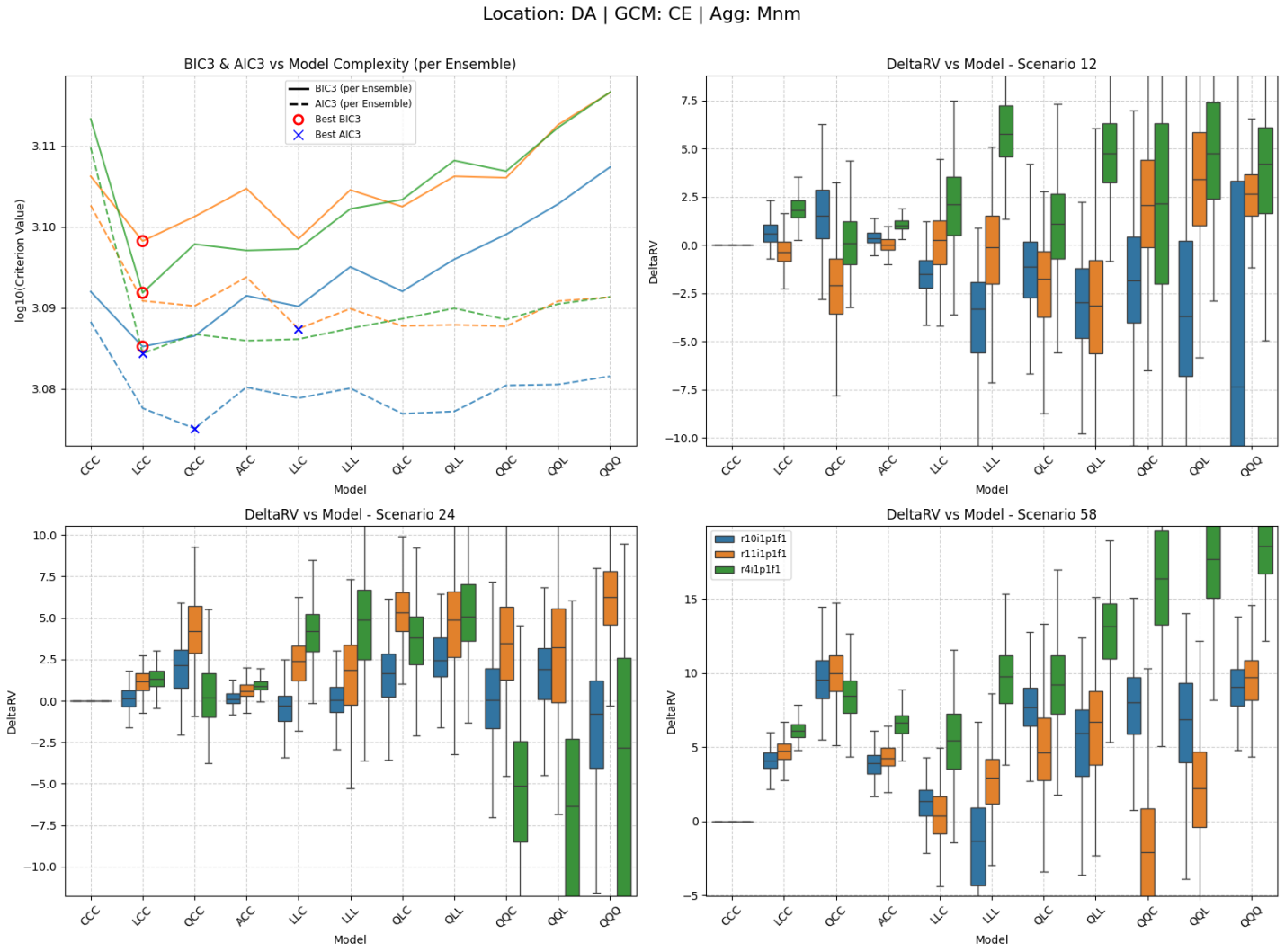

Figure SM42: Summary of scenario-coupled GEV regression for regional annual minima of the Dasht-e Lut region using `CESM2` GCM data. Top left: plots of BIC3 (solid line) and AIC3 (dashed line) for each available ensemble (distinguished by colour, see Table 2 of the main text and legend in bottom-right panel); optimal model choice using BIC3 (AIC3) indicated using red disc (blue cross). Top right: box-whisker plots summarising the distribution of the difference in the 100-year return value between 2025 and 2125 (ΔQ_1; see Equation 7) for climate scenario `SSP126` as a function of fitted model complexity (x-axis) and ensemble (distinguished by colour, with consistent ensemble colouring across panels); location of horizontal centre line of each box indicates posterior median of ΔQ_1; location of top (bottom) side of each box indicates 75%ile (25%ile) point, and top (bottom) of whiskers the 97.5%ile (2.5%ile) point of the posterior distribution. Bottom left and right: analogues of top right for scenarios `SSP245` (ΔQ_2) and `SSP585` (ΔQ_3). Value of ΔQ_j, $j = 1, 2, 3$ under model CCC is identically zero, and is omitted from bottom panels when convenient to provide better illustration of the variation in estimates under more complex models. For comparison with Figure 6 of the main text.

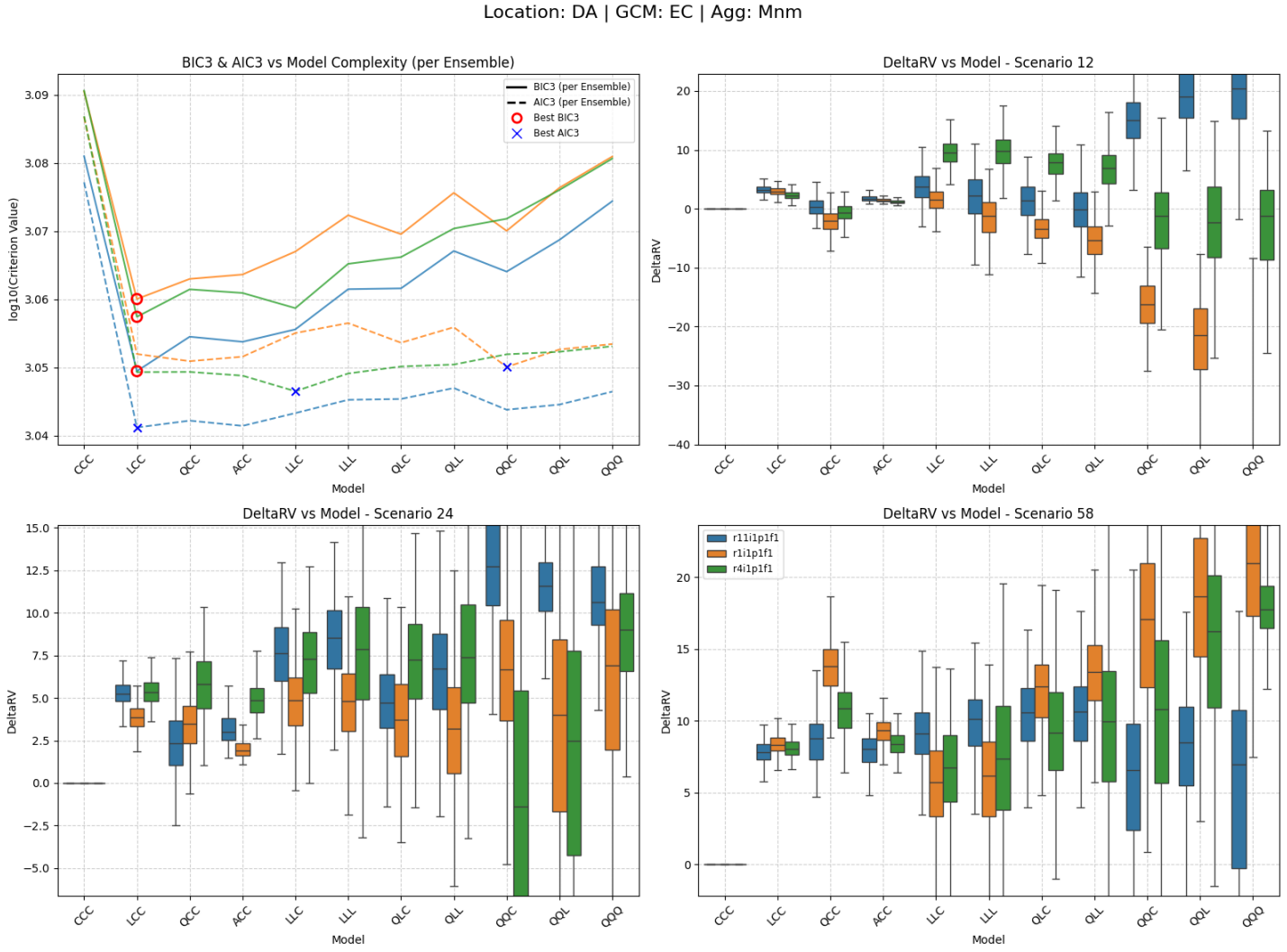

Figure SM43: Summary of scenario-coupled GEV regression for regional annual minima of the Dasht-e Lut region using `EC-Earth3` GCM data. Top left: plots of BIC3 (solid line) and AIC3 (dashed line) for each available ensemble (distinguished by colour, see Table 2 of the main text and legend in bottom-right panel); optimal model choice using BIC3 (AIC3) indicated using red disc (blue cross). Top right: box-whisker plots summarising the distribution of the difference in the 100-year return value between 2025 and 2125 (ΔQ_1; see Equation 7) for climate scenario `SSP126` as a function of fitted model complexity (x-axis) and ensemble (distinguished by colour, with consistent ensemble colouring across panels); location of horizontal centre line of each box indicates posterior median of ΔQ_1; location of top (bottom) side of each box indicates 75%ile (25%ile) point, and top (bottom) of whiskers the 97.5%ile (2.5%ile) point of the posterior distribution. Bottom left and right: analogues of top right for scenarios `SSP245` (ΔQ_2) and `SSP585` (ΔQ_3). Value of ΔQ_j, $j = 1, 2, 3$ under model CCC is identically zero, and is omitted from bottom panels when convenient to provide better illustration of the variation in estimates under more complex models. For comparison with Figure 6 of the main text.

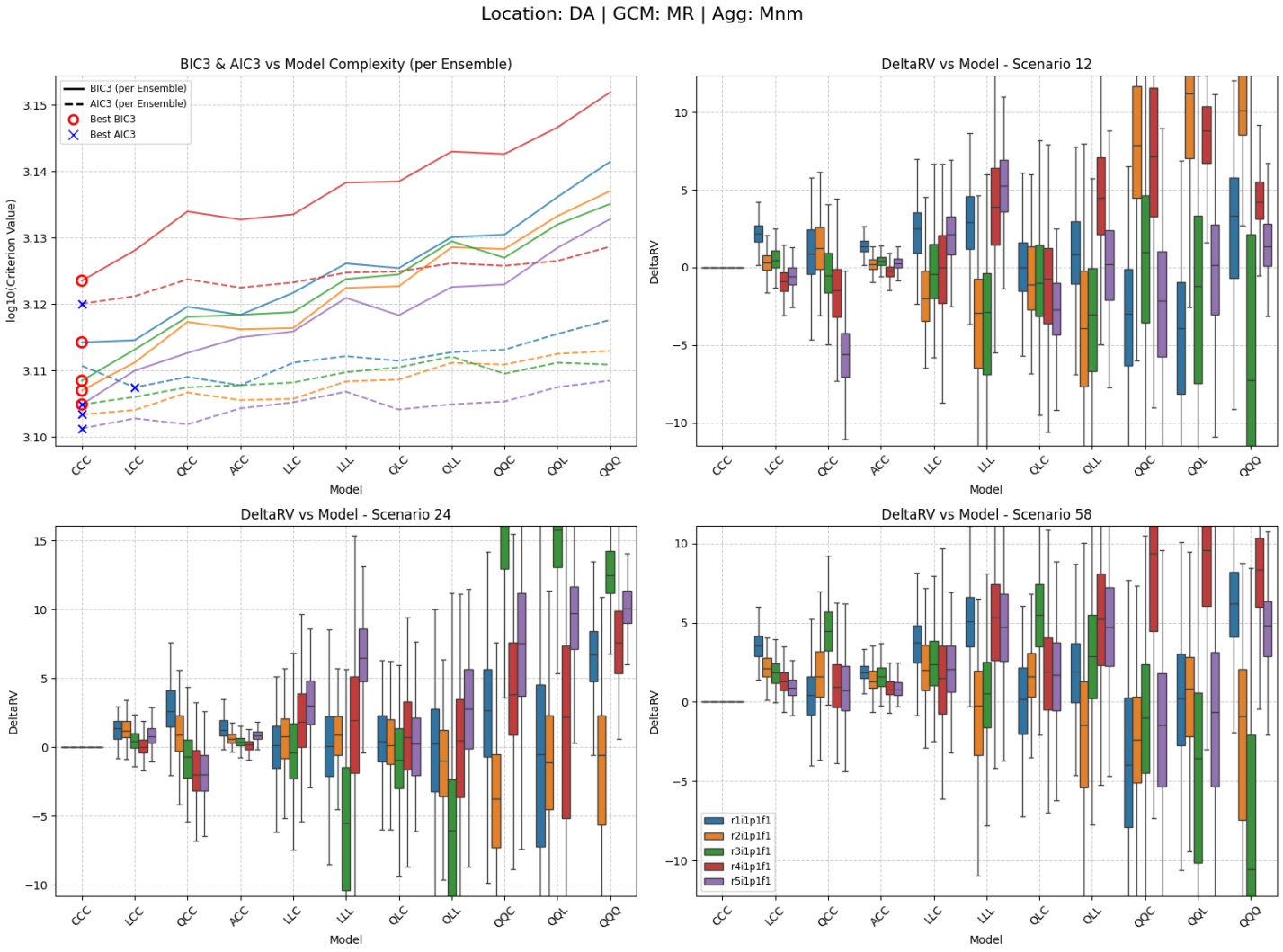

Figure SM44: Summary of scenario-coupled GEV regression for regional annual minima of the Dasht-e Lut region using `MRI-ESM2-0` GCM data. Top left: plots of BIC3 (solid line) and AIC3 (dashed line) for each available ensemble (distinguished by colour, see Table 2 of the main text and legend in bottom-right panel); optimal model choice using BIC3 (AIC3) indicated using red disc (blue cross). Top right: box-whisker plots summarising the distribution of the difference in the 100-year return value between 2025 and 2125 (ΔQ_1; see Equation 7) for climate scenario `SSP126` as a function of fitted model complexity (x-axis) and ensemble (distinguished by colour, with consistent ensemble colouring across panels); location of horizontal centre line of each box indicates posterior median of ΔQ_1; location of top (bottom) side of each box indicates 75%ile (25%ile) point, and top (bottom) of whiskers the 97.5%ile (2.5%ile) point of the posterior distribution. Bottom left and right: analogues of top right for scenarios `SSP245` (ΔQ_2) and `SSP585` (ΔQ_3). Value of ΔQ_j, $j = 1, 2, 3$ under model CCC is identically zero, and is omitted from bottom panels when convenient to provide better illustration of the variation in estimates under more complex models. For comparison with Figure 6 of the main text.

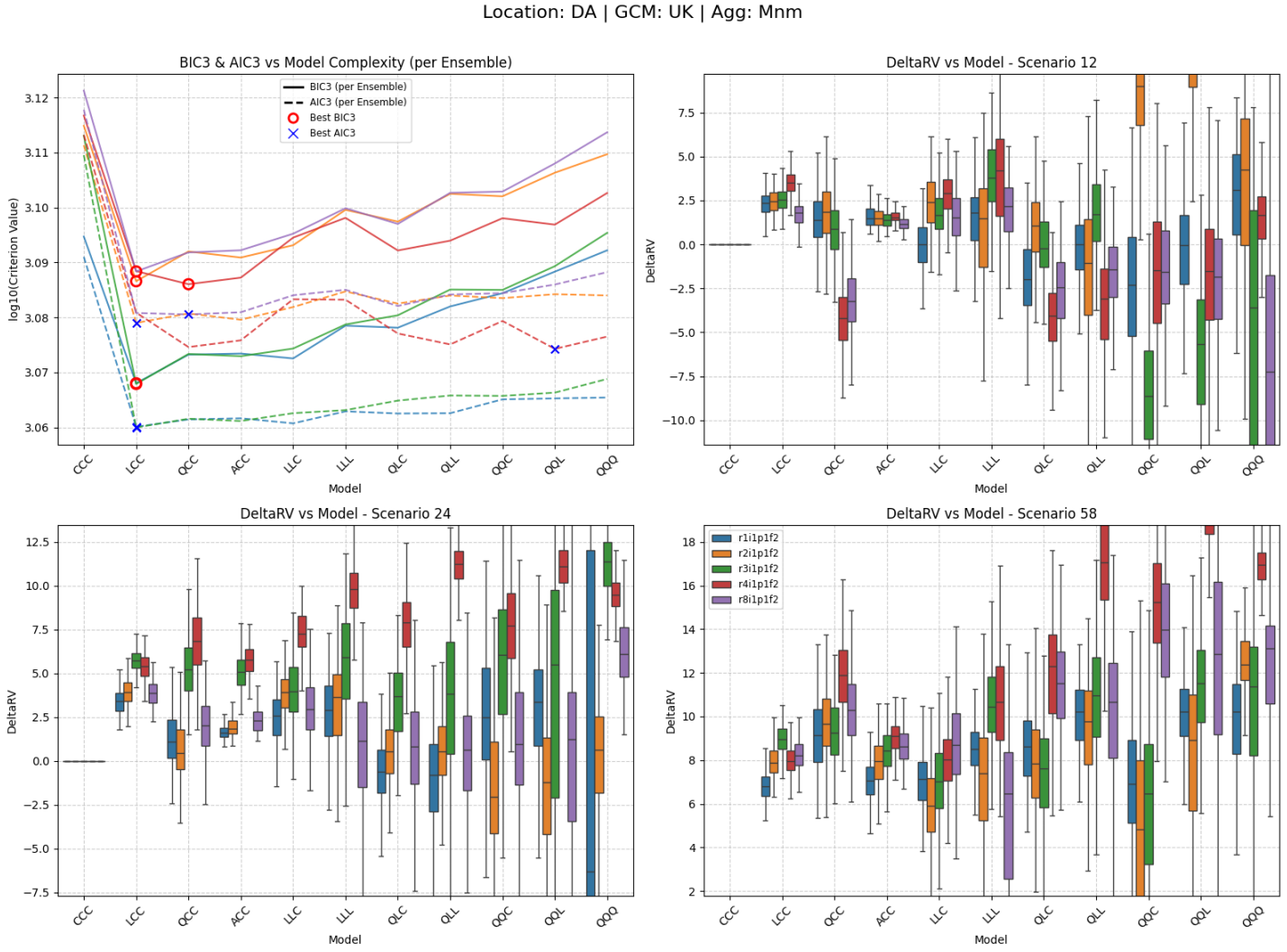

Figure SM45: Summary of scenario-coupled GEV regression for regional annual minima of the Dasht-e Lut region using `UKESM1-0-LL` GCM data. Top left: plots of BIC3 (solid line) and AIC3 (dashed line) for each available ensemble (distinguished by colour, see Table 2 of the main text and legend in bottom-right panel); optimal model choice using BIC3 (AIC3) indicated using red disc (blue cross). Top right: box-whisker plots summarising the distribution of the difference in the 100-year return value between 2025 and 2125 (ΔQ_1; see Equation 7) for climate scenario `SSP126` as a function of fitted model complexity (x-axis) and ensemble (distinguished by colour, with consistent ensemble colouring across panels); location of horizontal centre line of each box indicates posterior median of ΔQ_1; location of top (bottom) side of each box indicates 75%ile (25%ile) point, and top (bottom) of whiskers the 97.5%ile (2.5%ile) point of the posterior distribution. Bottom left and right: analogues of top right for scenarios `SSP245` (ΔQ_2) and `SSP585` (ΔQ_3). Value of ΔQ_j, $j = 1, 2, 3$ under model CCC is identically zero, and is omitted from bottom panels when convenient to provide better illustration of the variation in estimates under more complex models. For comparison with Figure 6 of the main text.

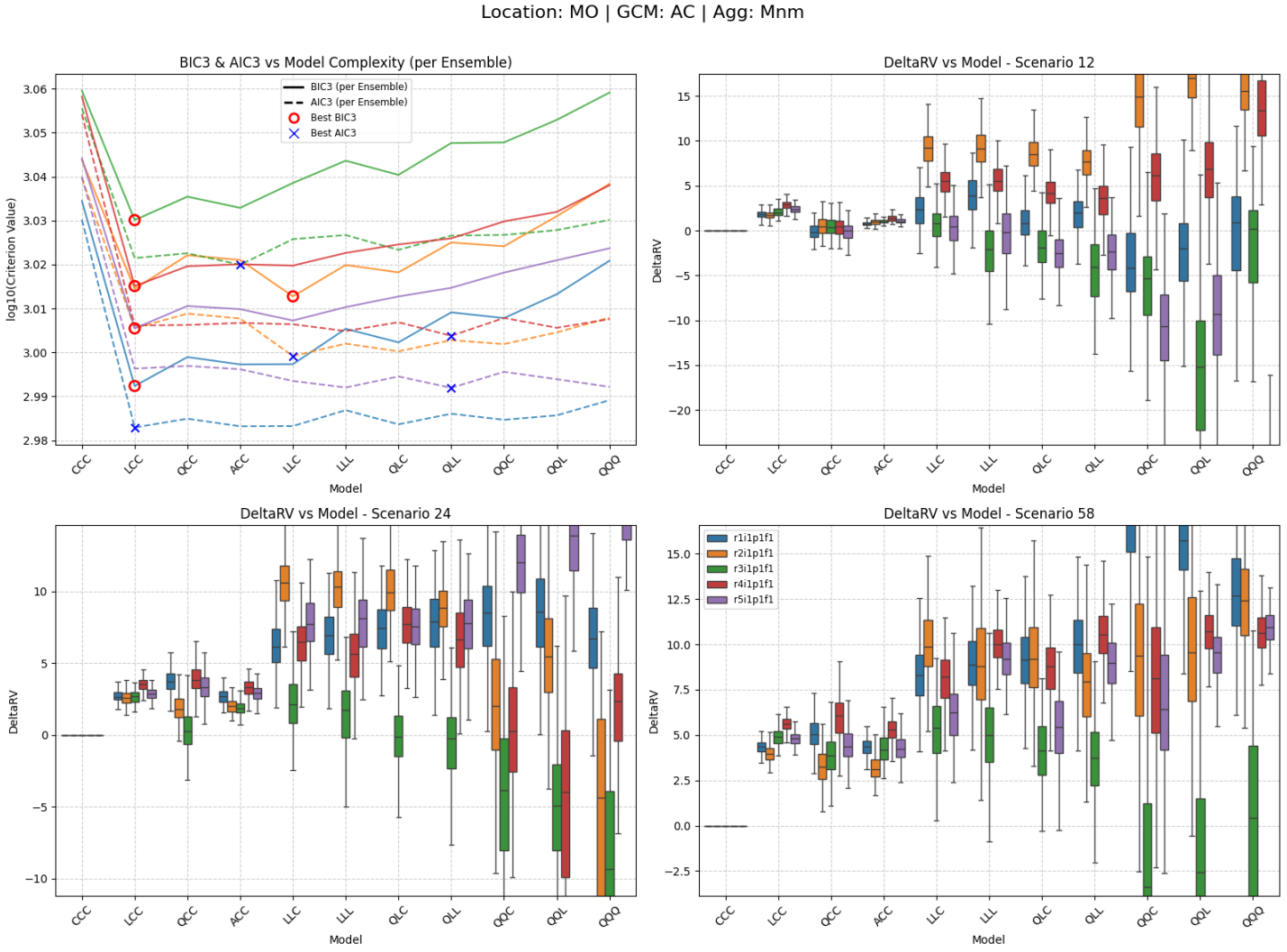

Figure SM46: Summary of scenario-coupled GEV regression for regional annual minima of the Mojave region using `ACCESS-CM2` GCM data. Top left: plots of BIC3 (solid line) and AIC3 (dashed line) for each available ensemble (distinguished by colour, see Table 2 of the main text and legend in bottom-right panel); optimal model choice using BIC3 (AIC3) indicated using red disc (blue cross). Top right: box-whisker plots summarising the distribution of the difference in the 100-year return value between 2025 and 2125 (ΔQ_1; see Equation 7) for climate scenario `SSP126` as a function of fitted model complexity (x-axis) and ensemble (distinguished by colour, with consistent ensemble colouring across panels); location of horizontal centre line of each box indicates posterior median of ΔQ_1; location of top (bottom) side of each box indicates 75%ile (25%ile) point, and top (bottom) of whiskers the 97.5%ile (2.5%ile) point of the posterior distribution. Bottom left and right: analogues of top right for scenarios `SSP245` (ΔQ_2) and `SSP585` (ΔQ_3). Value of ΔQ_j, $j = 1, 2, 3$ under model CCC is identically zero, and is omitted from bottom panels when convenient to provide better illustration of the variation in estimates under more complex models. For comparison with Figure 6 of the main text.

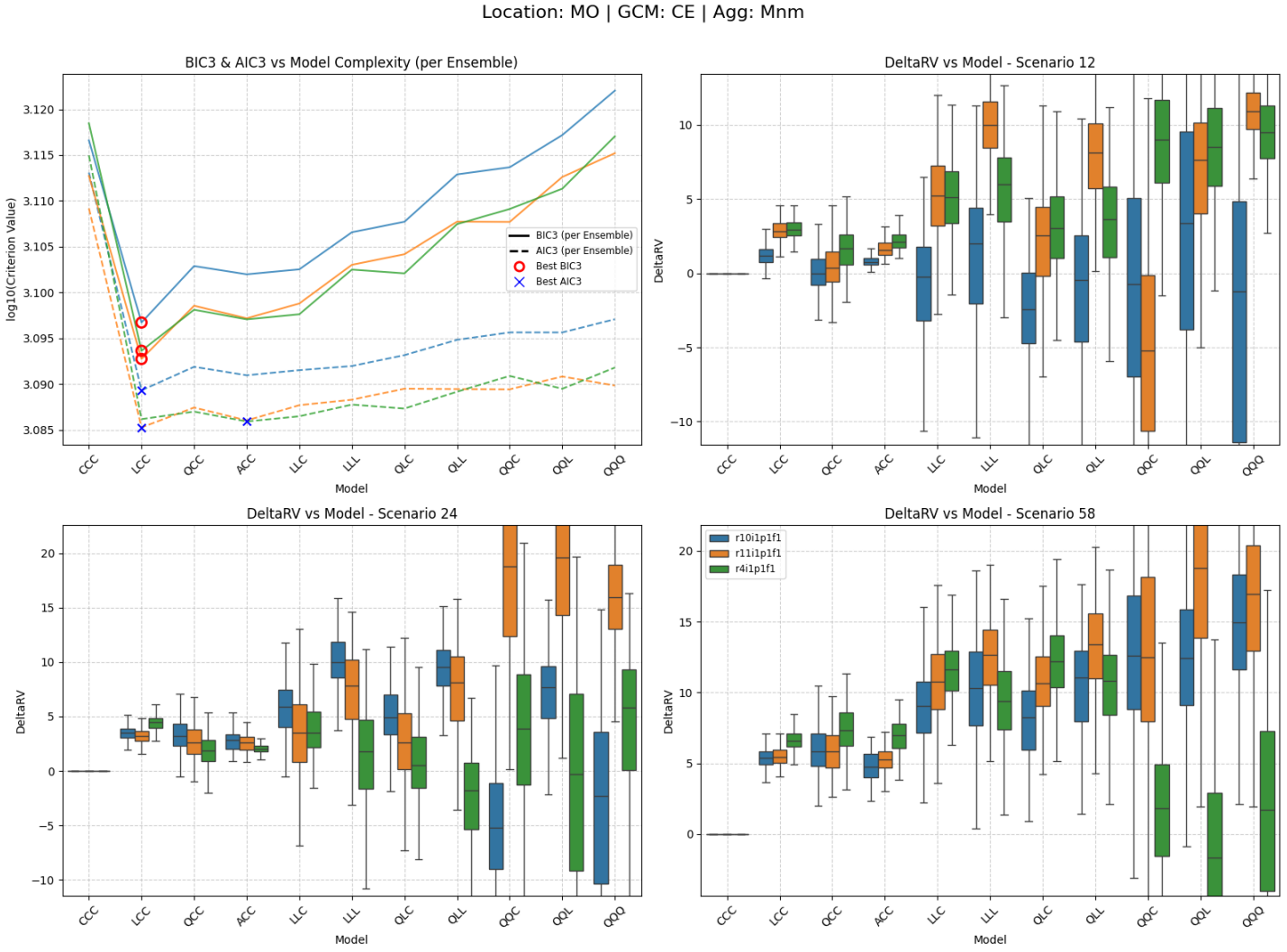

Figure SM47: Summary of scenario-coupled GEV regression for regional annual minima of the Mojave region using `CESM2` GCM data. Top left: plots of BIC3 (solid line) and AIC3 (dashed line) for each available ensemble (distinguished by colour, see Table 2 of the main text and legend in bottom-right panel); optimal model choice using BIC3 (AIC3) indicated using red disc (blue cross). Top right: box-whisker plots summarising the distribution of the difference in the 100-year return value between 2025 and 2125 (ΔQ_1; see Equation 7) for climate scenario `SSP126` as a function of fitted model complexity (x-axis) and ensemble (distinguished by colour, with consistent ensemble colouring across panels); location of horizontal centre line of each box indicates posterior median of ΔQ_1; location of top (bottom) side of each box indicates 75%ile (25%ile) point, and top (bottom) of whiskers the 97.5%ile (2.5%ile) point of the posterior distribution. Bottom left and right: analogues of top right for scenarios `SSP245` (ΔQ_2) and `SSP585` (ΔQ_3). Value of ΔQ_j, $j = 1, 2, 3$ under model CCC is identically zero, and is omitted from bottom panels when convenient to provide better illustration of the variation in estimates under more complex models. For comparison with Figure 6 of the main text.

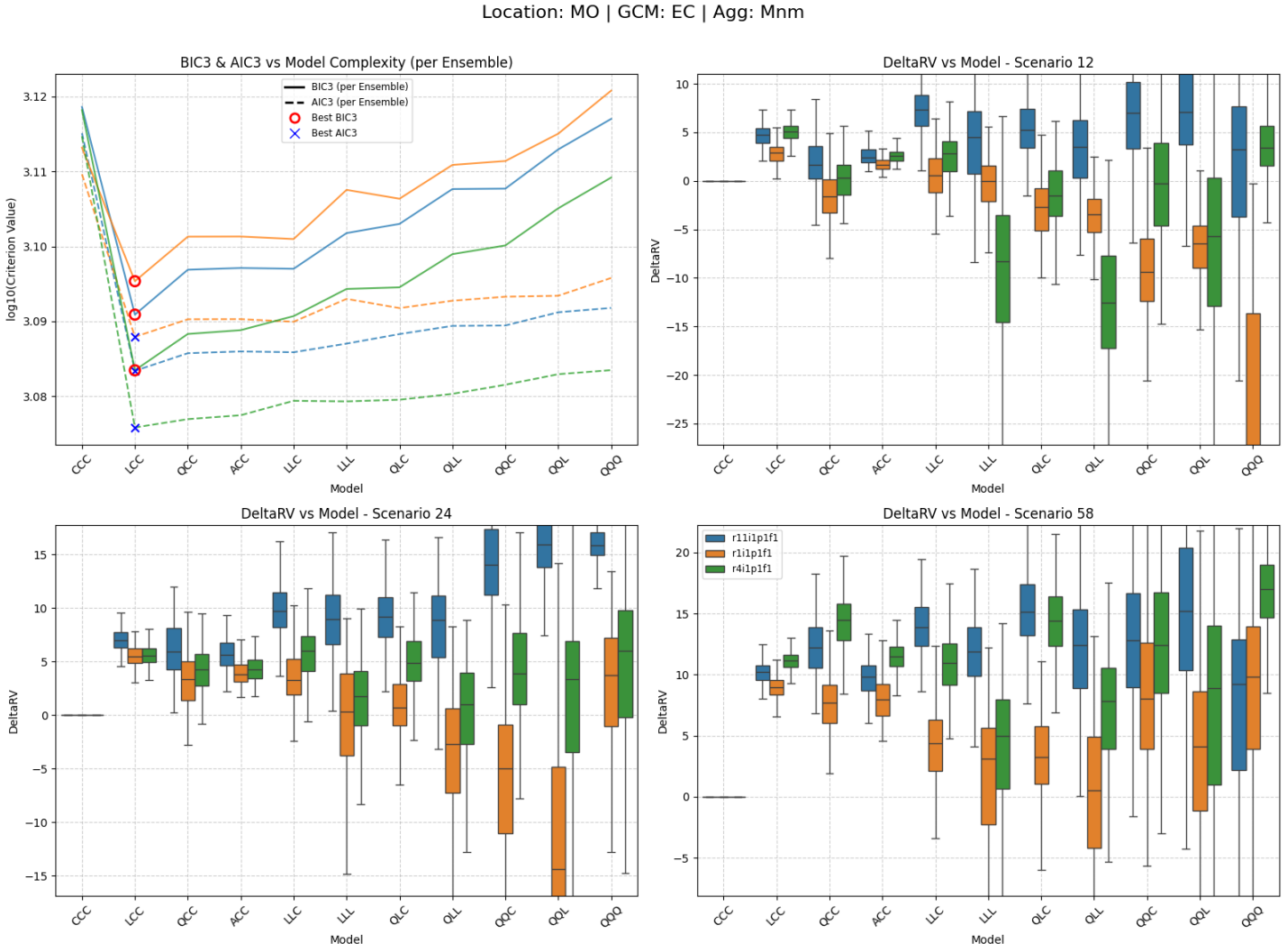

Figure SM48: Summary of scenario-coupled GEV regression for regional annual minima of the Mojave region using `EC-Earth3` GCM data. Top left: plots of BIC3 (solid line) and AIC3 (dashed line) for each available ensemble (distinguished by colour, see Table 2 of the main text and legend in bottom-right panel); optimal model choice using BIC3 (AIC3) indicated using red disc (blue cross). Top right: box-whisker plots summarising the distribution of the difference in the 100-year return value between 2025 and 2125 (ΔQ_1; see Equation 7) for climate scenario `SSP126` as a function of fitted model complexity (x-axis) and ensemble (distinguished by colour, with consistent ensemble colouring across panels); location of horizontal centre line of each box indicates posterior median of ΔQ_1; location of top (bottom) side of each box indicates 75%ile (25%ile) point, and top (bottom) of whiskers the 97.5%ile (2.5%ile) point of the posterior distribution. Bottom left and right: analogues of top right for scenarios `SSP245` (ΔQ_2) and `SSP585` (ΔQ_3). Value of ΔQ_j, $j = 1, 2, 3$ under model CCC is identically zero, and is omitted from bottom panels when convenient to provide better illustration of the variation in estimates under more complex models. For comparison with Figure 6 of the main text.

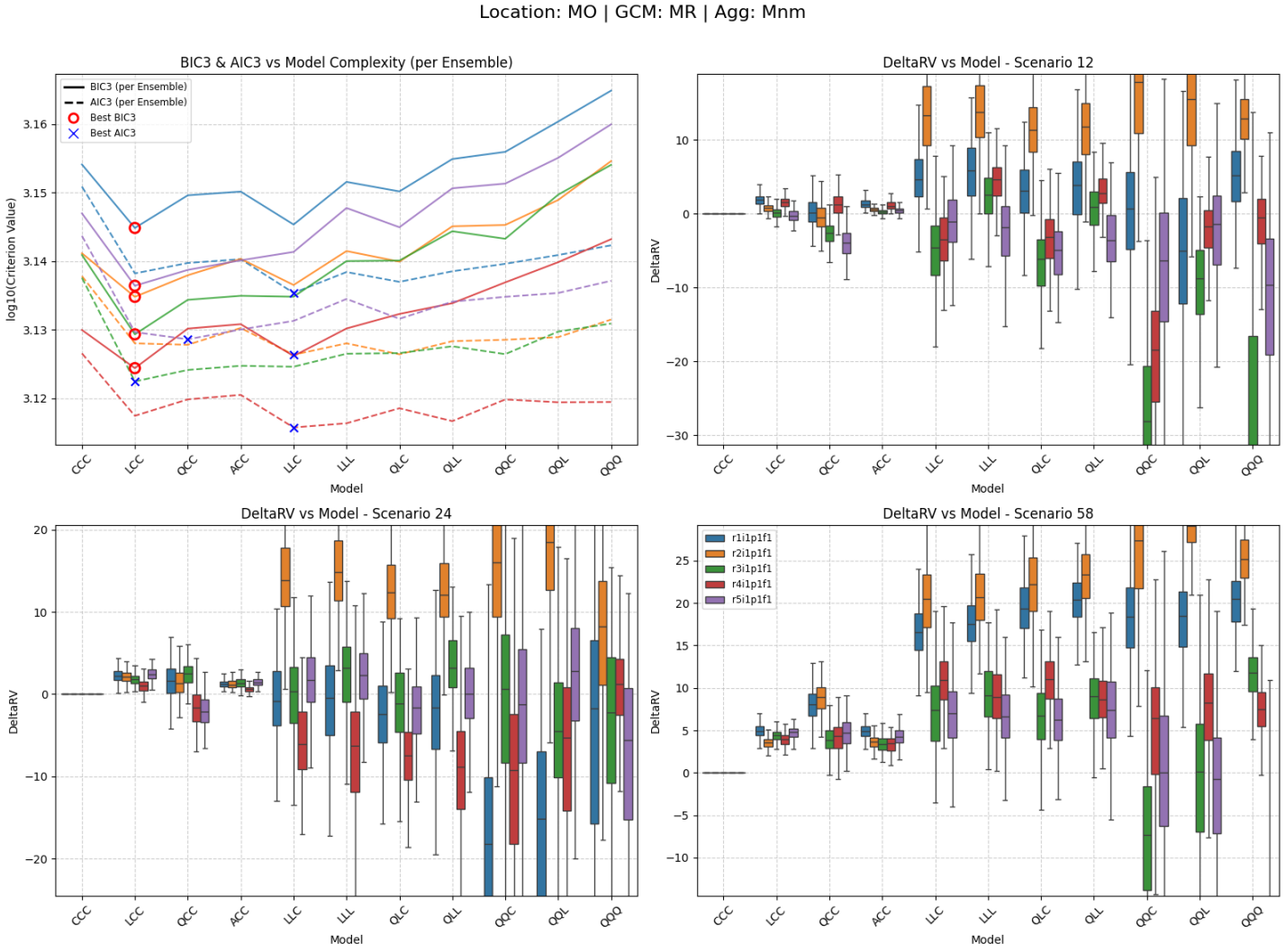

Figure SM49: Summary of scenario-coupled GEV regression for regional annual minima of the Mojave region using `MRI-ESM2-0` GCM data. Top left: plots of BIC3 (solid line) and AIC3 (dashed line) for each available ensemble (distinguished by colour, see Table 2 of the main text and legend in bottom-right panel); optimal model choice using BIC3 (AIC3) indicated using red disc (blue cross). Top right: box-whisker plots summarising the distribution of the difference in the 100-year return value between 2025 and 2125 (ΔQ_1; see Equation 7) for climate scenario `SSP126` as a function of fitted model complexity (x-axis) and ensemble (distinguished by colour, with consistent ensemble colouring across panels); location of horizontal centre line of each box indicates posterior median of ΔQ_1; location of top (bottom) side of each box indicates 75%ile (25%ile) point, and top (bottom) of whiskers the 97.5%ile (2.5%ile) point of the posterior distribution. Bottom left and right: analogues of top right for scenarios `SSP245` (ΔQ_2) and `SSP585` (ΔQ_3). Value of ΔQ_j, $j = 1, 2, 3$ under model CCC is identically zero, and is omitted from bottom panels when convenient to provide better illustration of the variation in estimates under more complex models. For comparison with Figure 6 of the main text.

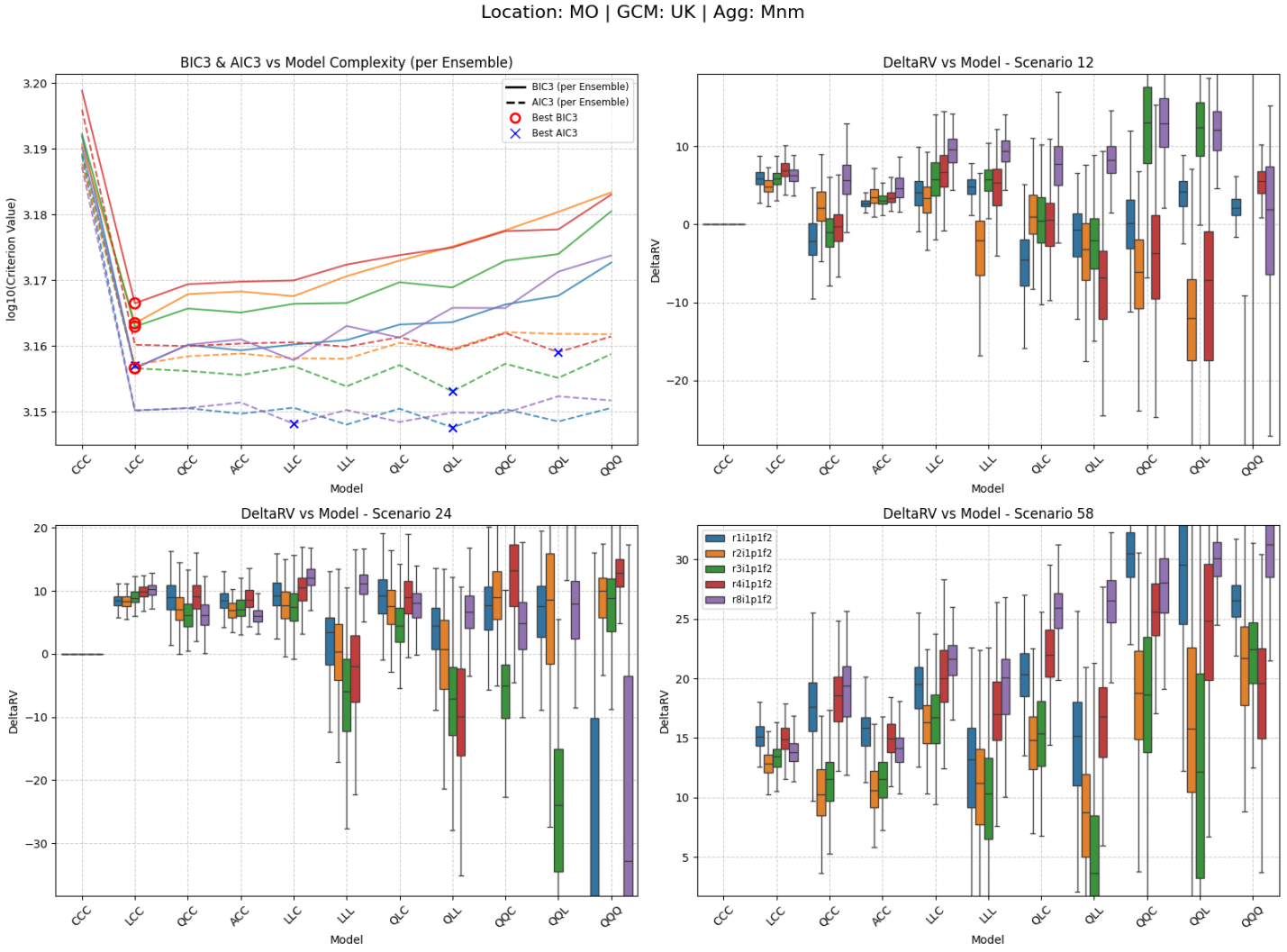

Figure SM50: Summary of scenario-coupled GEV regression for regional annual minima of the Mojave region using `UKESM1-0-LL` GCM data. Top left: plots of BIC3 (solid line) and AIC3 (dashed line) for each available ensemble (distinguished by colour, see Table 2 of the main text and legend in bottom-right panel); optimal model choice using BIC3 (AIC3) indicated using red disc (blue cross). Top right: box-whisker plots summarising the distribution of the difference in the 100-year return value between 2025 and 2125 (ΔQ_1; see Equation 7) for climate scenario `SSP126` as a function of fitted model complexity (x-axis) and ensemble (distinguished by colour, with consistent ensemble colouring across panels); location of horizontal centre line of each box indicates posterior median of ΔQ_1; location of top (bottom) side of each box indicates 75%ile (25%ile) point, and top (bottom) of whiskers the 97.5%ile (2.5%ile) point of the posterior distribution. Bottom left and right: analogues of top right for scenarios `SSP245` (ΔQ_2) and `SSP585` (ΔQ_3). Value of ΔQ_j, $j = 1, 2, 3$ under model CCC is identically zero, and is omitted from bottom panels when convenient to provide better illustration of the variation in estimates under more complex models. For comparison with Figure 6 of the main text.

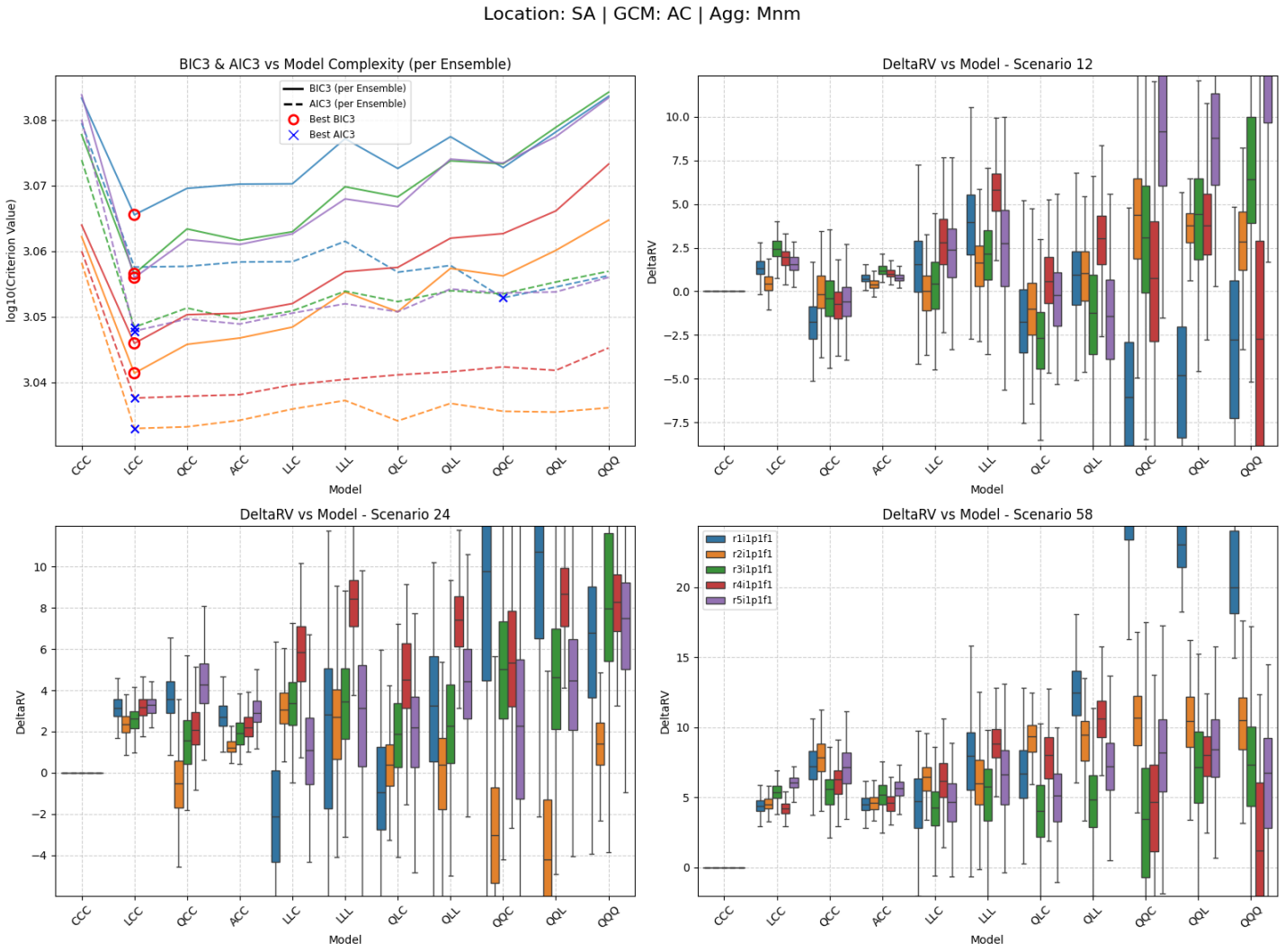

Figure SM51: Summary of scenario-coupled GEV regression for regional annual minima of the Sahara region using `ACCESS-CM2` GCM data. Top left: plots of BIC3 (solid line) and AIC3 (dashed line) for each available ensemble (distinguished by colour, see Table 2 of the main text and legend in bottom-right panel); optimal model choice using BIC3 (AIC3) indicated using red disc (blue cross). Top right: box-whisker plots summarising the distribution of the difference in the 100-year return value between 2025 and 2125 (ΔQ_1; see Equation 7) for climate scenario `SSP126` as a function of fitted model complexity (x-axis) and ensemble (distinguished by colour, with consistent ensemble colouring across panels); location of horizontal centre line of each box indicates posterior median of ΔQ_1; location of top (bottom) side of each box indicates 75%ile (25%ile) point, and top (bottom) of whiskers the 97.5%ile (2.5%ile) point of the posterior distribution. Bottom left and right: analogues of top right for scenarios `SSP245` (ΔQ_2) and `SSP585` (ΔQ_3). Value of ΔQ_j, $j = 1, 2, 3$ under model CCC is identically zero, and is omitted from bottom panels when convenient to provide better illustration of the variation in estimates under more complex models. For comparison with Figure 6 of the main text.

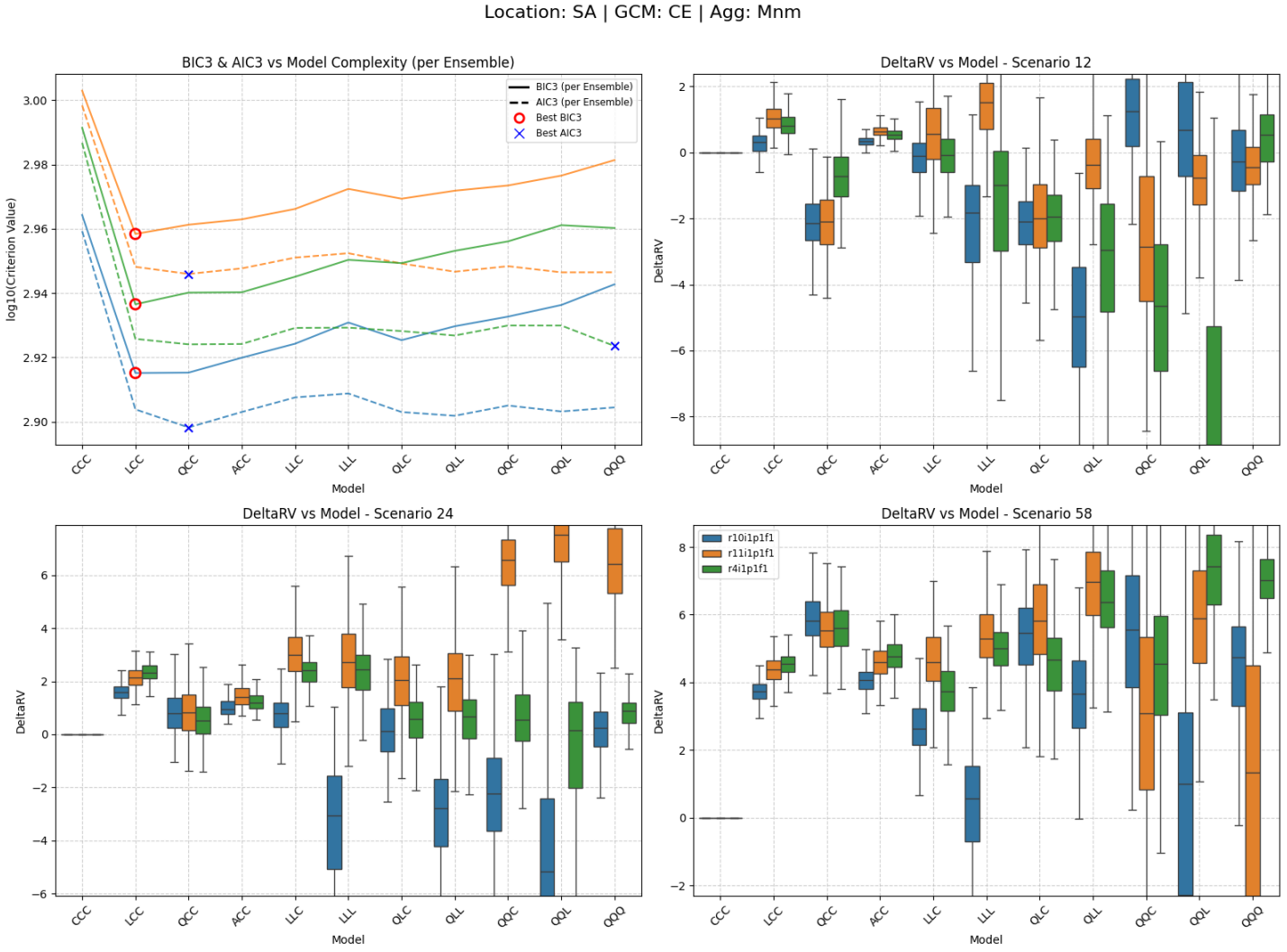

Figure SM52: Summary of scenario-coupled GEV regression for regional annual minima of the Sahara region using `CESM2` GCM data. Top left: plots of BIC3 (solid line) and AIC3 (dashed line) for each available ensemble (distinguished by colour, see Table 2 of the main text and legend in bottom-right panel); optimal model choice using BIC3 (AIC3) indicated using red disc (blue cross). Top right: box-whisker plots summarising the distribution of the difference in the 100-year return value between 2025 and 2125 (ΔQ_1; see Equation 7) for climate scenario `SSP126` as a function of fitted model complexity (x-axis) and ensemble (distinguished by colour, with consistent ensemble colouring across panels); location of horizontal centre line of each box indicates posterior median of ΔQ_1; location of top (bottom) side of each box indicates 75%ile (25%ile) point, and top (bottom) of whiskers the 97.5%ile (2.5%ile) point of the posterior distribution. Bottom left and right: analogues of top right for scenarios `SSP245` (ΔQ_2) and `SSP585` (ΔQ_3). Value of ΔQ_j, $j = 1, 2, 3$ under model CCC is identically zero, and is omitted from bottom panels when convenient to provide better illustration of the variation in estimates under more complex models. For comparison with Figure 6 of the main text.

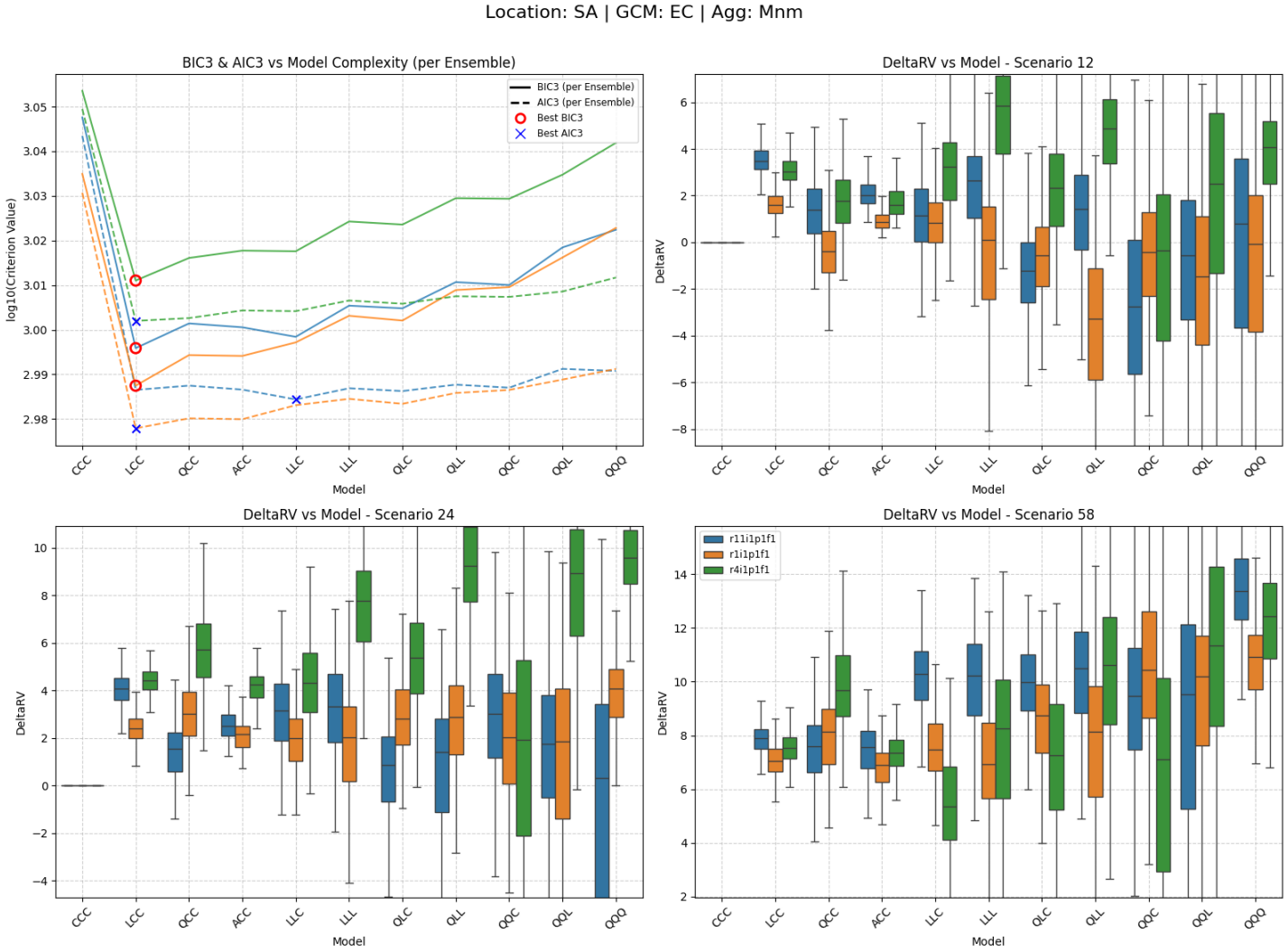

Figure SM53: Summary of scenario-coupled GEV regression for regional annual minima of the Sahara region using `EC-Earth3` GCM data. Top left: plots of BIC3 (solid line) and AIC3 (dashed line) for each available ensemble (distinguished by colour, see Table 2 of the main text and legend in bottom-right panel); optimal model choice using BIC3 (AIC3) indicated using red disc (blue cross). Top right: box-whisker plots summarising the distribution of the difference in the 100-year return value between 2025 and 2125 (ΔQ_1; see Equation 7) for climate scenario `SSP126` as a function of fitted model complexity (x-axis) and ensemble (distinguished by colour, with consistent ensemble colouring across panels); location of horizontal centre line of each box indicates posterior median of ΔQ_1; location of top (bottom) side of each box indicates 75%ile (25%ile) point, and top (bottom) of whiskers the 97.5%ile (2.5%ile) point of the posterior distribution. Bottom left and right: analogues of top right for scenarios `SSP245` (ΔQ_2) and `SSP585` (ΔQ_3). Value of ΔQ_j, $j = 1, 2, 3$ under model CCC is identically zero, and is omitted from bottom panels when convenient to provide better illustration of the variation in estimates under more complex models. For comparison with Figure 6 of the main text.

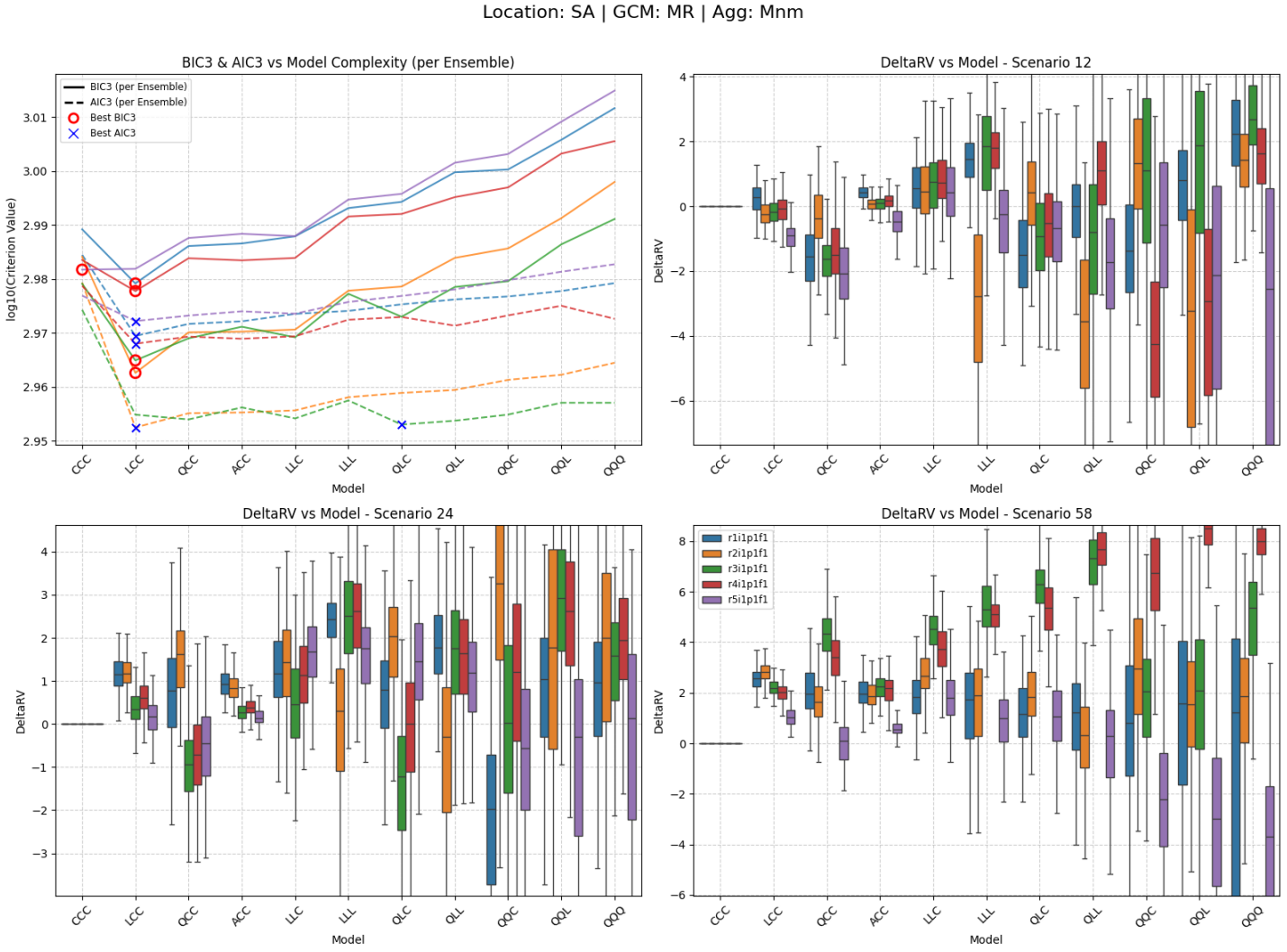

Figure SM54: Summary of scenario-coupled GEV regression for regional annual minima of the Sahara region using `MRI-ESM2-0` GCM data. Top left: plots of BIC3 (solid line) and AIC3 (dashed line) for each available ensemble (distinguished by colour, see Table 2 of the main text and legend in bottom-right panel); optimal model choice using BIC3 (AIC3) indicated using red disc (blue cross). Top right: box-whisker plots summarising the distribution of the difference in the 100-year return value between 2025 and 2125 (ΔQ_1; see Equation 7) for climate scenario `SSP126` as a function of fitted model complexity (x-axis) and ensemble (distinguished by colour, with consistent ensemble colouring across panels); location of horizontal centre line of each box indicates posterior median of ΔQ_1; location of top (bottom) side of each box indicates 75%ile (25%ile) point, and top (bottom) of whiskers the 97.5%ile (2.5%ile) point of the posterior distribution. Bottom left and right: analogues of top right for scenarios `SSP245` (ΔQ_2) and `SSP585` (ΔQ_3). Value of ΔQ_j, $j = 1, 2, 3$ under model CCC is identically zero, and is omitted from bottom panels when convenient to provide better illustration of the variation in estimates under more complex models. For comparison with Figure 6 of the main text.

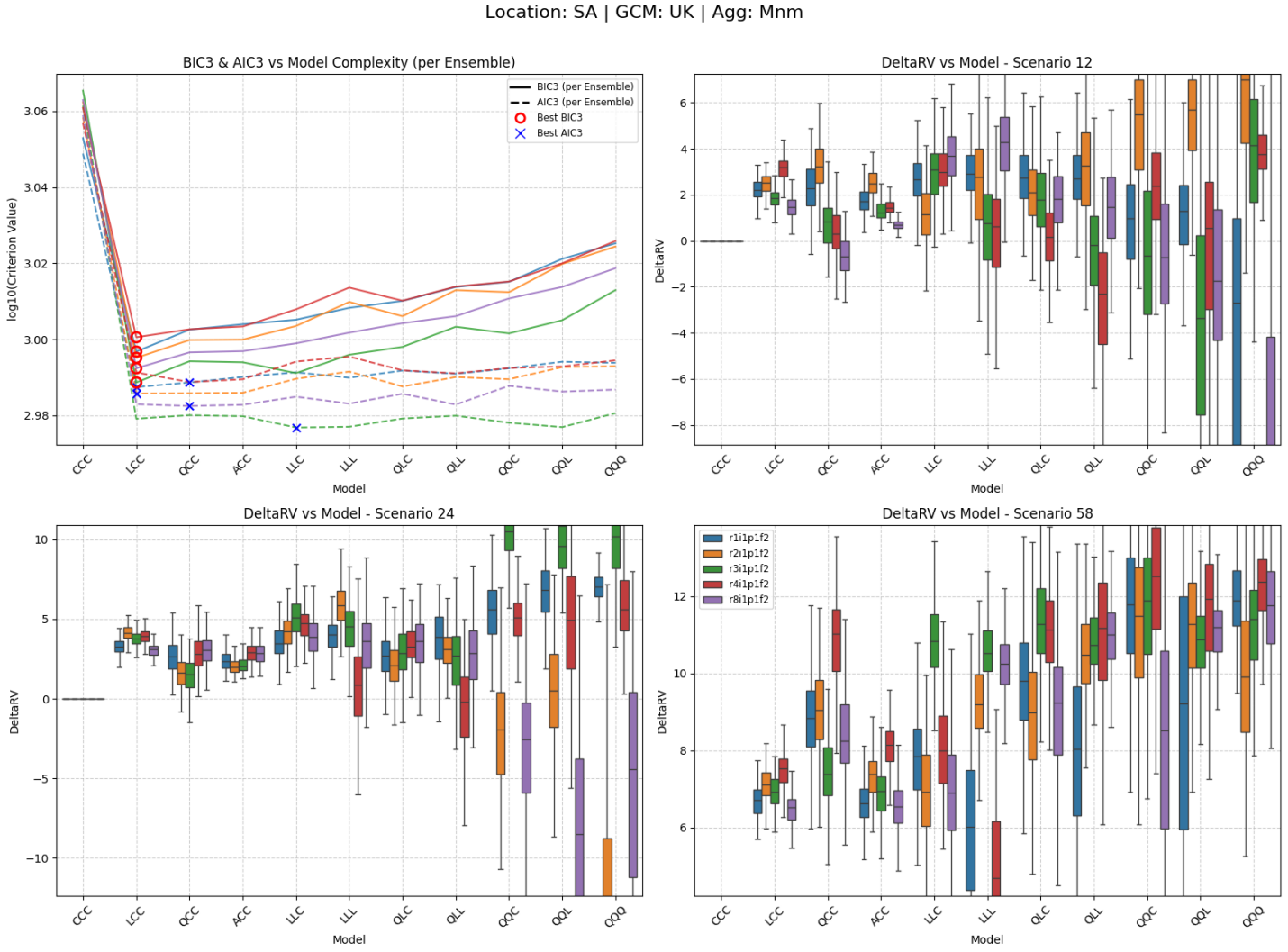

Figure SM55: Summary of scenario-coupled GEV regression for regional annual minima of the Sahara region using `UKESM1-0-LL` GCM data. Top left: plots of BIC3 (solid line) and AIC3 (dashed line) for each available ensemble (distinguished by colour, see Table 2 of the main text and legend in bottom-right panel); optimal model choice using BIC3 (AIC3) indicated using red disc (blue cross). Top right: box-whisker plots summarising the distribution of the difference in the 100-year return value between 2025 and 2125 (ΔQ_1; see Equation 7) for climate scenario `SSP126` as a function of fitted model complexity (x-axis) and ensemble (distinguished by colour, with consistent ensemble colouring across panels); location of horizontal centre line of each box indicates posterior median of ΔQ_1; location of top (bottom) side of each box indicates 75%ile (25%ile) point, and top (bottom) of whiskers the 97.5%ile (2.5%ile) point of the posterior distribution. Bottom left and right: analogues of top right for scenarios `SSP245` (ΔQ_2) and `SSP585` (ΔQ_3). Value of ΔQ_j, $j = 1, 2, 3$ under model CCC is identically zero, and is omitted from bottom panels when convenient to provide better illustration of the variation in estimates under more complex models. For comparison with Figure 6 of the main text.

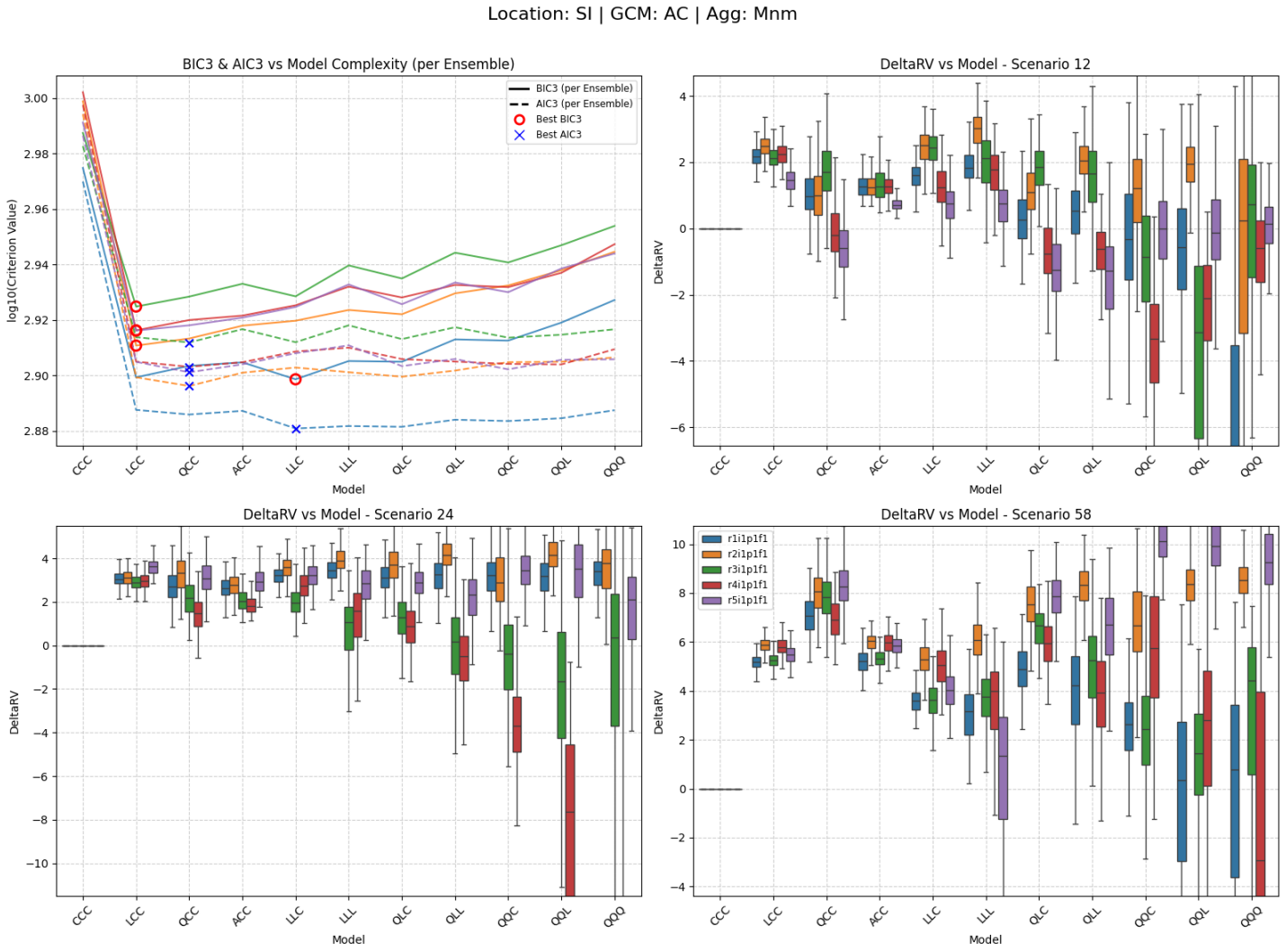

Figure SM56: Summary of scenario-coupled GEV regression for regional annual minima of the Simpson region using `ACCESS-CM2` GCM data. Top left: plots of BIC3 (solid line) and AIC3 (dashed line) for each available ensemble (distinguished by colour, see Table 2 of the main text and legend in bottom-right panel); optimal model choice using BIC3 (AIC3) indicated using red disc (blue cross). Top right: box-whisker plots summarising the distribution of the difference in the 100-year return value between 2025 and 2125 (ΔQ_1; see Equation 7) for climate scenario `SSP126` as a function of fitted model complexity (x-axis) and ensemble (distinguished by colour, with consistent ensemble colouring across panels); location of horizontal centre line of each box indicates posterior median of ΔQ_1; location of top (bottom) side of each box indicates 75%ile (25%ile) point, and top (bottom) of whiskers the 97.5%ile (2.5%ile) point of the posterior distribution. Bottom left and right: analogues of top right for scenarios `SSP245` (ΔQ_2) and `SSP585` (ΔQ_3). Value of ΔQ_j, $j = 1, 2, 3$ under model CCC is identically zero, and is omitted from bottom panels when convenient to provide better illustration of the variation in estimates under more complex models. For comparison with Figure 6 of the main text.

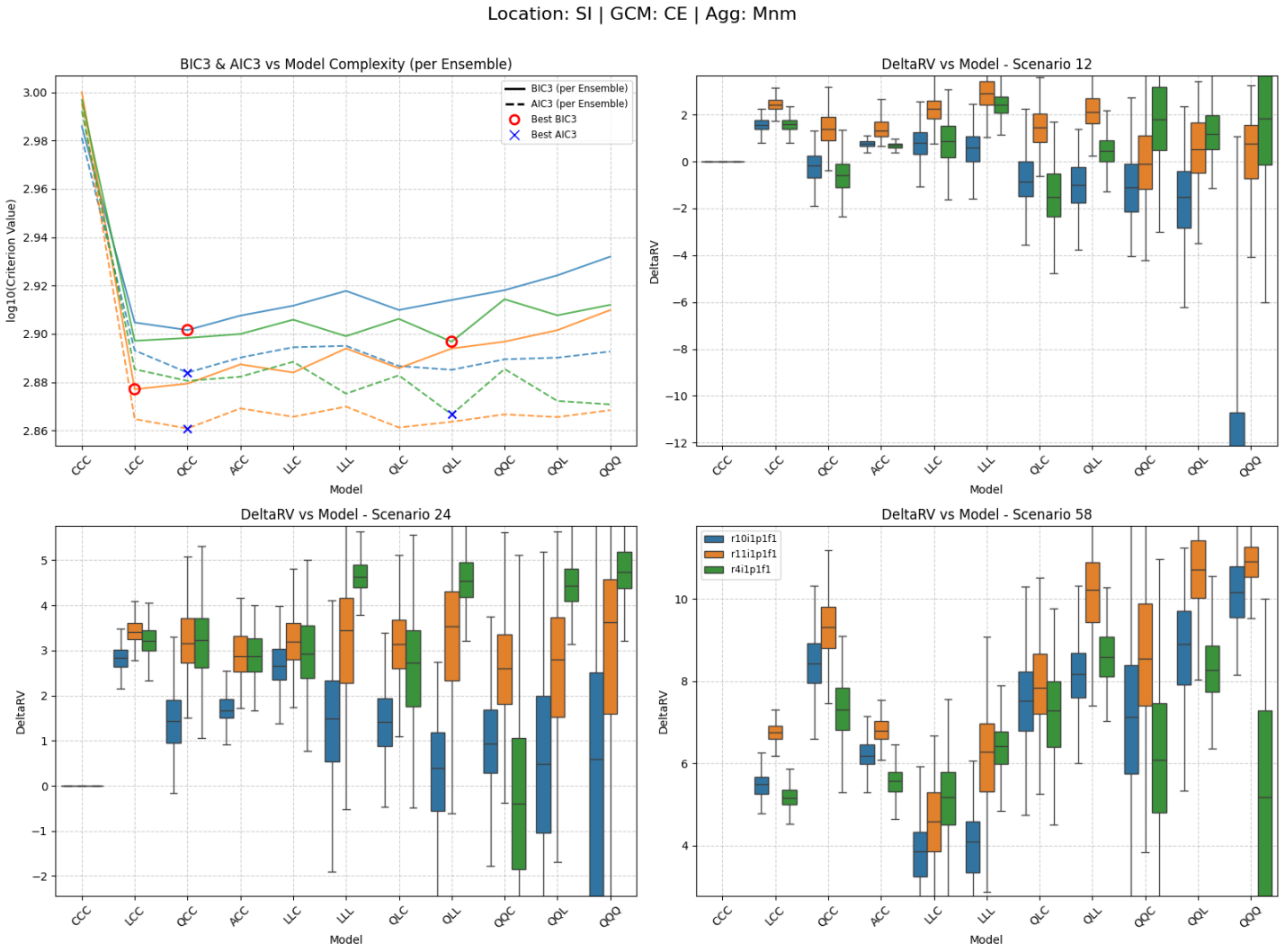

Figure SM57: Summary of scenario-coupled GEV regression for regional annual minima of the Simpson region using `CESM2` GCM data. Top left: plots of BIC3 (solid line) and AIC3 (dashed line) for each available ensemble (distinguished by colour, see Table 2 of the main text and legend in bottom-right panel); optimal model choice using BIC3 (AIC3) indicated using red disc (blue cross). Top right: box-whisker plots summarising the distribution of the difference in the 100-year return value between 2025 and 2125 (ΔQ_1; see Equation 7) for climate scenario `SSP126` as a function of fitted model complexity (x-axis) and ensemble (distinguished by colour, with consistent ensemble colouring across panels); location of horizontal centre line of each box indicates posterior median of ΔQ_1; location of top (bottom) side of each box indicates 75%ile (25%ile) point, and top (bottom) of whiskers the 97.5%ile (2.5%ile) point of the posterior distribution. Bottom left and right: analogues of top right for scenarios `SSP245` (ΔQ_2) and `SSP585` (ΔQ_3). Value of ΔQ_j, $j = 1, 2, 3$ under model CCC is identically zero, and is omitted from bottom panels when convenient to provide better illustration of the variation in estimates under more complex models. For comparison with Figure 6 of the main text.

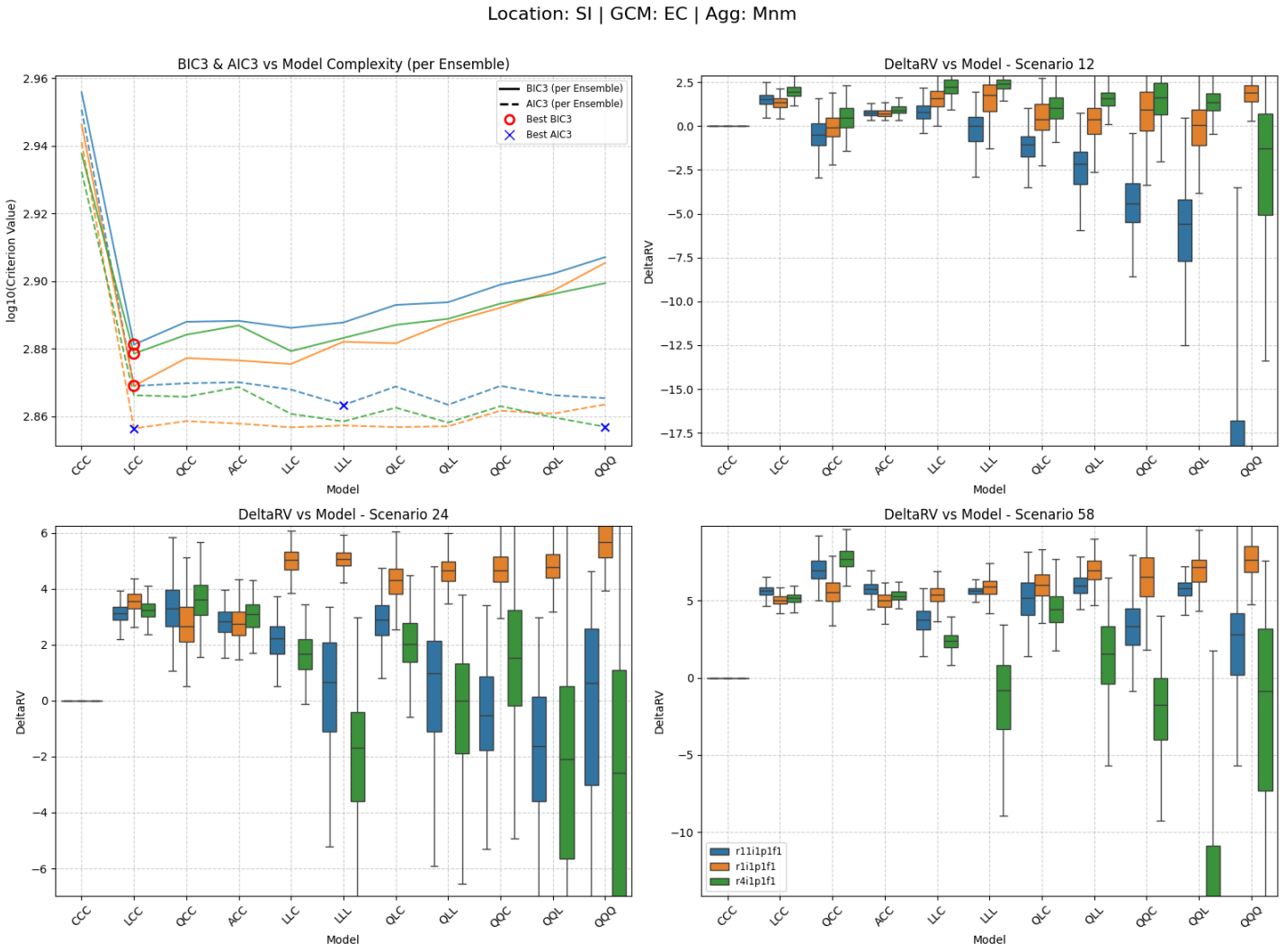

Figure SM58: Summary of scenario-coupled GEV regression for regional annual minima of the Simpson region using `EC-Earth3` GCM data. Top left: plots of BIC3 (solid line) and AIC3 (dashed line) for each available ensemble (distinguished by colour, see Table 2 of the main text and legend in bottom-right panel); optimal model choice using BIC3 (AIC3) indicated using red disc (blue cross). Top right: box-whisker plots summarising the distribution of the difference in the 100-year return value between 2025 and 2125 (ΔQ_1; see Equation 7) for climate scenario `SSP126` as a function of fitted model complexity (x-axis) and ensemble (distinguished by colour, with consistent ensemble colouring across panels); location of horizontal centre line of each box indicates posterior median of ΔQ_1; location of top (bottom) side of each box indicates 75%ile (25%ile) point, and top (bottom) of whiskers the 97.5%ile (2.5%ile) point of the posterior distribution. Bottom left and right: analogues of top right for scenarios `SSP245` (ΔQ_2) and `SSP585` (ΔQ_3). Value of ΔQ_j, $j = 1, 2, 3$ under model CCC is identically zero, and is omitted from bottom panels when convenient to provide better illustration of the variation in estimates under more complex models. For comparison with Figure 6 of the main text.

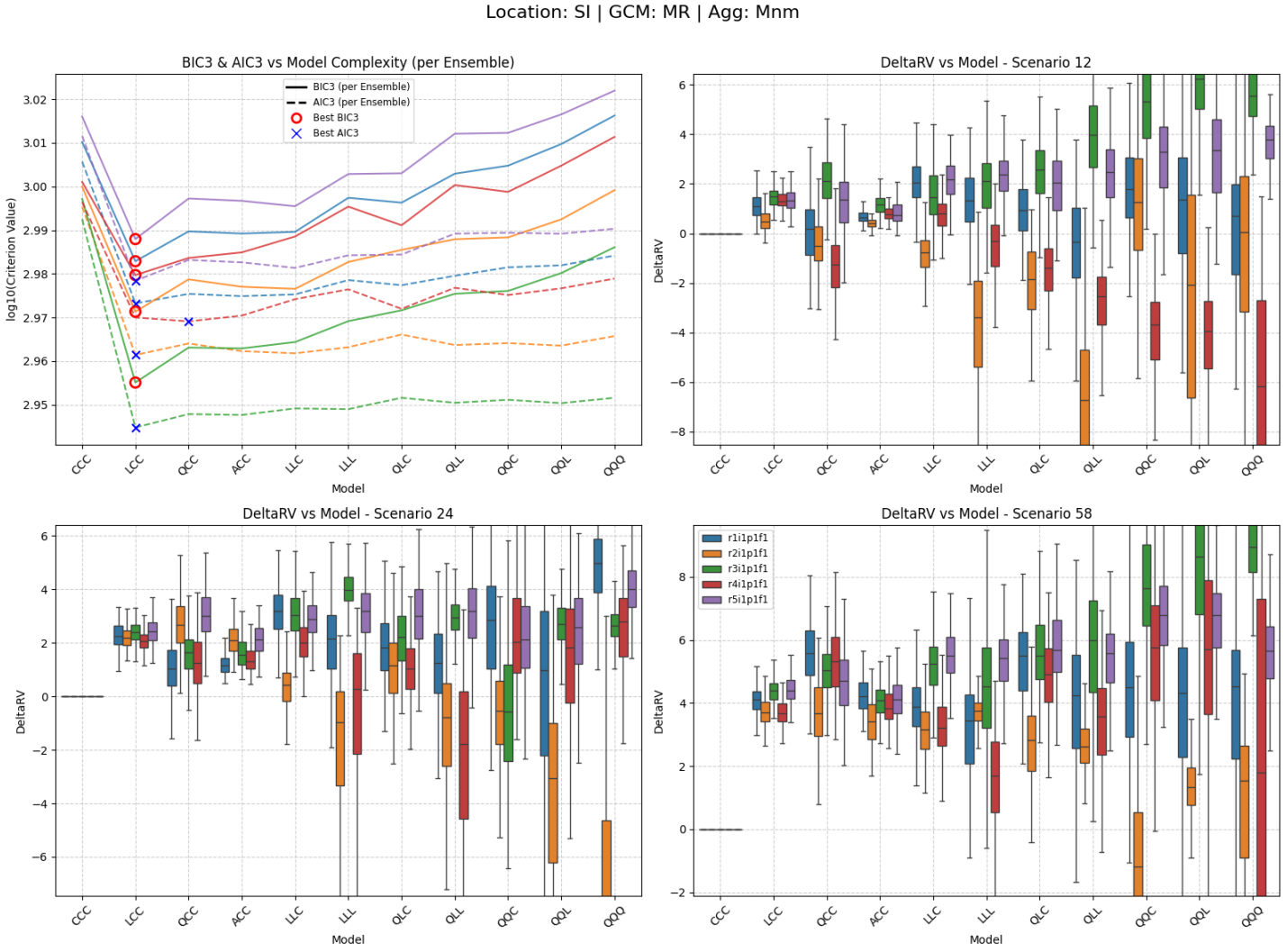

Figure SM59: Summary of scenario-coupled GEV regression for regional annual minima of the Simpson region using `MRI-ESM2-0` GCM data. Top left: plots of BIC3 (solid line) and AIC3 (dashed line) for each available ensemble (distinguished by colour, see Table 2 of the main text and legend in bottom-right panel); optimal model choice using BIC3 (AIC3) indicated using red disc (blue cross). Top right: box-whisker plots summarising the distribution of the difference in the 100-year return value between 2025 and 2125 (ΔQ_1; see Equation 7) for climate scenario `SSP126` as a function of fitted model complexity (x-axis) and ensemble (distinguished by colour, with consistent ensemble colouring across panels); location of horizontal centre line of each box indicates posterior median of ΔQ_1; location of top (bottom) side of each box indicates 75%ile (25%ile) point, and top (bottom) of whiskers the 97.5%ile (2.5%ile) point of the posterior distribution. Bottom left and right: analogues of top right for scenarios `SSP245` (ΔQ_2) and `SSP585` (ΔQ_3). Value of ΔQ_j, $j = 1, 2, 3$ under model CCC is identically zero, and is omitted from bottom panels when convenient to provide better illustration of the variation in estimates under more complex models. For comparison with Figure 6 of the main text.

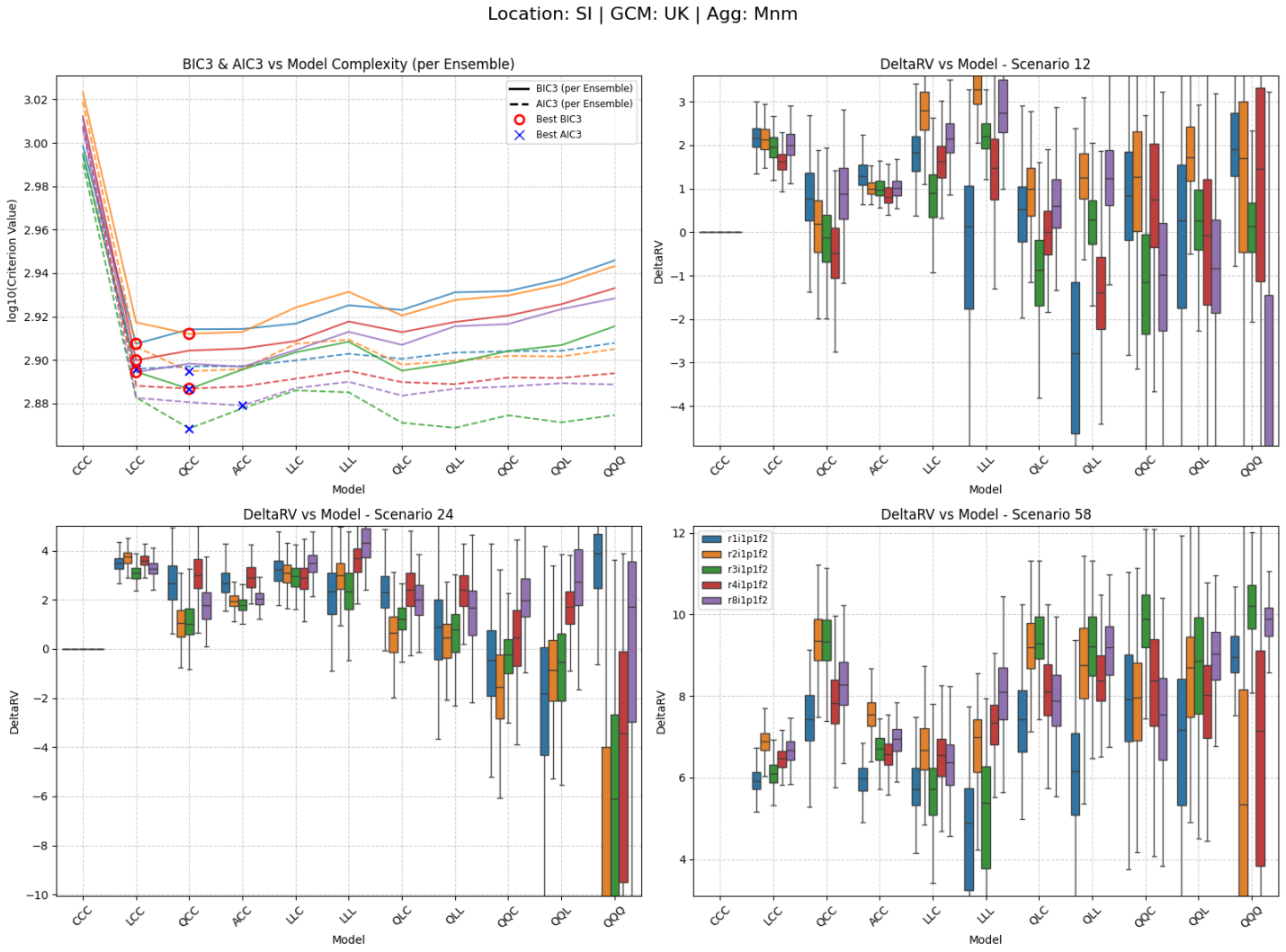

Figure SM60: Summary of scenario-coupled GEV regression for regional annual minima of the Simpson region using `UKESM1-0-LL` GCM data. Top left: plots of BIC3 (solid line) and AIC3 (dashed line) for each available ensemble (distinguished by colour, see Table 2 of the main text and legend in bottom-right panel); optimal model choice using BIC3 (AIC3) indicated using red disc (blue cross). Top right: box-whisker plots summarising the distribution of the difference in the 100-year return value between 2025 and 2125 (ΔQ_1; see Equation 7) for climate scenario `SSP126` as a function of fitted model complexity (x-axis) and ensemble (distinguished by colour, with consistent ensemble colouring across panels); location of horizontal centre line of each box indicates posterior median of ΔQ_1; location of top (bottom) side of each box indicates 75%ile (25%ile) point, and top (bottom) of whiskers the 97.5%ile (2.5%ile) point of the posterior distribution. Bottom left and right: analogues of top right for scenarios `SSP245` (ΔQ_2) and `SSP585` (ΔQ_3). Value of ΔQ_j, $j = 1, 2, 3$ under model CCC is identically zero, and is omitted from bottom panels when convenient to provide better illustration of the variation in estimates under more complex models. For comparison with Figure 6 of the main text.

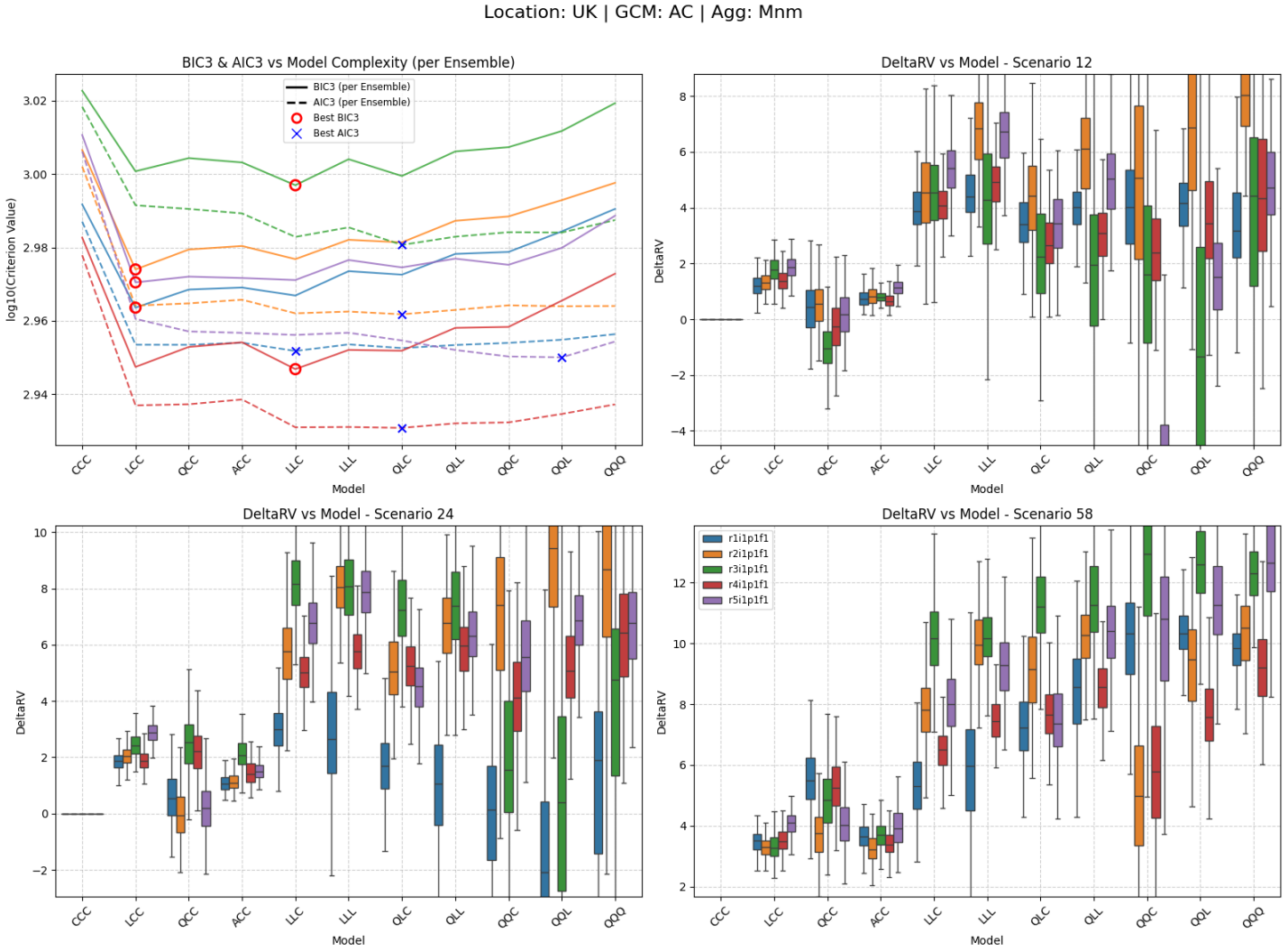

Figure SM61: Summary of scenario-coupled GEV regression for regional annual minima of the UK region using `ACCESS-CM2` GCM data. Top left: plots of BIC3 (solid line) and AIC3 (dashed line) for each available ensemble (distinguished by colour, see Table 2 of the main text and legend in bottom-right panel); optimal model choice using BIC3 (AIC3) indicated using red disc (blue cross). Top right: box-whisker plots summarising the distribution of the difference in the 100-year return value between 2025 and 2125 (ΔQ_1; see Equation 7) for climate scenario `SSP126` as a function of fitted model complexity (x-axis) and ensemble (distinguished by colour, with consistent ensemble colouring across panels); location of horizontal centre line of each box indicates posterior median of ΔQ_1; location of top (bottom) side of each box indicates 75%ile (25%ile) point, and top (bottom) of whiskers the 97.5%ile (2.5%ile) point of the posterior distribution. Bottom left and right: analogues of top right for scenarios `SSP245` (ΔQ_2) and `SSP585` (ΔQ_3). Value of ΔQ_j, $j = 1, 2, 3$ under model CCC is identically zero, and is omitted from bottom panels when convenient to provide better illustration of the variation in estimates under more complex models. For comparison with Figure 6 of the main text.

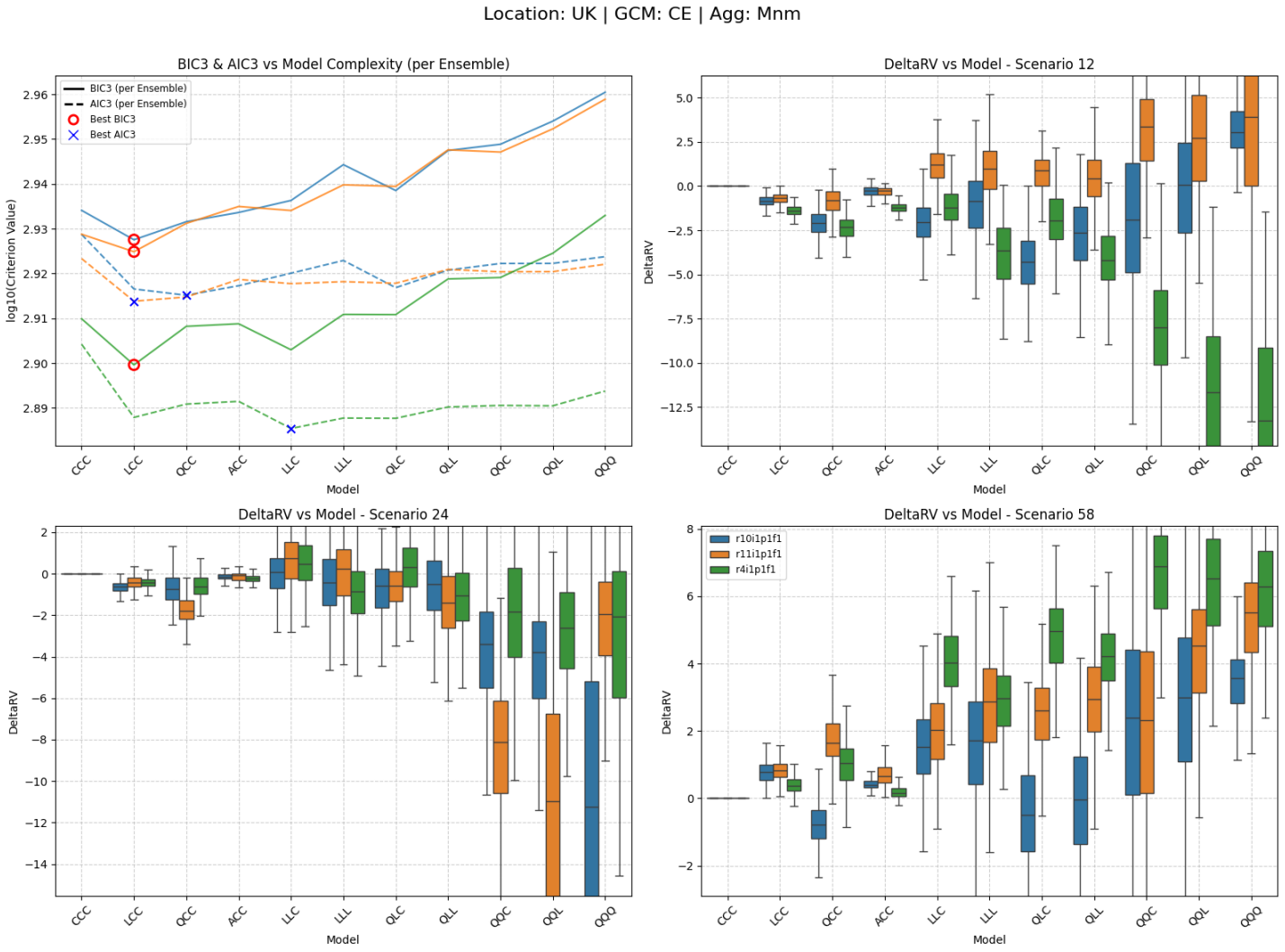

Figure SM62: Summary of scenario-coupled GEV regression for regional annual minima of the UK region using `CESM2` GCM data. Top left: plots of BIC3 (solid line) and AIC3 (dashed line) for each available ensemble (distinguished by colour, see Table 2 of the main text and legend in bottom-right panel); optimal model choice using BIC3 (AIC3) indicated using red disc (blue cross). Top right: box-whisker plots summarising the distribution of the difference in the 100-year return value between 2025 and 2125 (ΔQ_1; see Equation 7) for climate scenario `SSP126` as a function of fitted model complexity (x-axis) and ensemble (distinguished by colour, with consistent ensemble colouring across panels); location of horizontal centre line of each box indicates posterior median of ΔQ_1; location of top (bottom) side of each box indicates 75%ile (25%ile) point, and top (bottom) of whiskers the 97.5%ile (2.5%ile) point of the posterior distribution. Bottom left and right: analogues of top right for scenarios `SSP245` (ΔQ_2) and `SSP585` (ΔQ_3). Value of ΔQ_j, $j = 1, 2, 3$ under model CCC is identically zero, and is omitted from bottom panels when convenient to provide better illustration of the variation in estimates under more complex models. For comparison with Figure 6 of the main text.

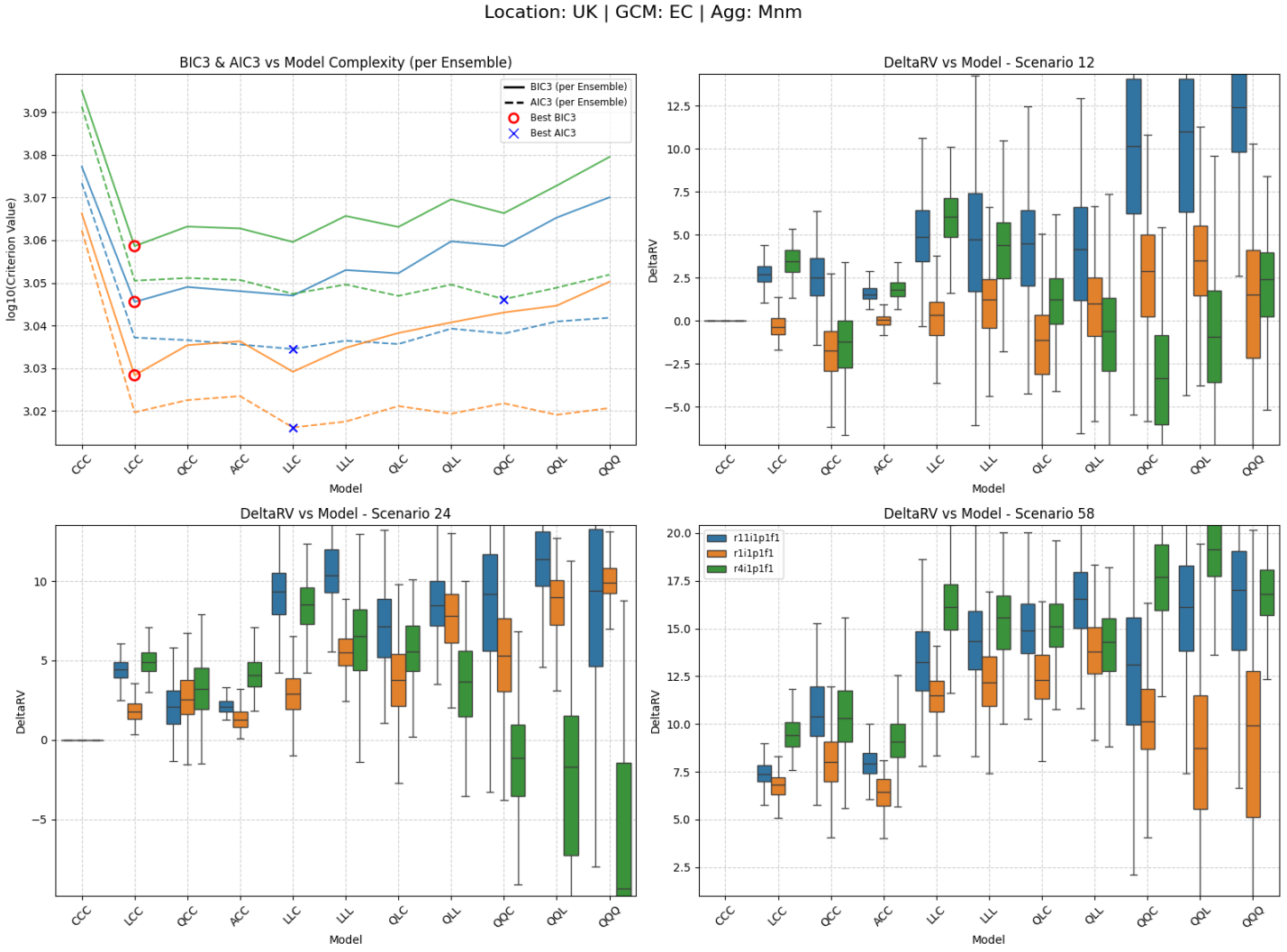

Figure SM63: Summary of scenario-coupled GEV regression for regional annual minima of the UK region using `EC-Earth3` GCM data. Top left: plots of BIC3 (solid line) and AIC3 (dashed line) for each available ensemble (distinguished by colour, see Table 2 of the main text and legend in bottom-right panel); optimal model choice using BIC3 (AIC3) indicated using red disc (blue cross). Top right: box-whisker plots summarising the distribution of the difference in the 100-year return value between 2025 and 2125 (ΔQ_1; see Equation 7) for climate scenario `SSP126` as a function of fitted model complexity (x-axis) and ensemble (distinguished by colour, with consistent ensemble colouring across panels); location of horizontal centre line of each box indicates posterior median of ΔQ_1; location of top (bottom) side of each box indicates 75%ile (25%ile) point, and top (bottom) of whiskers the 97.5%ile (2.5%ile) point of the posterior distribution. Bottom left and right: analogues of top right for scenarios `SSP245` (ΔQ_2) and `SSP585` (ΔQ_3). Value of ΔQ_j, $j = 1, 2, 3$ under model CCC is identically zero, and is omitted from bottom panels when convenient to provide better illustration of the variation in estimates under more complex models. For comparison with Figure 6 of the main text.

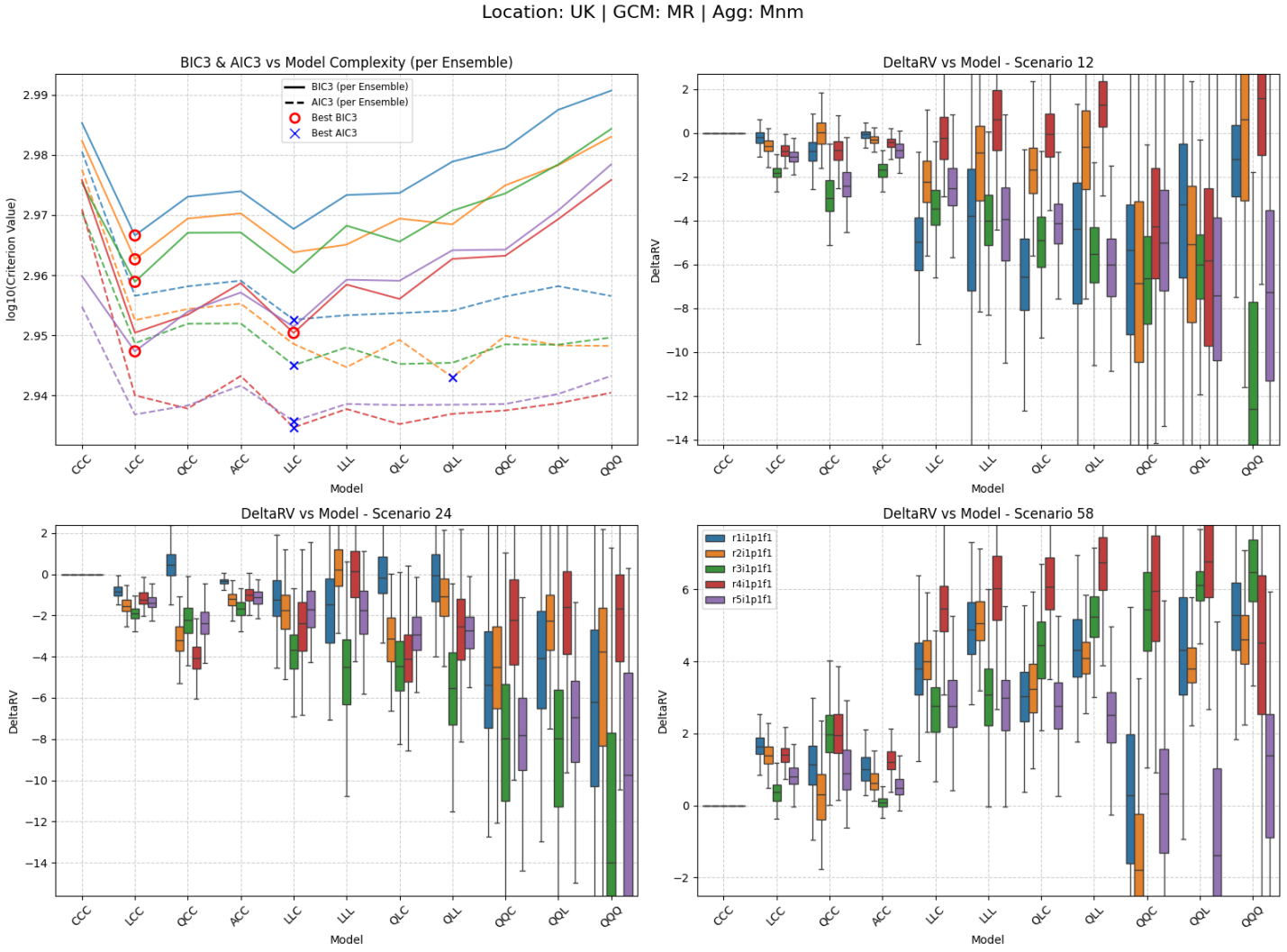

Figure SM64: Summary of scenario-coupled GEV regression for regional annual minima of the UK region using `MRI-ESM2-0` GCM data. Top left: plots of BIC3 (solid line) and AIC3 (dashed line) for each available ensemble (distinguished by colour, see Table 2 of the main text and legend in bottom-right panel); optimal model choice using BIC3 (AIC3) indicated using red disc (blue cross). Top right: box-whisker plots summarising the distribution of the difference in the 100-year return value between 2025 and 2125 (ΔQ_1; see Equation 7) for climate scenario `SSP126` as a function of fitted model complexity (x-axis) and ensemble (distinguished by colour, with consistent ensemble colouring across panels); location of horizontal centre line of each box indicates posterior median of ΔQ_1; location of top (bottom) side of each box indicates 75%ile (25%ile) point, and top (bottom) of whiskers the 97.5%ile (2.5%ile) point of the posterior distribution. Bottom left and right: analogues of top right for scenarios `SSP245` (ΔQ_2) and `SSP585` (ΔQ_3). Value of ΔQ_j, $j = 1, 2, 3$ under model CCC is identically zero, and is omitted from bottom panels when convenient to provide better illustration of the variation in estimates under more complex models. For comparison with Figure 6 of the main text.

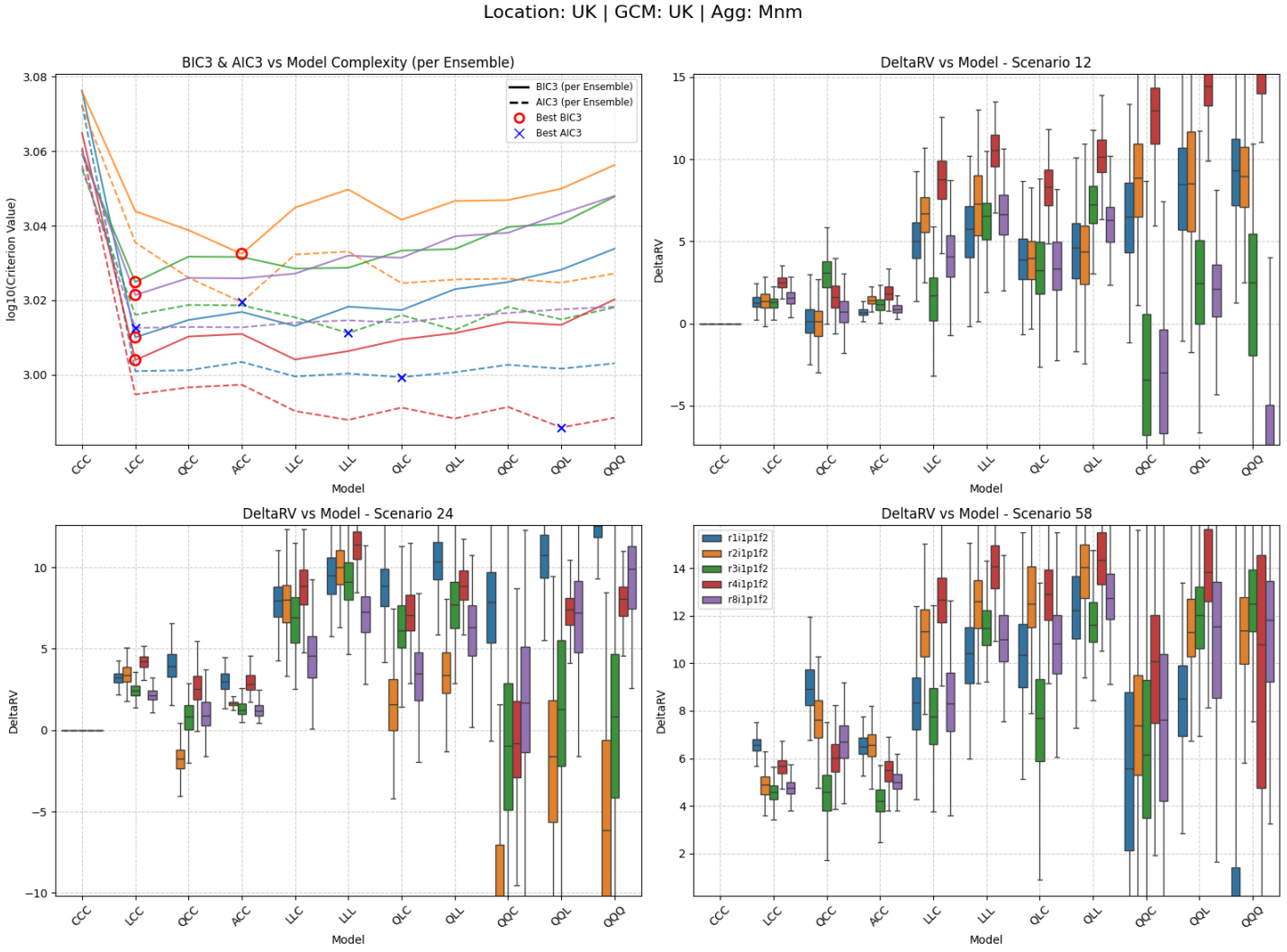

Figure SM65: Summary of scenario-coupled GEV regression for regional annual minima of the UK region using `UKESM1-0-LL` GCM data. Top left: plots of BIC3 (solid line) and AIC3 (dashed line) for each available ensemble (distinguished by colour, see Table 2 of the main text and legend in bottom-right panel); optimal model choice using BIC3 (AIC3) indicated using red disc (blue cross). Top right: box-whisker plots summarising the distribution of the difference in the 100-year return value between 2025 and 2125 (ΔQ_1; see Equation 7) for climate scenario `SSP126` as a function of fitted model complexity (x-axis) and ensemble (distinguished by colour, with consistent ensemble colouring across panels); location of horizontal centre line of each box indicates posterior median of ΔQ_1; location of top (bottom) side of each box indicates 75%ile (25%ile) point, and top (bottom) of whiskers the 97.5%ile (2.5%ile) point of the posterior distribution. Bottom left and right: analogues of top right for scenarios `SSP245` (ΔQ_2) and `SSP585` (ΔQ_3). Value of ΔQ_j, $j = 1, 2, 3$ under model CCC is identically zero, and is omitted from bottom panels when convenient to provide better illustration of the variation in estimates under more complex models. For comparison with Figure 6 of the main text.

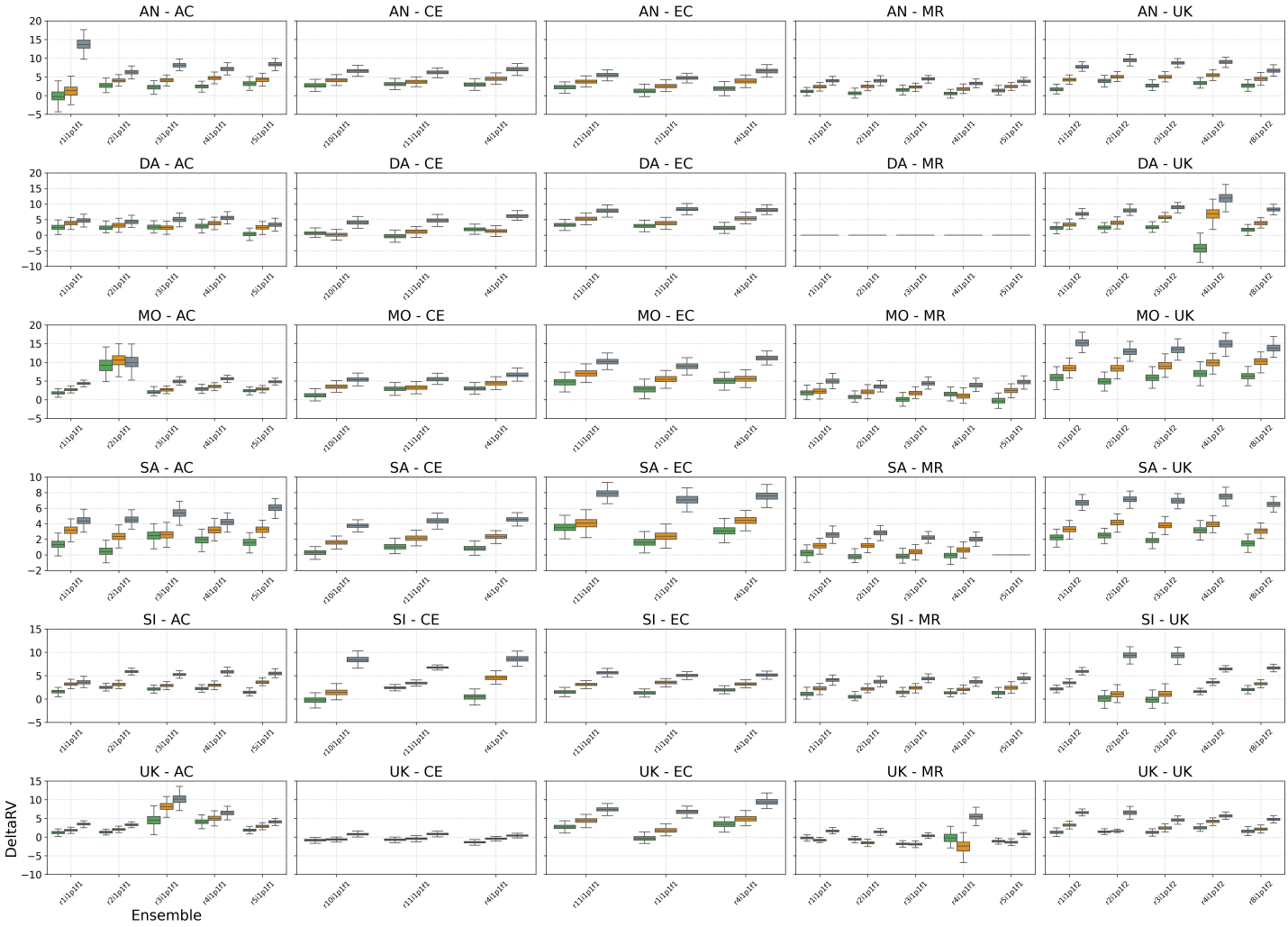

Figure SM66: Summary of inferences for return value differences ΔQ_j, $j = 1, 2, 3$ (see Equation 7) of regional annual minima using BIC3 for model selection. Each panel shows box-whisker plots summarising the posterior distribution of ΔQ for climate scenarios `SSP126` ($j = 1$, green), `SSP245` ($j = 2$, orange) and `SSP585` ($j = 3$, grey) for each of up to five climate ensembles. Different panels show inferences for specific combinations of regions and locations; see Tables 1 and 2 for region and GCM acronyms.

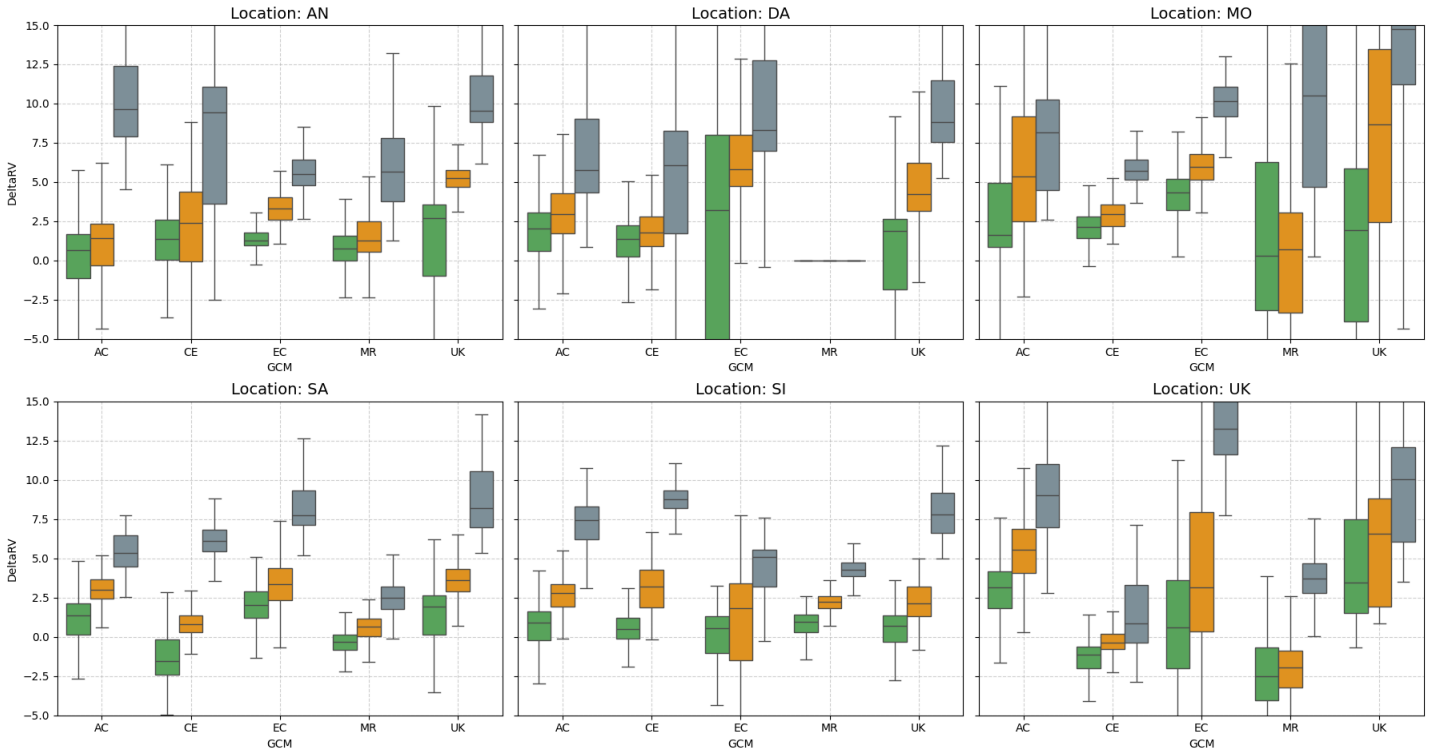

Figure SM67: Summary of inferences for return value differences ΔQ_j, $j = 1, 2, 3$ (see Equation 7) of regional annual minima using AIC3 for model selection, aggregated over climate ensemble. Each panel shows box-whisker plots summarising the posterior distribution of ΔQ for climate scenarios `SSP126` ($j = 1$, green), `SSP245` ($j = 2$, orange) and `SSP585` ($j = 3$, grey) and each of five GCMs (`ACCESS-CM2`, `CESM2`, `EC-Earth3`, `MRI-ESM2-0`, `UKESM1-0-LL`). Left to right, top to bottom, panels show inferences for the Antarctic, Dasht-e Lut, Mojave, Sahara, Simpson and UK regions. For comparison with Figure 10.

Figure SM68: Summary of inferences for return value differences ΔQ_j, $j = 1, 2, 3$ (see Equation 7) of regional annual minima using AIC3 for model selection. Each panel shows box-whisker plots summarising the posterior distribution of ΔQ for climate scenarios `SSP126` ($j = 1$, green), `SSP245` ($j = 2$, orange) and `SSP585` ($j = 3$, grey) for each of up to five climate ensembles. Different panels show inferences for specific combinations of regions and locations; see Tables 1 and 2 for region and GCM acronyms.

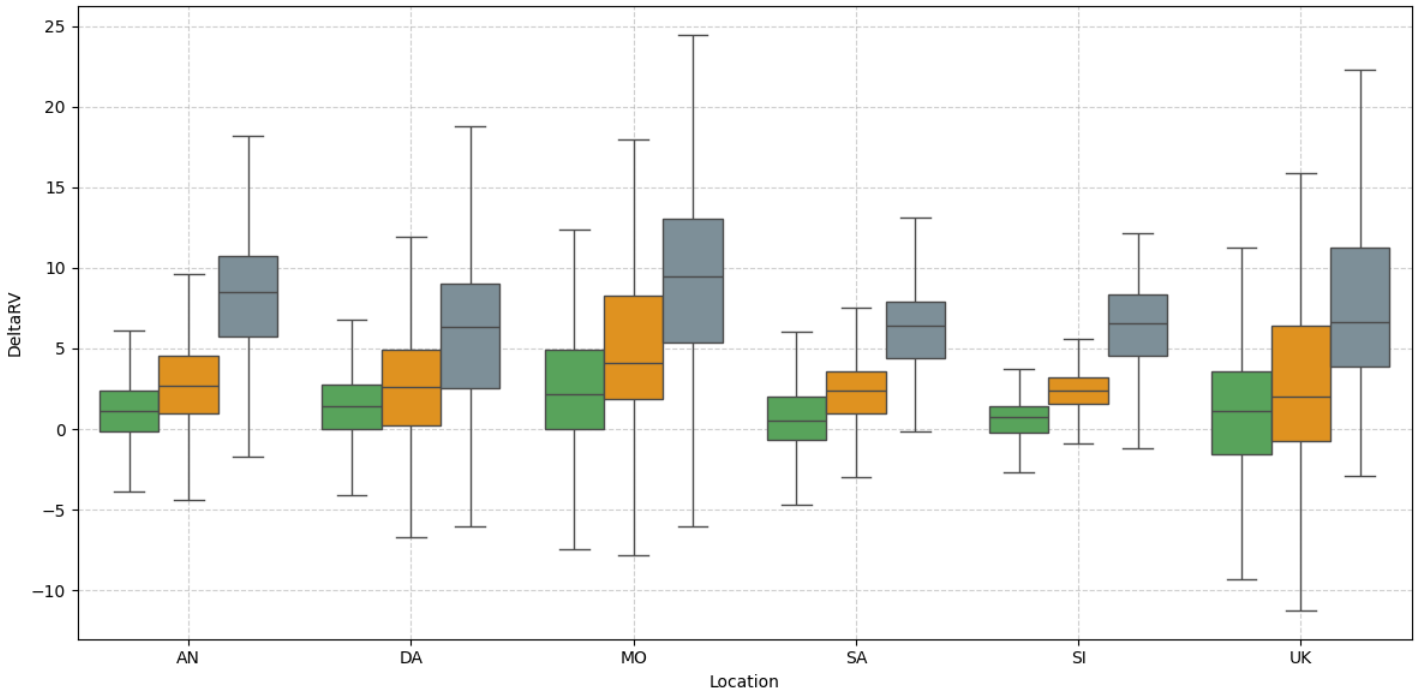

Figure SM69: Summary of inferences for return value differences ΔQ_j, $j = 1, 2, 3$ (see Equation 7) of regional annual minima using AIC3 for model selection, aggregated over climate ensemble and GCM. Box-whisker plots summarise the posterior distribution of ΔQ for climate scenarios `SSP126` ($j = 1$, green), `SSP245` ($j = 2$, orange) and `SSP585` ($j = 3$, grey) for the Antarctic, Dasht-e Lut, Mojave, Sahara, Simpson and UK regions.

SM6 Differences between changes in return value for maxima and minima

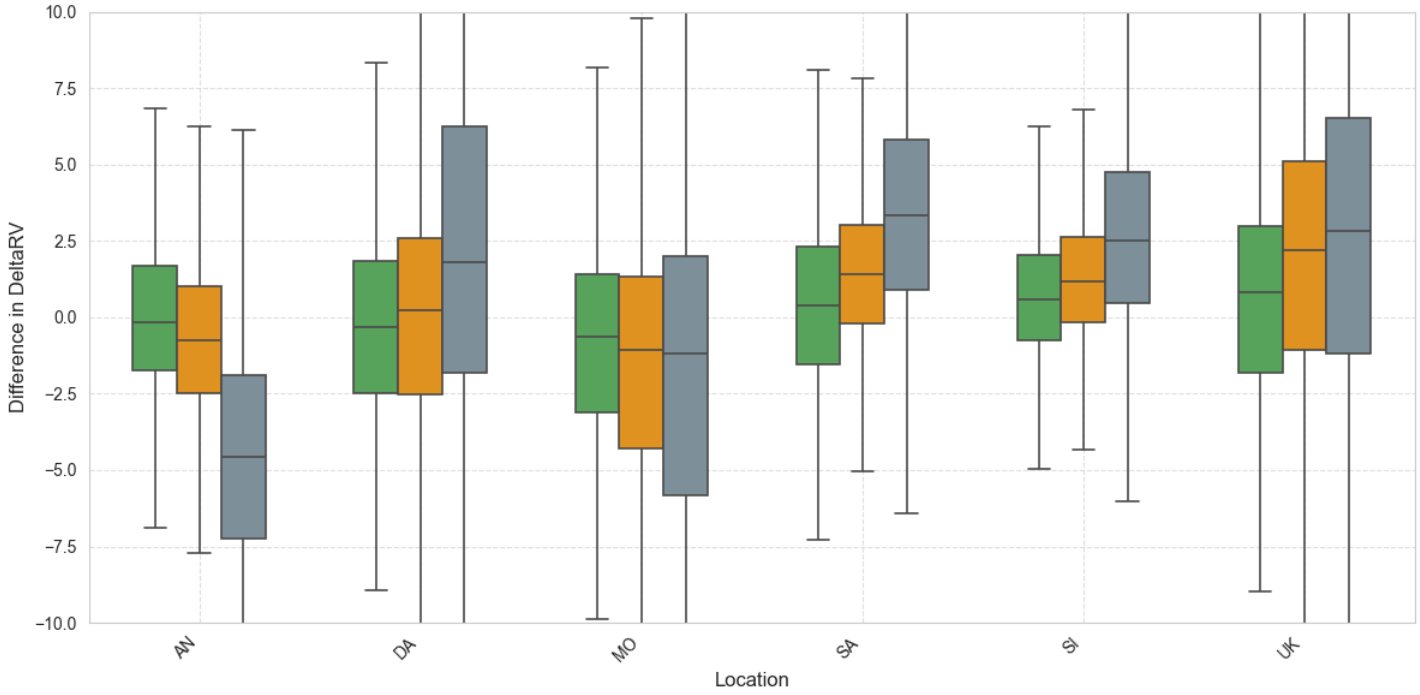

Figure SM70: Summary of inferences for the difference $\Delta\Delta Q_j$, $j = 1, 2, 3$ (see Equation 12) between ΔQ values of regional annual maxima and minima. AIC3 was used for model selection, and posterior distributions aggregated over climate ensemble and GCM. For other details, see Figure 8. For comparison with Figure 12.

SM7 Locations of regional annual maxima and minima in time

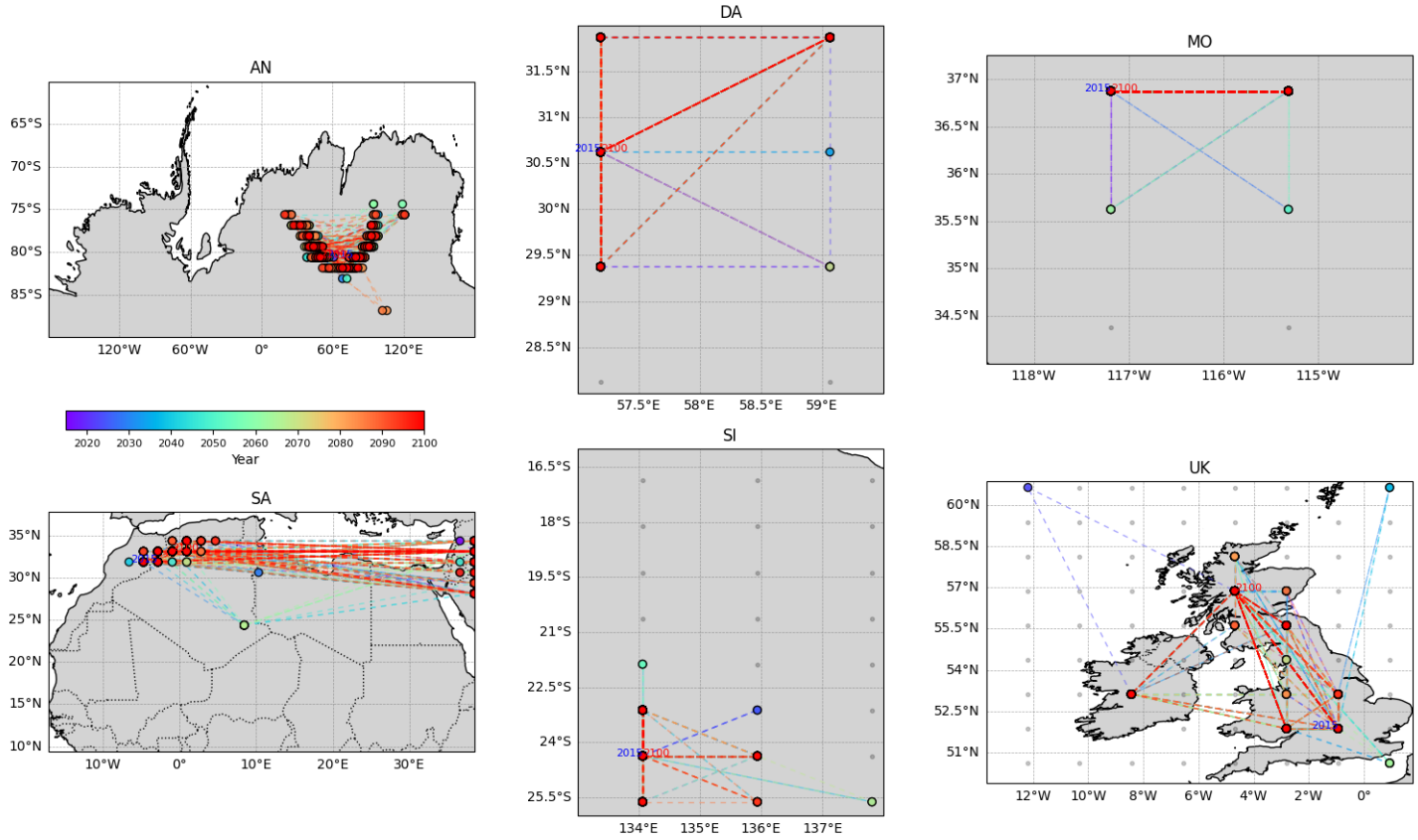

Figure SM71: Locations of regional annual minima (coloured discs) per region (panels) over time for the period (2015,2100) from the `UKESM1-0-LL` GCM. Lines connect discs corresponding to adjacent years; disc and line colours indicate the year; grey dots indicate GCM grid locations for Dasht-e Lut (DA), Mojave (MO), Simpson (SI) and UK (UK), suppressed for Antarctic (AN) and Sahara (SA). For comparison with Figure 13.

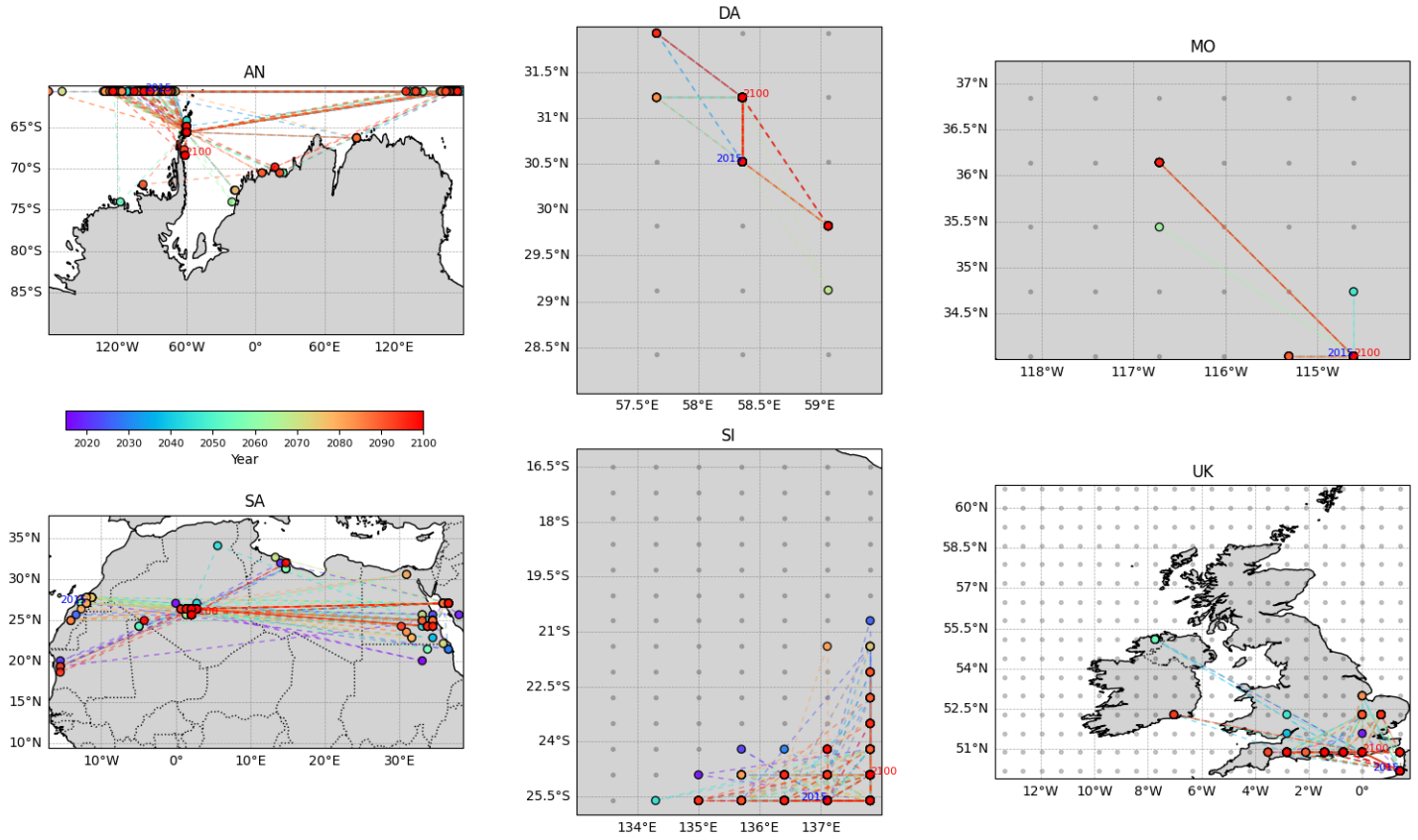

Figure SM72: Locations of regional annual maxima (coloured discs) per region (panels) over time for the period (2015,2100) from the `EC-Earth3` GCM. For other details, see Figure SM71.

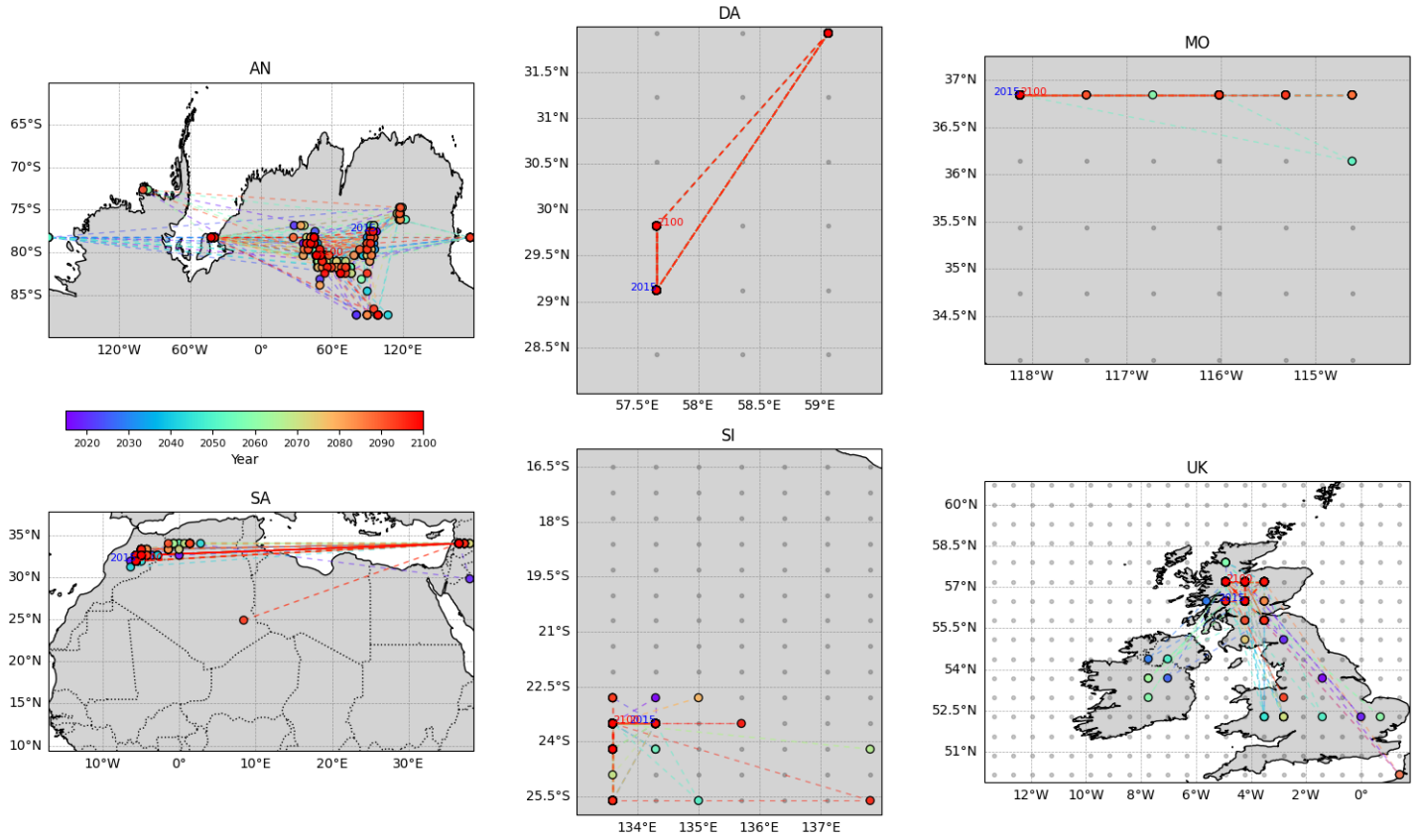

Figure SM73: Locations of regional annual minima (coloured discs) per region (panels) over time for the period (2015,2100) from the `EC-Earth3` GCM. For other details, see Figure SM71.

SM8 Distribution of complexity of fitted models

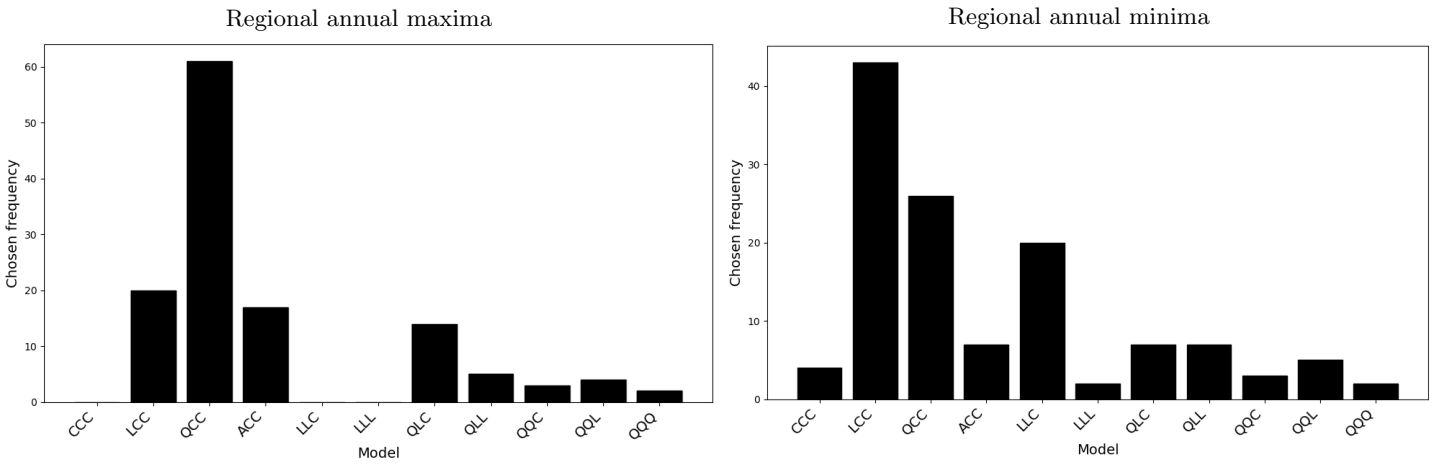

Figure SM74: Complexities of optimal fitted models for regional annual maxima (left) and minima (right) using AIC3 for model selection.

SM9 Bayesian model averaging

This section should be read in conjunction with Section 6.4 of the main text. Consider using sample $x = \{x_1, x_2, ..., x_P\}$ of annual maxima to estimate n_M different models M_1, M_2, ..., M_{n_M}, with which to make a prediction of some future q. In the context of the current work, the $n_M = 11$ models correspond to the different models CCC, LCC, ..., QQQ, and q to the vector of values of ΔQ for the difference in 100-year return value between 2025 and 2125, for three climate scenarios `SSP126`, `SSP245` and `SSP585`. Instead of selecting a single "best" model from the set of n_M models, we can use a weighted average of all the models for prediction. Specifically, the Bayesian model average for the density $f(q|x)$ of q given sample x takes the form

$$f(q|x) = \sum_{m=1}^{n_M} f(q|M_m, x) f(M_m|x) \tag{SM1}$$

where $f(q|M_m, x)$ is the posterior predictive density of q under model M_m, $m = 1, 2, ..., n_M$, and $f(M_m|x)$ is the posterior probability of model M_m given x. We can estimate $f(q|M_m, x)$ relatively straightforwardly using Bayesian inference, e.g., using MCMC as in the current work, since

$$f(q|M_m, x) = \int_{\theta_m} f(q|\theta_m, M_m) f(\theta_m|M_m, x) d\theta \tag{SM2}$$

where $f(\theta_m|M_m, x)$ is the posterior density of parameters θ_m of model M_m from the MCMC, and $f(q|\theta_m, M_m)$ is the known density of q given M_m and its parameters θ_m. We can also attempt to estimate the posterior probability of model M_m using the expression

$$f(M_m|x) = \frac{f(x|M_m) f(M_m)}{\sum_{m'=1}^{n_M} f(x|M_{m'}) f(M_{m'})} \tag{SM3}$$

where $f(x|M_m)$ is the marginal probability of x under model M_m, given by

$$f(x|M_m) = \int_{\theta_m} f(x|\theta_m, M_m) f(\theta_m|M_m) d\theta \tag{SM4}$$

where $f(x|\theta_m, M_m)$ is the known density of x given model M_m with parameters θ_m. The remaining densities $f(M_m)$ in Equation SM3 and $f(\theta_m|M_m)$ in Equation SM4 are prior specifications of the models M_m, $m = 1, 2, ..., n_M$ and their parameters θ_m. In principle, once the priors are specified we can therefore use Equations SM1 - SM4 to estimate the model average density for q.

In practice however, specifying $f(M_m)$ and $f(\theta_m|M_m)$, $m = 1, 2, ..., n_M$ is problematic. Practitioners often revert to trying different possible choices of prior, and confirming whether plausible estimates for $f(q|x)$ result. Model stacking provides a data-driven alternative to prior specification. The stacked model average density $f_S(q|x)$ is given by

$$f_S(q|x) = \sum_{m=1}^{n_M} w_m f(q|M_m, x) \tag{SM5}$$

where weight vector $w = (w_1, w_2, ..., w_{n_M})$ is found by a cross-validation strategy

$$w = \underset{w'}{\text{argmax}} \sum_{i=1}^{P} \log \left(\sum_{m=1}^{n_M} w'_m f(x_i|M_m, x_{-i}) \right) \tag{SM6}$$

where $f(x_i|M_m, x_{-i})$ is the posterior predictive density of observation x_i, $i = 1, 2, ..., n$, under model M_m estimated using all observations in x except for x_i. $f(x_i|M_m, x_{-i})$ is evaluated using

$$f(x_i|M_m, x_{-i}) = \int_{\theta_m} f(x_i|\theta_m, M_m) f(\theta_m|M_m, x_{-i}) d\theta \tag{SM7}$$

where, as before, $f(x_i|\theta_m, M_m)$ is a known density, and $f(\theta_m|M_m, x_{-i})$ is the posterior density of parameters θ_m of model M_m estimated using sample x_{-i}, which can be sampled using MCMC. Comparison of Equations SM1 and SM5 suggests that the stacking weight vector w acts as an estimate of the set of the posterior probabilities $f(M_m|x)$, $m = 1, 2, ..., n_M$.

To then evaluate the RMSE for BMA in Section 6.4, we use the expression

$$\text{RMSE} = \left(\frac{1}{3 n_R n_S} \sum_{j=1}^{3} \sum_{k=1}^{n_R} \sum_{s=1}^{n_S} \left(\Delta Q_j^* - \sum_{m=1}^{n_M} (w_m|D_k) \left(\Delta Q_{j(s)}|M_m, D_k \right) \right)^2 \right)^{1/2}. \tag{SM8}$$

where ΔQ_j^* is the true value, and $\Delta Q_{j(s)}|M_m, D_k$ is posterior estimate of ΔQ_j, $j = 1, 2, 3$ corresponding to iteration s, $s = 1, 2, ..., n_S$ from the MCMC chain for data realisation D_k, $k = 1, 2, ..., n_R$ and model M_m, $m = 1, 2, ..., n_M$, and $w_m|D_k$ is the BMA weight of model M_m for data realisation D_k.

Note that many different metrics (or "scoring rules") are available, as alternatives to RMSE, to evaluate the performance of our models for ΔQ. We chose RMSE for its simplicity; an attractive option might be the Jensen-Shannon (JS) divergence. Clearly, the choice of preferred model selection criterion in the simulation study of S4 of the main text (namely BIC3 using RMSE) might be different were we to use JS divergence as our metric.

An issue with applications of leave-out methods to environmental extreme value modelling is that the support of an estimated marginal model $f(x|M_m)$ may be bounded above if the posterior density of the shape parameter is zero for non-negative values. As a result, it is possible in particular that the density $f(x|M_m, x_{-i})$ of withheld observation x under model M_m estimated using sample x_{-i} is zero; that is, that the value x lies beyond the upper end point of the estimated GEV distribution. To mitigate this issue, we impose a constraint on the Bayesian inference using MCMC, for each geographic region considered, that temperatures up to 20% higher than the largest observed temperature (over all combinations of GCM, scenario and ensemble member) must have non-zero density. Formally, we insist that

$$\mu - \frac{\sigma}{\xi} > x^*_{\min} + 1.2 \times (x^*_{\max} - x^*_{\min}) \tag{SM9}$$

for each geographic region, where $x^*_{\min}$ and $x^*_{\max}$ are the minimum and maximum values observed anywhere over the region, over all combinations of GCM, scenario and ensemble member.

References

H. M. Abdelmoaty and S. M. Papalexiou. Changes of extreme precipitation in CMIP6 projections: should we use stationary or nonstationary models? *J. Clim.*, 36:2999–3014, 2023.

H. Akaike. A new look at the statistical model identification. *IEEE Trans. Autom. Control*, 19:716–723, 1974.

G. Auld, G. C. Hegerl, and I. Papastathopoulos. Changes in the distribution of annual maximum temperatures in Europe. *Adv. Stat. Clim. Meteorol. Oceanogr.*, 9:45–66, 2023.

L. R. Belzile, C. Dutang, P. J. Northrop, and T. Opitz. A modeler's guide to extreme value software. *Extremes*, 26:595–638, 2023.

J. Castillo-Mateo, J. Asin, A. C. Cebrian, J. Mateo-Lazaro, and J. Abaurrea. Bayesian variable selection in generalized extreme value regression: modeling annual maximum temperature. *Mathematics*, 11, 2023.

A. Diop and M. A. Niang. Variable selection in generalized extreme value regression model using Bootstrap method. *Qeios*, 2023. doi: 10.32388/WC481X.

K. Ewans and P. Jonathan. Uncertainties in estimating the effect of climate change on 100-year return period significant wave heights. *Ocean Eng.*, 272:113840:1–17, 2023.

D. S. Faulkner, S. Longfield, S. Warren, and J. A. Tawn. Modelling non-stationary flood frequency in England and Wales using physical covariates. *Hydrol. Res.*, 55:205–220, 2024.

D. P. Foster and E. I. George. The risk inflation criterion for multiple regression. *Ann. Stat.*, 22:1947–1975, 1994.

P. Friederichs and T. L. Thorarinsdottir. Forecast verification for extreme value distributions with an application to probabilistic peak wind prediction. *Environmetrics*, 23:579–594, 2012.

D. Gamerman and H. F. Lopes. *Markov chain Monte Carlo: stochastic simulation for Bayesian inference*. Chapman and Hall / CRC, Boca Raton, USA, 2006.

A. Gardini. Functional and variables selection in extreme value models for regional flood frequency analysis. *Environ. Ecol. Stat.*, 30:715–739, 2023.

A. Gelman, J. B. Carlin, H. S. Stern, and D. B. Rubin. *Bayesian data analysis*. Chapman and Hall/CRC, 2004.

A. Gelman, J. Hwang, and A. Vehtari. Understanding predictive information criteria for Bayesian models. *Stat. Comput.*, 24:997–1016, 2014.

E. J. Hannan and B. G. Quinn. The determination of the order of an autoregression. *Econometrica*, 47:71–84, 1979.

P. D. Hoff. *A first Course in Bayesian statistical methods.* Springer Texts in Statistics. Springer New York, 2009.

C. M. Hurvich and C. Tsai. Regression and time series model selection in small samples. *Biometrika*, 76:297–307, 1989.

M. J. Jones, D. Randell, K. Ewans, and P. Jonathan. Statistics of extreme ocean environments: non-stationary inference for directionality and other covariate effects. *Ocean Eng.*, 119:30–46, 2016.

V. V. Kharin and F. W. Zwiers. Estimating extremes in transient climate change simulations. *J. Clim.*, 18:1156–1173, 2005.

V. V. Kharin, F. W. Zwiers, X. Zhang, and M. Wehner. Changes in temperature and precipitation extremes in the CMIP5 ensemble. *Climatic Change*, 119:345–357, 2013.

V. V. Kharin, F. W. Zwiers, X. Zhang, and G. J. Flato. Estimating changes in temperature and precipitation extremes from the CMIP6 ensemble. *Earth's Future*, 6:704–715, 2018.

H. T. Kiiveri. A general approach to simultaneous model fitting and variable elimination in response models for biological data with many more variables than observations. *BMC Bioinformatics*, 9:195, 2008.

J. Kim, Y. Sun, J.-S. Kim, S. Kang, and J.-H. Lee. Appropriate model selection methods for nonstationary generalized extreme value models. *J. Hydrol.*, 549:538–550, 2017.

C. Leach and P. Jonathan. Scenario-coupled climate extreme-value regression (SCCER). https://github.com/Callum-Leach/SCCER, 2026.

J. Lee, Y. Fan, and S.A. Sisson. Bayesian threshold selection for extremal models using measures of surprise. 85:84–99, 2015.

C. Li, F. W. Zwiers, X. Zhang, G. Li, Y. Sun, and M. Wehner. Changes in annual extremes of daily temperature and precipitation in CMIP6 models. *J. Clim.*, 34:3441–3460, 2021.

R. J. Matear and P. J. Reddy. A machine learning tool for determining the required sample size for GEV fitting in climate applications. *Geophys. Res. Lett.*, 52:e2024GL112737, 2025.

B. Nasri, S. El Adlouni, and T. B. M. J. Ouarda. Bayesian estimation for GEV B-spline model. *Open Journal of Statistics*, 3:118–128, 2013.

A. Phatak, C. Chan, and H. Kiiveri. Fast variable selection for extreme values. In *Proc. 5th International Congress on Environmental Modelling and Software, Ottawa, Ca. 183.*, 2010.

J. Piironen and A. Vehtari. Comparison of Bayesian predictive methods for model selection. *Stat. Comput.*, 27:711–735, 2017.

D. Randell, K. Turnbull, K. Ewans, and P. Jonathan. Bayesian inference for non-stationary marginal extremes. *Environmetrics*, 27:439–450, 2016.

J. Richards and R. Huser. Regression modelling of spatiotemporal extreme U.S. wildfires via partially-interpretable neural networks. *Journal of Computational and Graphical Statistics*, 2026. doi: https://doi.org/10.1080/10618600.2025.2609641.

J. Rissanen. Modeling by shortest data description. *Automatica*, 14:465–471, 1978.

G. O. Roberts and J. S. Rosenthal. Examples of adaptive MCMC. *J. Comp. Graph. Stat.*, 18:349–367, 2009.

G. Schwarz. Estimating the dimension of a model. *Ann. Stat.*, 6:461–464, 1978.

D. J. Spiegelhalter, N. G. Best, B. P. Carlin, and A. van der Linde. Bayesian measures of model complexity and fit. *J. Roy. Statist. Soc. B*, 64:583–639, 2002.

A. Vehtari, A. Gelman, and J. Gabry. Practical Bayesian model evaluation using leave-one-out cross-validation and WAIC. *Statistics and Computing*, 27:1413–1432, 2017.

S. Watanabe. A widely applicable Bayesian information criterion. *J. Mach. Learn. Res.*, 14:867?897, 2013.

J. Zhang, Y. Yang, and J. Ding. Information criteria for model selection. *Wiley Interdiscip. Rev. Comput. Stat.*, 15:e1607, 2023.

F. W. Zwiers, X. Zhang, and Y. Feng. Anthropogenic influence on long return period daily temperature extremes at regional scales. *J. Clim.*, 24:881–892, 2011.